An Investigation of Micro-Hydro Power Generator Characteristics

Salma A. S. Alarefi

A thesis submitted for the degree of *Doctor of Philosophy*

School of Computer Science and Electronic Engineering

University of Essex

Date of Submission: Friday 17th August, 2018

Abstract

Research on the electrical characteristics of hydroelectric power systems has to the author's knowledge, not received much attention. However, renewed interest in hydropower microgeneration has created a need to understand the underlying properties. This thesis presents a pioneering empirical investigation into the electrical characteristics of micro-hydro power generators (MHPGs). An ohmic characteristic behaviour in MHPGs with constant source impedance, even with varying water flow is demonstrated for the first time. Experimental results showed variable flow correlation between the MHPGs voltage and current at the maximum power point, which coincides with 50% V_{oc} and 50% of I_{sc}. A novel heuristic model for hydroelectric power generator is then derived and validated through MATLAB-Simulink simulation.

In pursuit of MHPG maximum utilisation efficiency, a new Seesaw maximum power point tracking (MPPT) controller is presented. The simple but accurate analogue Seesaw MPPT, which incorporates feedforward control of the output voltage only in a current-mode operation, proved fast tracking control under rapidly varying operational conditions. Only one voltage sensor is required. The renewed application of the classical feedforward mechanism offers superior MPPT response (μ seconds). This approach is unlike previous work in that it uses the current-voltage characteristics rather than the power, which reduces the design complexity. Maximum power delivery from the source to the load is guaranteed through the load-side control.

The introduction of shunt measurement in the hydraulic analogy through a parallel combination of high-flow rate sensing (via MHPGs) and highly sensitive ultrasonic mL/min sensor would allow micro-leaks to be detected. Unlike conventional water leakage detection systems, the proposed automated system is highly sensitive (detected leaks of 1 mL/min.) and does not impede the main flow. Wavelet de-noising analyses carried out removed background noise and further isolated micro-leakage signals.

Acknowledgements

I would like to extend thanks to the many people, who so generously contributed to the work presented in this thesis.

Special gratitude goes to my supervisor, Professor Stuart Walker. I am sincerely appreciative to him for his generous support, patience, motivation, and immense knowledge during my Ph.D. research. His continual intellectual and moral support have been invaluable.

Similar, profound thanks go to my supervisory board members: Dr. Nick Zakhleniuk and Dr. Arsenia Chorti for their insightful comments and suggestions. To Mr. Nick Warren for his help with fabricating the PCBs for my experimental validations, and Dr Felix Ngobigha for his advice and assistant. A special mention goes to my friend and colleague Dr. Naseem Ramli for her inspiring guidance and much intellectually stimulating discussion throughout this research.

I am greatly appreciative to the Libyan Ministry of Higher Education for providing me with the financial support to complete my Ph.D. in the U.K.

My heartfelt appreciation goes to my dear husband, Mohamed Breish, my family, and my friends for their continuous love and unconditional support throughout my studies. I am truly indebted to my parents, Almabrok and Halima, for more than words can express and I dedicate this thesis to them.

Contents

List of Figures

List of Tables

Nomenclature

ANN	Artificial Neural Network
CCTV	Closed-Circuit Television
DC	Direct Current
DMA	District Metered Area
ESC	Extremum Seeking Control
FIT	Feed-in-Tariff
GSM	Global System for Mobile Communications
HCS	Hill Climb Searching
HPCS	Hydro Power Conversion System
HPG	Hydropower Generator
IC	Incremental Conductance
I-V	Current-Voltage
IR	Infrared Radiation
MHPG	Micro Hydro Power Generator
Micro-CHP	Micro Combined Heat and Power
MPP	Maximum Power Point
MPPT	Maximum Power Point Tracking
PCB	Printed Circuit Board
PCS	Power Conversion System
pH	Potential of Hydrogen
P-R	Power-Resistance
PSF	Power Signal Feedback
P-V	Power-Voltage
PV	Photovoltaics
SMS	Short Message Service
TSR	Tip Speed Ratio
USB	Universal Serial Bus
WPCS	Wind Power Conversion System
WT	Wavelet Transform

Chapter 1

Introduction

Microgeneration continues to emerge as a promising candidate for greener and more sustainable energy sources. This has renewed interest in prospects for small-scale hydropower generation. Despite significant advances in the development of small hydro turbines [1–3], the electrical properties of hydropower conversion systems (HPCSs) have received little attention. This chapter introduces the research motivation behind this work and identifies current challenges in this domain. It states the research objectives in tackling the problem. The major contributions made by this thesis to bridge these research gaps are also listed. In closing, highlights of each chapter are presented to illustrate the structure of the thesis.

1.1 Research motivation

From a fluid-dynamic prospective, HPCSs have a rich knowledge base. This is in sharp contrast to the electrical performance and control aspects for such renewable systems. It appears that there is a lack of understanding of electrical performance and key aspects, such as the characteristic impedance, have been overlooked [4–6].

Today, the advancement of power electronic circuitry has contributed significantly to the rapid development of sustainable energy systems. In particular, wind power conversion systems (WPCSs) and solar photovoltaic (PV) systems electrical characteristics have been the subject of detailed research. Advanced power control mechanisms, which rely on the system's electrical properties, are concerned mostly with wind turbine and solar technology. Research on the control of HPCSs highlighted the gap in studying operational performance of these systems [7]. The literature suggests that most research effort on HPCSs differences and opportunities has been based on WPCSs with claimed synergies in system performance synthesis [8, 9]. Although, the underlying electrical properties of HPCSs remain to be investigated, hydropower generation is manifested through non-linear performance characteristics [9–11].

Maximising the energy yield of a sustainable power conversion system such as a HPCS remains a challenging control problem. That is because the intermittent nature of hydropower sources influences the maximum power available for harnessing under different environmental conditions (i.e. water flow rate). Maximum power point tracking (MPPT) controllers are therefore used to maximise the yield and improve efficiency. Unlike HPCSs, MPPT is a mature control technology for WPCSs and solar PV systems. The development of small hydropower generators has made it possible to investigate power controllers for HPCSs within controlled environments.

1.2 Challenges

While it is true that great strides have been made in the field of sustainable power control systems, there are still many avenues that need to be pursued and remain challenging. Among other open research issues, some are identified here that provide the impetus for the work presented in this thesis:

- **System non-linearity:** renewable power conversion system PCSs such as WPCSs and solar PV systems are inherently non-linear in nature, so that the change of the output with respect to the input is not proportionate. The subtle nature of such systems poses challenges in tracking the output parameters. Advanced control strategies are therefore required to track and control the output power [12]. Although most research on HPCS power control assumes nonlinear performance [11], its electrical characteristics remain undetermined.

- **Power source intermittency:** the variable nature of sustainable power sources controls the maximum potential power available from the source. As a result, the maximum operating voltage V_{mpp} and current I_{mpp}, and hence operation point of a PCS are affected [13]. This challenges power conversion controllers to promptly track the rapidly varying output power. Power controllers based on approximated linearity between open circuit voltage V_{oc}, short circuit current I_{sc} and V_{mpp}, I_{mpp}, respectively, are presented in [14, 15]. Not only does the open circuit voltage and short circuit current control lead to near optimum operation but it also suffers temporal power loss caused by disconnecting the generator to measure V_{oc} and I_{sc} [16].

- **Variable system dynamics:** the dynamics of renewable PCSs are mostly operating point and environmental variables dependent; for example, the characteristic impedance of solar PV systems varies with solar irradiance and temperature. The fact that significant power losses can be caused by a mismatch between the load and the power source impedances, adds to the challenges of power conversion efficiency enhancement. Although lookup table methods reported in [17, 18] can offer a fast estimate to the MPP, its model dependency limits it compatibility.

- **Power conversion efficiency:** maximising the power conversion relative to the input parameters is a major drawback of most conventional MPPT controllers. Such optimisers fail in delivering maximum harvested power to the load. The advantages of implementing MPPT through output parameters are introduced in the literature [19]. Moreover, conventional direct, indirect or classical numerical MPPT algorithms [20] are mostly based on the systems' power characteristics. This requires prior knowledge of initial conditions usually not satisfied in practice which causes the system to oscillate around the MPP leading to significant power loss. Such approaches also involve an iterative process to calculate the instantaneous power, which increase complexity and the tracking time [21, 22].

1.3 Main objectives and outcomes

The main objectives of this research have focused on the field of hydropower microgeneration as means of investigating potential sustainable sources for emergency situations in developing countries (e.g. powering devices in blackouts). In this regard, the research has been to investigate the underlying electrical characteristics of micro-hydropower generators MHPGs.

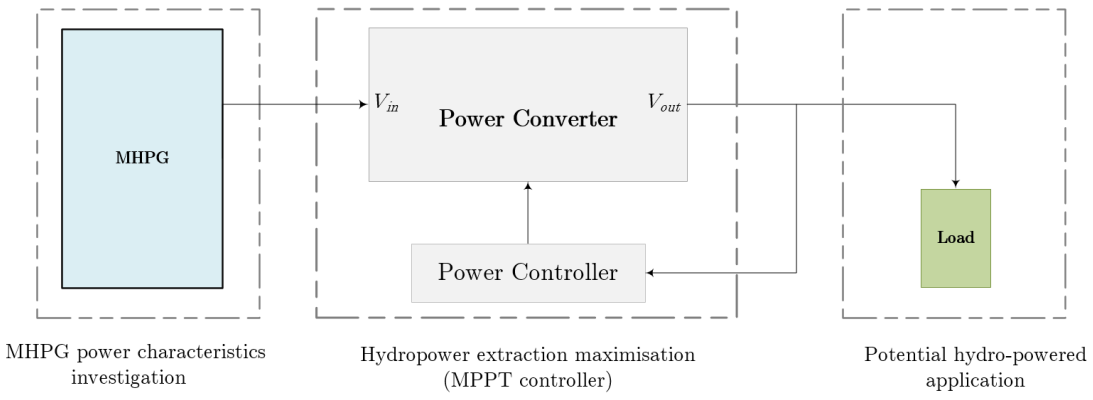

Figure 1.1: Conceptual scheme of the overall research objectives.

Following the understanding of MHPGs electrical performance, the research has investigated MPPT optimisation methods appropriate to HPCSs. The scope of the research has expanded further to include the study of a potential micro-hydropowered application in the field of water management systems (i.e. leakage detection). The work reported in this thesis has been validated empirically. Experiments have been conducted on a built-in-house hydropower emulator. These results were analysed using MATLAB software. Main results obtained are:

- A demonstration of linear power characteristics for MHPGs at various flow rates. Three different configurations of MHPGs were examined. A constant source impedance for MHPGs at various flow rates was observed. Analysis of the electric-hydraulic analogy explained the relationship between MHPG electrical performance and the flow dynamics. Measurements showed a linear dependency between MHPG voltage at the maximum power point (MPP) V_{mpp} and open circuit voltage V_{oc} (i.e.$V_{mpp} = 50\%V_{oc}$). Those results were accepted for publication in the proceedings of a peer-reviewed IEEE International Conference on Industrial Technology (ICIT2018).

- A heuristic model characterising MHPG electrical power performance was derived from empirical findings. MATLAB-Simulink simulation results showed agreement with practical results. The key electrical characteristics for MHPG were compared to that of WCSs and solar PV systems. The results of these analyses were also included in the paper accepted for publication in ICIT2018.

- A demonstration of a new load-side, constant voltage, feed-forward, Seesaw MPPT controller conducted on MHPG incorporated into a laboratory hydropower emulator. The Seesaw MPPT controller tracked the maximum power point under various flow rates. The experimental validation of the Seesaw MPPT for load voltage control showed a potential for the controller in the application of battery charging control.

- An optimised 2x2 parallel series arrangement of 4 commercially-available MHPGs incorporated in a house water inlet produced $4W$ into 330Ω at typical UK domestic pressures and flow-rates ($\approx$ 3bar/300 kPa and $\approx$17 L/min.). The results of these experiments were published in the proceedings of the peer-reviewed IEEE Conference on Renewable and Sustainable Energy (IRSEC) [23].

- A demonstration of the shunt measurement in hydraulic analogies for flow rate measurements. The incorporation of a highly sensitive flow meter allowed for water leakage of micro flow rates (i.e. 1 mL/min) to be detected. The results were presented and published in the peer-reviewed IEEE Conference in [24] and were also orally presented in STEM for BRITAIN 2017 (See Appendix B.1).

1.4 Contribution to research

The work carried out during this Ph.D. project has made a number of contributions to the field of hydropower microgeneration. To the author's knowledge, below is a brief account of the novelty of this work.

- **MHPG characteristics impedance**

  The investigations of MHPG characteristics represent the first demonstration of a constant source impedance and linear system performance. These new findings demonstrated interconnections between MHPG electrical properties and the flow dynamics in relation to the impedance. The linear relationship between the MHPG maximum voltage V_{oc} and the MPP voltage V_{mpp} describes a new understanding of MHPGs. In addition, the heuristic analysis of MHPG introduces a new model could prove valuable in simulations studies for HPCSs.

- **Feed-forward maximum power conversion optimisation**

  The concept of feed-forward for maximum power optimisation is not new, but here for the first time it is believed, a constant-voltage, load side, current-mode-controlled MPPT controller is attempted. The state-of-the-art lies in maximising the output power as a function of the output voltage only. Not only does the Seesaw promptly tracks the MPP under rapid changing operational conditions but also guarantees maximum power delivery to the load. The use I-V characteristics rather than the power, conventionally, adds to the novelty of the scheme.

- **Shunt water flow measurement**

  The novelty in the use of shunt measurement in fluid analogies is in the concept of detecting micro flow rates through a sensitive shunt flow meter. The wavelet de-noising analysis on water flow rate signals is the first application in residential water management systems. This analysis further enhanced the detection sensitivity. The automated system detected leaks on any scale, anywhere in the world. This latter feature is beyond the reach of the complex conventional detection methods.

1.5 Structure of the thesis

The thesis is organised as follows:

Chapter **2** provides the theoretical background of the work presented in later chapters. It constitutes an overview of hydropower microgeneration status. In setting the scene for hydropower microgeneration, it highlights the classification of hydropower schemes in terms of storage capacity in particular. Two major related MPPT control methods, namely direct and indirect controller, are described at length. Finally, an overview of a potential hydro-powered system in the field of water management systems is included.

Chapter **3** discusses the demonstration of MHPG characteristic impedance measurement. A brief review of the measurement principles is outlined. An overview of the system design and experimental implementation is then described highlighting the characteristics of the key components. The experimental results of three different MHPGs are presented. A comparative summary between HPCSs, WPCSs and Solar PV systems is also given. The derivation of a hydroelectric power heuristic model based on empirical findings is explained. Finally, Simulink simulation results of the heuristic model are included.

Chapter **4** presents the Seesaw feed-forward, load side MPPT controller. The operation principles of the controller are detailed including the control algorithm. It highlights principles of impedance transformation through a buck-boost power converter. The chapter also addresses the mechanism and features of output parameters control. This is followed by outlines of the experimental implementation of the controller including specifications of the main system components characteristics. The empirical results of the Seesaw controller demonstration in tracking the MPP under different operation conditions are presented and discussed. In closing, the chapter closes with highlights on the application of the Seesaw MPPT for battery charging control drawn from practical demonstrations.

Chapter **5** introduces a new shunt measurement for water leakage detection systems through MHPGs. The chapter states the principles of shunt measurement in the hydraulic analogies in the light of water-electricity analogies. The principles of wavelet de-noising in the application of flow rate signal analysis are overviewed. Outlines of the autonomous water monitoring system features and implementations are included. These include the realisation of self-powered water flow sensors and the demonstration of shunt measurement in water analogies to measure water flow rate. The practical implementation and

results of using a highly sensitive ultrasonic flow meter to measure micro flow rates that features micro leakage detection are presented.

Chapter **6** summarises the results and addresses the conclusions drawn from the conducted research. The thesis closes with suggestions for future work in the research field.

Chapter 2

Overview on Microgeneration of Hydropower

2.1 Introduction

Microgeneration is the generation of electricity or production of heat from mostly or exclusively a zero or low-carbon source at a small scale. In addition to its role in decarbonising energy generation, it adds to the diversity and security of the energy supply. Indeed, it is emerging as a promising technology with great potential towards distributed generation, whereby power is generated at the point of consumption [25]. The microgeneration capacity in the U.K. is limited to 50 kW for electricity and embraces a variety of renewable technologies [26]. This includes solar photovoltaic (PV) arrays, micro-wind and micro-hydropower generation.

In the U.K. the residential sector accounts for nearly a third of the total energy consumption [27]. A number of incentive schemes have therefore been introduced to increase the uptake of microgeneration [28], an example being, the Feed-in-Tariffs (FITs) scheme which offers a set of rates to households for every unit of energy generated by approved microgeneration installations [29]. Since the introduction of the FITs in 2010,

the total installed capacity of microgeneration has increased from 0.65GW in 2011 to 5.6GW in March 2017 [30]. As a result, greenhouse gas emission has reduced by 24% in 2015 [30] compared to 13% in 2012 [31]. However, with a modest growth of just 6% between 2016 and 2017 [30], the overall household contribution to microgeneration remains low, accounting for under 0.3% of the total energy supplied to households [32]. Evidently from Figure 2.1 hydropower, the most widely-used renewable power source, represents a small installed microgeneration capacity (0.17 GW) for the U.K. [30].

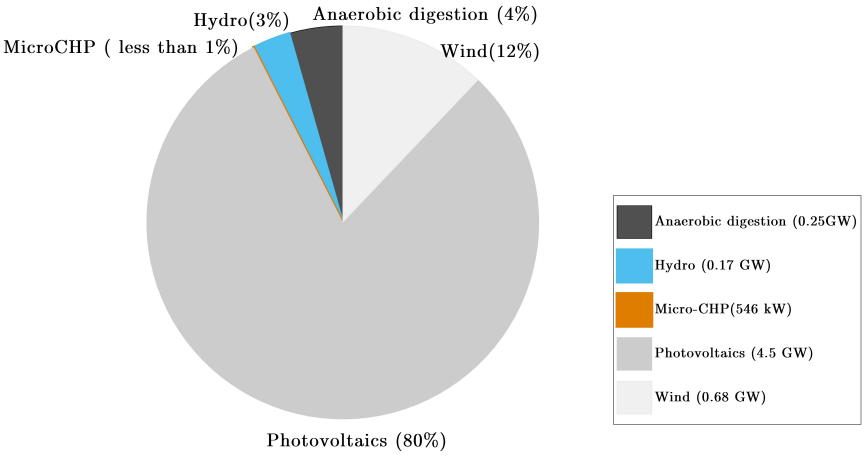

Figure 2.1: The total cumulative installed capacity for microgeneration technologies in the U.K. according to the Central Feed-in Tariff Register in 2017.

This chapter sets the scene for the research reported in this thesis. It starts with an overview of hydroelectric power generation in the U.K. and briefly discusses the classification of, HPCS schemes. It states the problem of hydropower generators HPGs characteristics analysis and MPPT optimisation control. It further surveys the background of a potential micro-hydro powered system (i.e. water monitoring system). The chapter closes with a critical review which restates the main research problems and knowledge gap in relation to micro-HPCS.

2.2 Overview on hydroelectric power generation

Harvesting energy from water has existed since the industrial revolution. However, its modest power output alongside the widespread distribution of mains electricity, made microgeneration of hydropower unprofitable. The thrust of hydroelectric generation was then shifted to large size hydro plants [33]. Hydropower remains today the leading renewable source for electricity generation, with the global hydroelectric installed capacity exceeding 1,064 GW at the end of 2015, accounting for 71% of the global power generation capacity from renewable sources and 16.4% of the world's net electricity production [34]. Hydroelectricity has advantages over conventional sources of primary generations such as:

- It is a non-carbon-dioxide power source and generates no direct greenhouse emissions, although the construction of the plants can be polluting,
- It is the only renewable source that stores energy in a clean environmentally-friendly manner (i.e. pumped storage and reservoir plants),
- The water can be stored and controlled to supply electricity on demand,
- The fuel (water) can be reused to produce additional electricity,
- Modern hydro turbines have a high energy conversion efficiency of 90% [2].

However, 10,000 TWh/year of potential worldwide hydropower remains unexploited [34]. The annual technically exploitable capability of hydropower plants in the U.K. alone is estimated to be about 14TWh [35]. Nevertheless, the overall amount of the installed hydroelectric capacity remains significantly modest contributing 1.5% of the U.K. total electricity generation. Although the U.K.'s potential for further large-scale development is limited to the availability of sites, opportunities for small-scale development exist [36]. That said, a recent review on the uptake of small-scale hydropower projects categorises the U.K. among countries with only a modest contribution in comparison to Spain and

Norway [37]. The U.K. in fact has 175.7 MW of existing small-hydro plants (>5 MW) [30], only 3% is contributed by the domestic sector [38], and at least 850 MW of unutilised potential [39]. The cumulative number of hydropower installations between 2010 and 2016 as confirmed by the U.K. Central Feed-in Tariff Register in [30] is illustrated in Figure (2.2) (*The data used to produce Figure (2.2) are available in [30]*). .

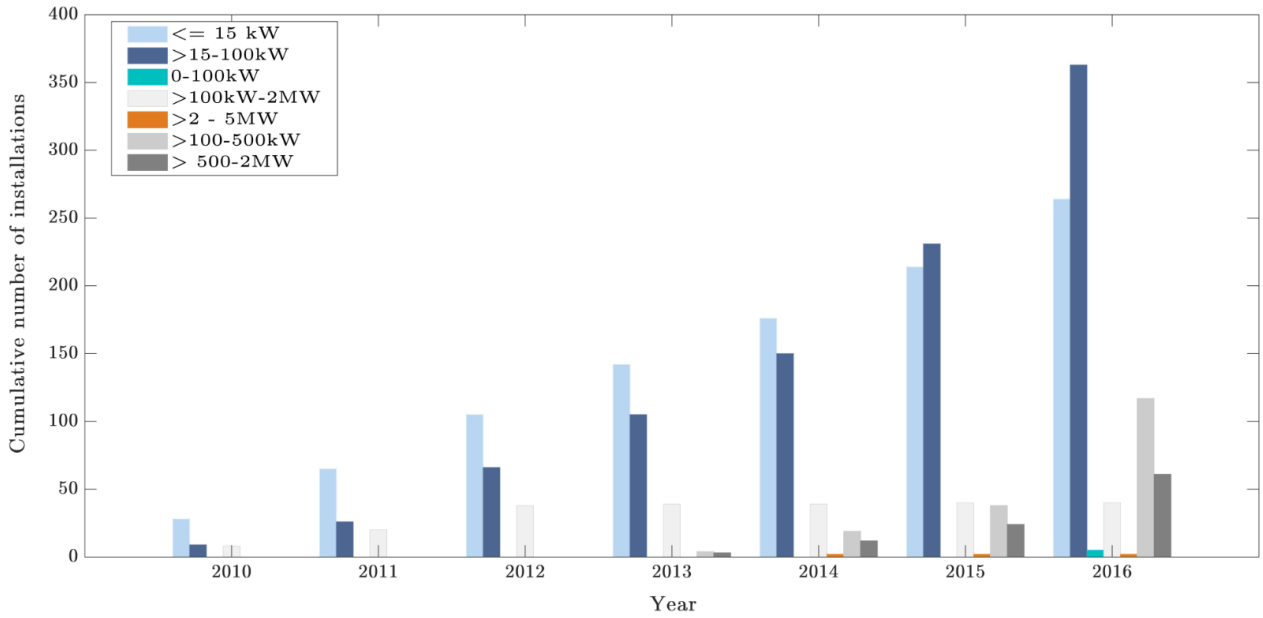

Figure 2.2: The cumulative number of hydro installations by tariff type for years from 2010 to 2016 in the U.K. according to the Central Feed-in Tariff Register.

The growing concern about developing domestic renewable energy supplies alongside the shortage for undeveloped suitable sites has renewed interest in reviewing the prospects for small-scale hydropower generation. Development of small hydro turbines towards low environmental impact has been an active area of research [1–3]. The development of hydro-electric microgeneration emerges as an alternative trade-off between no carbon emissions and a negligible local environmental footprint.

2.3 Classifications of hydropower schemes

The operation of hydropower schemes can be defined by the available input (i.e. head, and storage capacity) and the output demand. Thus, depending on the hydrological characteristics, hydropower systems can be classified into different mutually exclusive categories and offer flexibility in demand-meeting and energy supply. For example, a hydropower system can be standalone or grid connected. The operation of the latter is influenced by the consumers and the power available from all other plants connected to the grid. In this case, a peak-load plant supplies power at peak demand, and a base-load plant provides a continuous power supply regardless of the total power demand and may serve both where hydropower is abundant [40, 41]. Hydropower schemes can be further classified based on the generation capacity, storage capacity, available head and load type as shown in Figure (2.3).

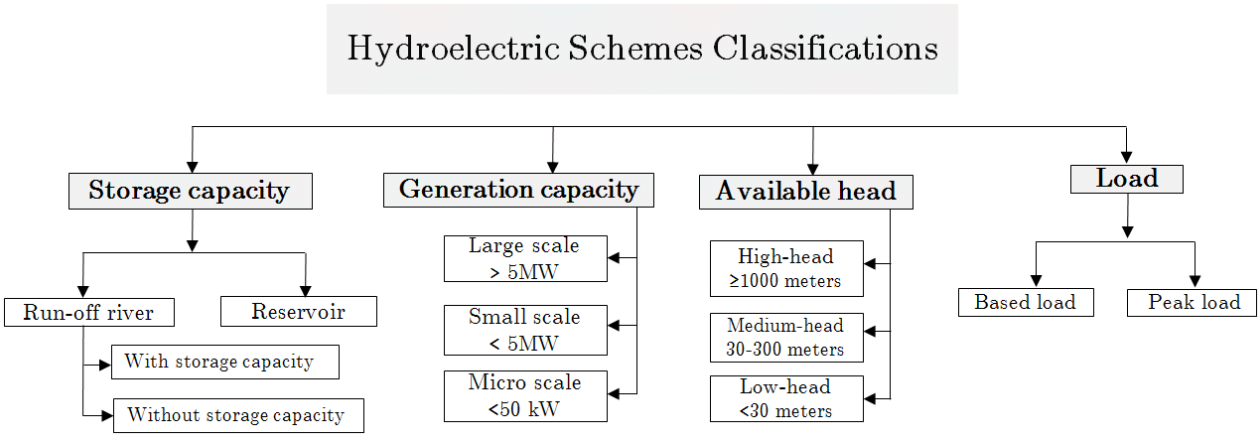

Figure 2.3: Overall classifications of hydropower schemes.

2.3.1 Hydroelectric storage capacity and head schemes

Based on the storage capacity, hydropower systems can be subdivided into run-of-river, reservoir and pumped storage plants. In contrast to the run-of-river, the significant water storage capacity of reservoir type schemes provides a means of energy storage which is a

key asset in meeting power demand fluctuations. Among these schemes, pumped storage plants are highly efficient and cost-effective energy storage schemes when incorporated with base-load power plants [41].

The available water head defines the vertical change in elevation, expressed in feet or meters, between the upstream and downstream of the water level. In this respect, a hydropower plant can be categorised as high-head (>1000 m), medium-head (30-300 m) or low-head (< 30 m). Although most hydro systems have a substantial head, it is possible to generate a modest amount of electric power with a low head [42].

2.3.2 Hydroelectric generation capacity schemes

The size of a HPCS can be defined in terms of its generation capacity. To date there is no internationally agreed definition and category size varies between countries with different environmental legislation and generation policies. In the U.K. a hydroelectric power system based on its generation capacity is defined as a large, small or micro scheme as stated in Table (2.1). The research reported in this thesis focuses on micro-hydropower generation, MPPT control optimizations and potential applications.

Table 2.1: The U.K. categories of HPCS schemes based on the generation capacity.

Hydroelectric Scheme	**Power Generation Capacity**
Large-scale capacity	> 5MW
Small-scale capacity	< 5MW
Micro-scale capacity	< 50kW

2.4 Review of MPPT techniques for HPCS

The amount of power available from a source of an intermittent nature such as hydro, wind and solar power varies with changing environmental conditions (i.e. water flow rate, wind velocity and temperature). For a particular water flow rate for instance, there is a power point at which the potential power available for harvesting is at a maximum (the power characteristics for hydro, solar and wind systems are compared in the following chapter (section 3.6)). Power system controllers are therefore used to maximise the energy yield and improve efficiency.

MPPT is a mature control issue for wind and solar systems and has been the subject of detailed research but not as widely established for HPCS [9, 43]. The research to date has tended to reference the differences and opportunities associated with the HPC control issue to that of WPCS [44]. Indeed, significant differences between the two technologies do exit [45]. These originate from: the performance characteristics of a hydro turbine in relation to its narrow tip speed ratio TSR range where a minute change in the optimum TSR can significantly affect the systems efficiency; the accuracy of water velocity measurement is inherently affected by turbulence and flow complexity; the water is 199% denser than air which means that a small change in the water velocity, hence flow rate, can substantially affect the power output [43, 44].

In contrast to the challenges it inherently imposes in terms of power control requirements, various opportunities over other technologies can be recognised. Among these is the variation in the water flow rate; unlike with wind and solar, where the speed of the wind or the moving clouds varies dramatically over a time scale of seconds, the dominant water speed and level variations may occur within minutes to hours. This imposes fewer constraints on the tracking rate of the power controller, and hence relaxes the bandwidth requirements [44].

From a fluid-dynamics perspective, hydropower systems have a rich knowledge base. This is in sharp contrast, to the electrical performance and control aspects for such renewable systems as mentioned above. It appears that there is a lack of understanding of electrical performance and key aspects, such as the characteristic impedance have been overlooked [4–6]. In consequence, the adoption of advanced power control mechanisms, which rely on the system's electrical properties, is concerned mostly with WPCSs and solar PV technology.

Prior to the experimental development of MPPT optimisation control for HPCSs, existing methods adopted from wind and solar systems are reviewed. A brief survey of the potential MPPT control for HPCSs yields two generic categories namely, indirect and direct MPPT control. Unlike direct controllers, which directly maximise the output electrical power P_{out}, indirect controllers rely on the turbine characteristics to maximise the captured mechanical hydro power P_{hydro} not the actual electrical power P_{out}. The relationship between the electrical output power P_{out} and mechanical hydro power P_{hydro} is given in Equation (2.1), where the hydraulic turbine efficiency $\eta_h (0 \leq \eta_h \leq 1)$ depends upon the turbine design and operational conditions. The hydro mechanical power can be expressed by Equation (2.2), where P_{hydro} is the power in watts available from fluid (density ρ kg/m^3) flow Q (m^3/sec) with head h (meters) and gravitation acceleration g (m/sec^2) [9].

$$P_{out} = \eta_h P_{hydro} \tag{2.1}$$

$$P_{hydro} = Q\rho hg \tag{2.2}$$

2.4.1 Indirect MPPT control

In the indirect MPPT optimisation, prior knowledge of the turbine characteristics is required. This information is usually obtained from off-line tests or simulations. That is then stored into look-up tables and used by the controller as a reference to MPP. Examples of such optimisation methods are the Tip Speed Ratio and Power Signal feedback.

2.4.1.1 Tip speed ratio (TSR)

In its basic form, TSR control regulates the turbine rotor speed around an optimum point at which maximum power can be extracted, as identified from the characteristics of the turbine (i.e. power-rotor speed). The TSR is determined dynamically, relative to the measurements of the rotor speed and water velocity, and mapped onto the turbine's optimum TSR as shown in Figure (2.4) taken from [9]. Prior knowledge of the model-dependent optimum TSR point is a precondition. The optimum tip speed ratio λ_{opt} is defined in Equation (2.3) as an index of the optimum rotor rotational speed ω^*_{rot} in rad/s or radius R in meters against the fluid velocity V_{fluid} in m/s .

$$\lambda_{opt} = \frac{\omega^*_{rot} R}{V_{fluid}} \tag{2.3}$$

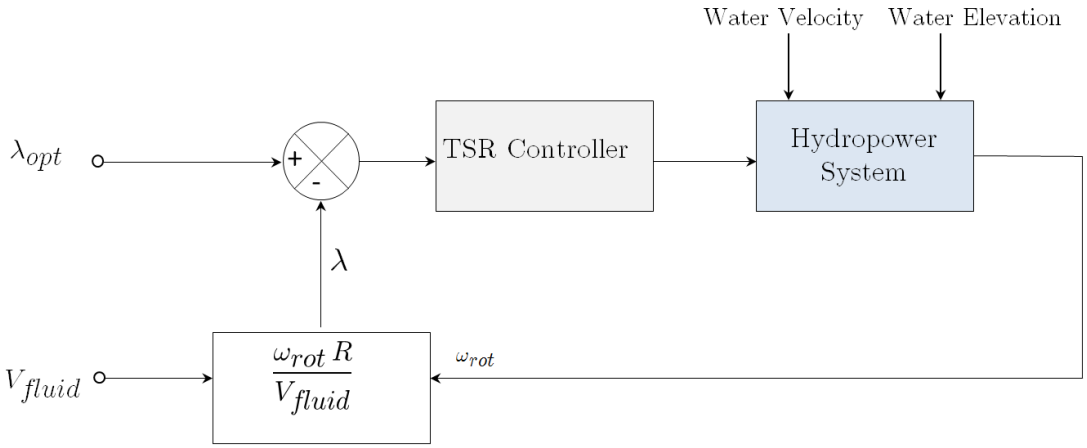

Figure 2.4: Outlines of a TSR MPPT control mechanism.

The development of TSR power controllers is widely reviewed in the literature [46–49]. Although, superior steady-state characteristics can be achieved through the conceptually simple technique, its dependency on the turbine's specifications limits its application. Further, the requirement for additional velocity measurement sensors reduces its cost effectiveness.

2.4.1.2 Power signal feedback (PSF)

The PSF method relies on the prior knowledge of the unitised maximum power performance curves (i.e. power-speed characteristics as in [50, 51] or torque-speed characteristics in [52, 53]). A power signal feedback is obtained based on the difference error and is non-linearly adjusted to the optimum rotor tracking speed. The tracking reference is determined dynamically relative to the output power as shown in Figure (2.5), which is adopted from [9]. Unlike TSR, the water velocity measurement is irrelevant; rather it is mapped onto the turbine power-speed characteristics. Different topologies of power signal feedback MPP have been developed in the literature [47, 54]. The example in [55] proposed a control scheme based on the pre-acquired optimum power characteristics from pilot testing. Further, the use of the lookup table approach, although offering fast tracking control, is specific to the turbine model.

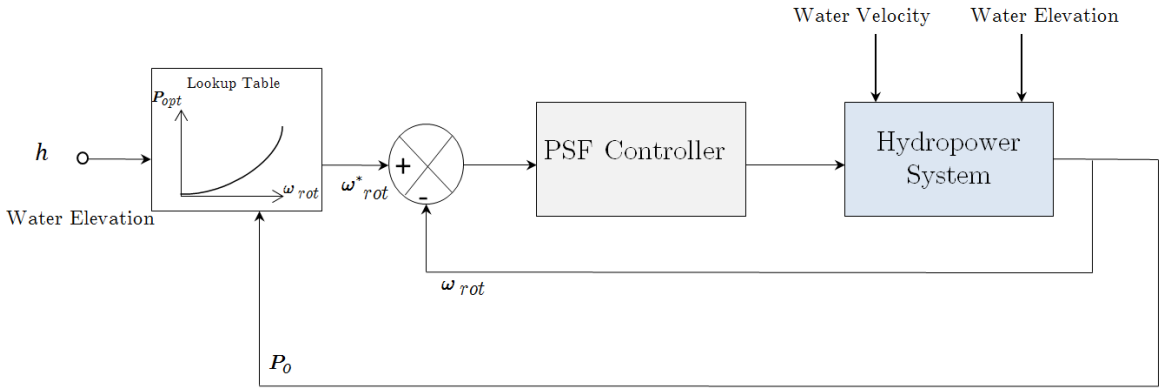

Figure 2.5: Outlines of a PSF MPPT control mechanism.

In addition, the localisation of the MPP for PSF is determined on a trial and error basis, which increases the likelihood of sub-optimal operation [9]. Although methods to enhance power capture have been proposed, the overall power tracking efficiency remains questionable [56]. This, along with the pre-required simulation and pilot testing of individual turbines to acquire the power characteristics, increases the associated cost and complexity.

2.4.2 Direct MPPT control

In principle, direct control optimisation is independent of the turbine characteristics. It utilises algorithms that use system parameters such as voltage, current, output power and rotational speed. Among these methods, three that have a potential in hydro power application are reviewed here.

2.4.2.1 Hill climb searching (HCS)

In theory, HCS does not rely on any system information and continuously adjusts the operating point to the MPP (as in Figure 2.6, which is adopted from [9]). The principle lies in disturbing the control variable by step-size and observing its effect on the resulting power. The variation of power and/or speed is then monitored periodically at specific time intervals. The power of the previous step is compared with that for the next step. If an incremental change in the output power is observed for an increase in the reference speed, the direction of the search-point remains unchanged and vice versa [16]. The operation can be interpreted by a discrete-time expression such as in Equation (2.4) [9].

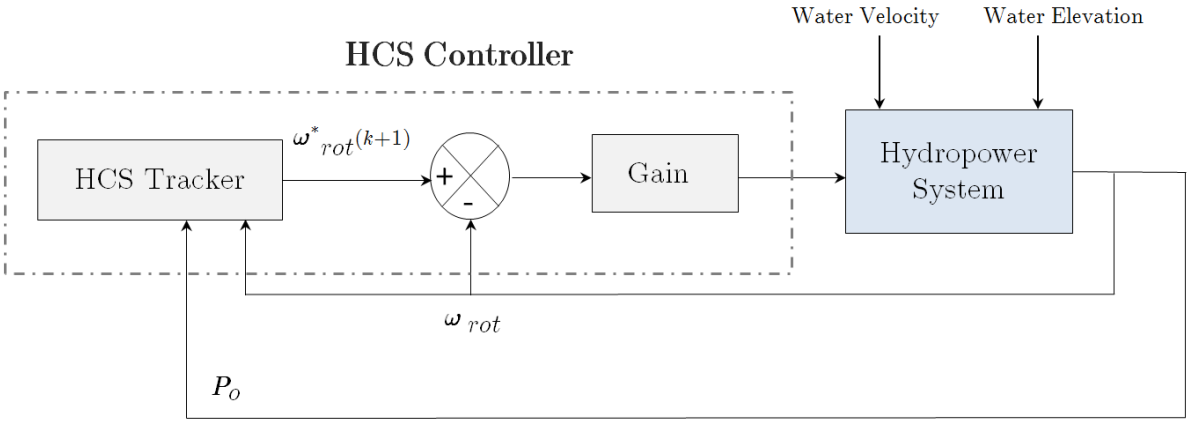

Figure 2.6: Outlines of a HCS MPPT control mechanism.

$$\omega^*_{rot}(k+1) = \omega^*_{rot}(k) + \Delta\omega^*_{rot} \tag{2.4}$$

Here $\omega^*_{rot}(k)$, $\omega^*_{rot}(k+1)$ and $\Delta\omega^*_{rot}$ correspond to the previous reference speed, new reference speed and the perturbation step respectively. The direction and size of the step are conventionally defined by Equations (2.5) and (2.6) respectively [57], where $\Delta\omega_{rot}$ is the change in rotor speed, ΔP_o is the relative change in output power and k_t is the HCS optimiser gain. If an increase in the rotor speed results in increased power, this direction is retained. However, if a change in the rotor speed resulted in reducing output power, the reference speed is decreased in the next perturbation as shown in Figure (2.7). Table (2.2) summarises the operating principles (adopted from [57]). This process continuous until the MPP is found.

$$sign(\Delta\omega_{rot}, \Delta P_o) = sign(\Delta\omega_{rot}) \times sign(\Delta P_o) \tag{2.5}$$

$$|\Delta\omega^*_{rot}| = k_t|\Delta P_o| \tag{2.6}$$

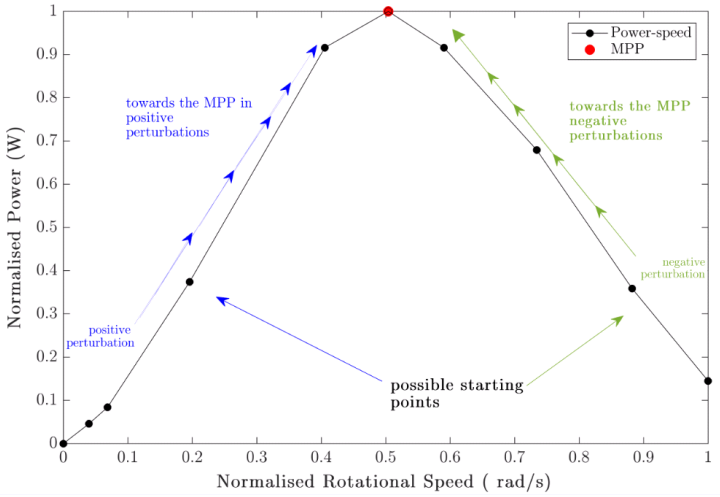

Figure 2.7: Principles of HCS MPPT control operation.

Table 2.2: The operating principles of HCS MPPT.

Previous perturbation	Change in output power	Next perturbation
Positive	Positive	Positive
Positive	Negative	Negative
Negative	Negative	Positive
Negative	Positive	Negative

2.4.2.2 Incremental conductance (IC)

Incremental conductance is another type of direct control MPPT that has been developed to overcome the limitations of HCS. This method depends primarily on the derivative of the power-voltage characteristic curve (Figure 2.8). It is based on the fact that the derivative of power as a function of the voltage (incremental conductance) ($\frac{dP}{dV}$) is null at the MPP, positive on the left of MPP and negative on the right of MPP (i.e. Figure 2.9). The slope, defined by the direct relation between the output generated power P_o, voltage V and current I, is given by Equation (2.7) [58].

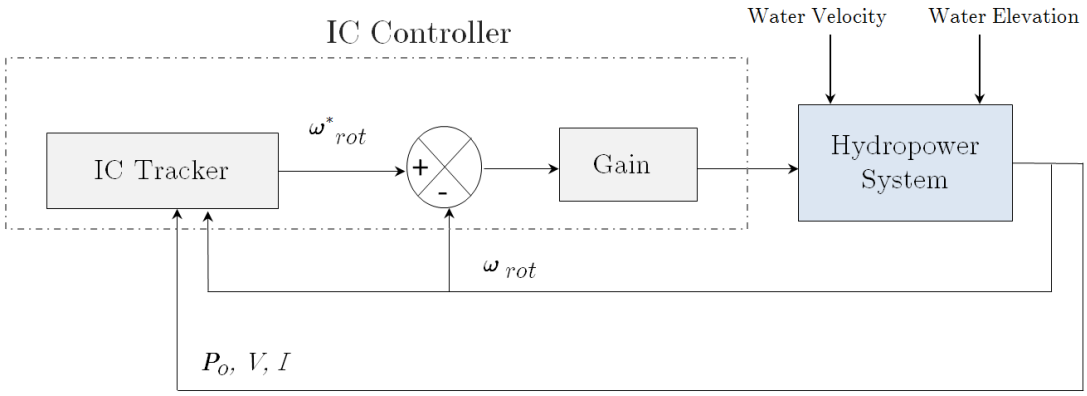

Figure 2.8: Outlines of an IC MPPT control mechanism.

$$\frac{dP_o}{dV} = \frac{d}{dV}.(V \times I) = I.\frac{dV}{dV} + V.\frac{dI}{dV} = I + V.\frac{dI}{dV} \tag{2.7}$$

$$\begin{aligned} \frac{\Delta I}{\Delta V} &= -\frac{I}{V} \quad when \quad \frac{dP_o}{dV} = 0 \quad \omega_{rot} = \omega^*_{rot} \\ \frac{\Delta I}{\Delta V} &> -\frac{I}{V} \quad when \quad \frac{dP_o}{dV} > 0 \quad \omega_{rot} < \omega^*_{rot} \\ \frac{\Delta I}{\Delta V} &< -\frac{I}{V} \quad when \quad \frac{dP_o}{dV} < 0 \quad \omega_{rot} > \omega^*_{rot} \end{aligned} \tag{2.8}$$

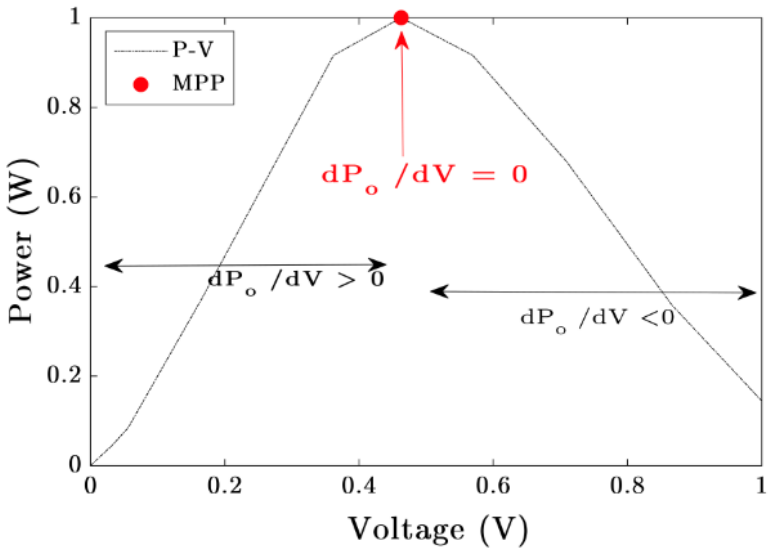

Figure 2.9: Principles of IC MPPT control operation.

The IC controller determines the perturbation direction by comparing the instantaneous conductance $\frac{I}{V}$ to the incremental conductance $\frac{\Delta I}{\Delta V}$ as defined in Equation (2.8). The iteration then continues until the MPP is reached.

2.4.2.3 Extremum seeking control (ESC)

Extremum seeking is a non-linear adaptive control that is model-free and offers real-time optimisation for dynamic systems where limited knowledge of the system characteristics is available. In principle this method establishes a feedback system which produces an oscillatory behaviour around the extremum (i.e. maximum or minimum). Conventional ESC applies the principles of perturbation and establishes the control action with respect to the output power system response. Fundamentally, a perturbation signal (i.e. sinusoidal with amplitude a_x and angular frequency ω_x) is superimposed onto the power system input. The gradient estimated from the rate of change in the output P_o with respect to the input control signal u (i.e. $k_x = \frac{\Delta P_o}{\Delta u}$) is then forced to zero. The operating point is therefore converged to a neighbourhood to the MPP, relative to the amplitude of the probing signal, and performs a limit cycle [59]. Figure 2.10 (adopted from [9]) outlines the control mechanism.

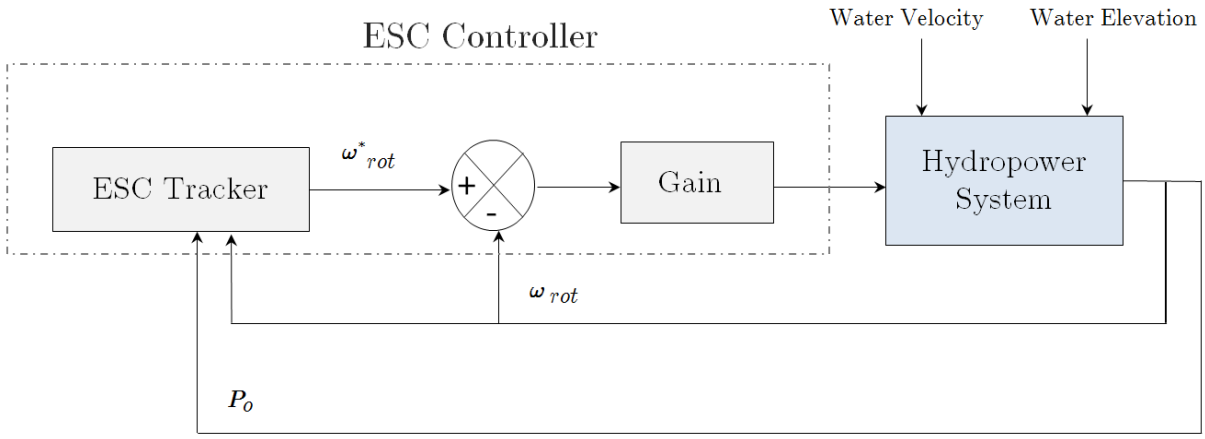

Figure 2.10: Outlines of a ESC MPPT control mechanism .

In summary, the reliability of enhanced indirect MPPT (i.e. lookup-table based MPPT) decreases with ageing factors and varying generator-converter subsystems efficiencies [60]. While adoptive TSR and PSF MPPTs, such as those reported in [61, 62], aimed at improving optimisation efficiency, the reliance on turbine characteristic remains a major drawback. Arguably, satisfactory application of such MPPTs methods is challenged by the fact that the MPP of HPCS coincided with a higher rotational speed than that resulting at the MPP of the actual generator [63].

Furthermore, direct maximum power point tracking controllers such as the Hill Climb Searching (HCS) has have been the current trend for most PCSs [64]. Although, favoured for its simplicity as a model-independent optimisation approach, the dynamics of the turbine are to be taken into consideration when determining the step size [9]. However, the fact that it requires the system to settle down before a decision on the next perturbation is made, slows the controller response. Unlike HCS, which oscillates around the MPP, an Incremental Conductance MPPT controller determines when the MPP is reached. This is achieved however at the cost of increased complexity and additional sensors to measure the voltage and the current [58].

In contrast to other direct based methods which requires the power system dynamics to settle before optimisation, ESC allows fast convergence to the extremum point. Examples of using the ESC MPPT optimisation method for micro-HPCSs have reported an improved tracking capability [9, 59, 64]. This direct control does not require measurement of the water elevation or velocity. However, the requirement to adjust a large number of control parameters associated with the stability of the feedback, adds to the controller complexity, and hence reduces its efficiency.

2.5 Water leakage detection technologies overview

Microgeneration of hydropower has great potential in supplying low power applications (e.g. smart meters). The advancement of sustainable digital devices has given rise to potential hydro-powered water leakage management systems. Water leakage management includes: methods of leakage assessment focusing on the amount of water lost; methods of leakage detection for leakage allocation; and methods of leakage control which effectively controls current and future leakage levels. This section briefly reviews methods of water leakage detection in water network systems. It concludes with highlights of the research gap in water leakage detection methods pertinent to residential applications.

2.5.1 Visual detection methods

This is the classic technique that uses image and video sensors inside or outside the pipe to detect water leaks. Among these are the closed-circuit television (CCTV) [65] and optical sensors [66]. Thermography IR cameras are also employed to detect the thermal contrasts caused by water leakage [67,68], whereby the infrared thermal cameras visualises the leakage point based on temperature variation on the surface above the pipeline. Although such a non-destructive detector provides real-time detection over large areas, its detection efficiency is greatly affected by the camera's limited sensitivity (i.e. within $\pm$ 0.2 °C [69]). This diminishes its capability of detecting unapparent leaks found at residential environments.

2.5.2 Acoustic detection methods

This is a non-destructive leak detection method which utilises acoustic sensors such as a piezoelectric sensor, hydrophones, vibration sensor and laser interferometers incorporated inside or outside the pipeline. It is formed on inspecting the vibration and noise generated by a fluid turbulently escaping a pipeline [70]. In the early 1900s, wooden listening sticks

were used to detect leaks; this was then enhanced by the emergence of microphones and the electronic age by the 1960s [71]. Further advancement continued with the advent of correlators which gave rise to the currently used methods ranging from electro-acoustic methods [72] to the advanced correlators with computerised analysis [73]. These methods however are labour intensive; sensors are required to be placed inside the pipe fittings [73, 74].

2.5.3 Transient analysis detection methods

This is an alternative to the previously described approaches and is based on the leak hydraulic phenomenon. Ideally any change in the propagation of the water imposes a wave reflection to an incoming transient signal and hence affects the water's flow and pressure response. The identification of these modifications can reveal useful information about the nature of the originating event. If an event has a unique signature then comparing the pressure signal recorded by monitoring devices with the signal observed when the system is leak-free can help locate the leak. Alternatively the leak's effect in pressure relief can be used to identify the leak. Transient-based leakage detection methods are categorised into time and frequency domain techniques [75, 76].

2.5.3.1 Time domain techniques

Time domain based analysis helps to pinpoint leakages in pipeline networks. Examples of these are:

- **Impulse response analysis** This is based on the reflection of the energy in the transient wave due to the leakage. Information on the arrival time of the reflected signal and the flow rate is used to locate the leak. A point of reference is generated on the leak-free system and compared with the transient response of the system. The leak reflection creates inconsistencies between the two responses. This technique is

feasible only when a point of reference can be easily determined [75].

- **Inverse transient analysis** Usually network analysis works with the forward problem in which the system's characteristics are defined and the resulting pressure and flow are to be determined. In the inverse problem, the system state is defined (i.e. pressure, flow) and some parameters are undefined (i.e. pipe roughness, leaks). The system's state variables are measured during a transient event and compared to the measurements when the system is leak-free. Irregularities are tested until both system states are matched [76–78]. The leakage magnitude is determined by minimizing the deviation between the actual measured data and simulated data by the transient model. The objective function for optimisation OF is given in Equation (2.9) [79],

$$min : OF = \sum_{i=1}^{N} |H_i^m| - |H_i^p| \tag{2.9}$$

where, i is the time interval point for number of data points N, $|H_i^m|$ is the measured head, $|H_i^p|$ is the predicted head. The accuracy of the transient model is the key challenge for the inverse transient analysis.

2.5.3.2 Frequency domain techniques

Real time noise handling and data gathering poses a challenge for real time transient analysis. The fact that frequency domain analysis is less computational in nature makes the investigation of irregularity detection and behavioural changes comparatively easy. Examples of frequency domain analysis based methods are:

- **Pressure-peak method** This suggests that the frequency response diagram of a pressure signal can reveal irregularity whereby the leak is represented by the peaks with lower amplitude than the leak-free signals [76].

- **Peak-sequencing method** This is based on the fact that leaks introduce a sinusoidal pattern on the peaks frequency response diagram. As a result the frequency response domain shows attenuation due to the presence of leaks. The distinguishable pattern of the leak-induced signal is then analysed to further locate the leak [80].

- **Wavelet transform (WT)** WT decomposes the signal into frequency components but provides a global presentation of the signal. It is a very useful tool to analyse non-stationary signals with time-varying frequency content. It divides the signal into an approximation and details and the approximation is also broken down into a second level of approximation and details and the process is continual (Figure 2.11 (adopted from [75])). Whereas approximations are the high-scale low-frequency component, the details are the low-scale high-frequency component [75]. The noise removal properties of WT makes it possible to detect leaks of small flows.

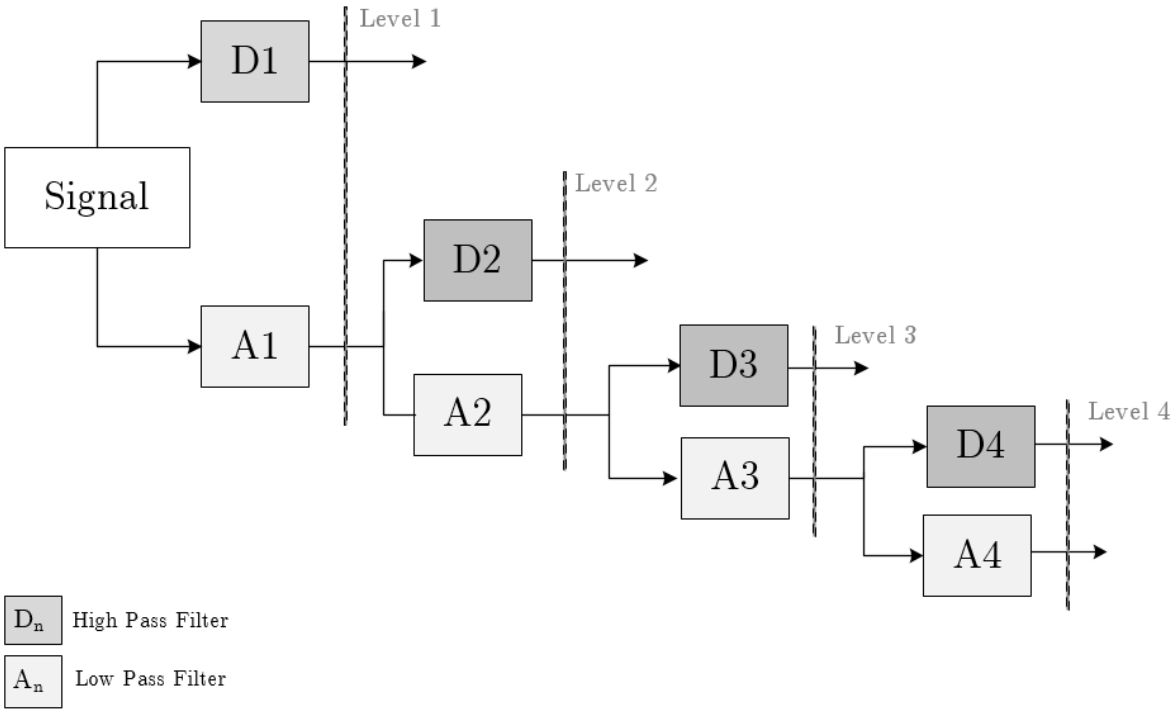

Figure 2.11: An outline of wavelet levels decomposition.

The analysis of transient water leakage events involves detailed fluid flow hydraulic and significant computer processing capabilities. Pattern recognition technologies have been introduced for water leakage detection to overcome that, to a limited extent. The example in [81] introduced artificial neural networks (ANN) to monitor water-pipe networks. The ANN is trained on various sets of input data that describes the water-pipe network under leakage and leakage-free operating conditions. These are then classified to identify any abnormality in the network. As well as neural networks, the application of pattern recognition includes fuzzy logic [82, 83]. However, among the state-of-the-art approaches, many are based on measurements of either flow, pressure or both gathered from multiple monitoring points [84, 85]. These are inappropriate for household scenarios with a single flow measurement point.A breaif comaritive summary of the main leakage detection features and limitaions is tabulated in Table 2.3.

Table 2.3: Comparative summary of the research on water leakage detection technologies.

Detection Method	Features	Limitations
Visual detection	Leakage allocation	Accuracy dependant on sensor's sensitivity
Acoustic detection	Non-destructive	Labour intensive and subject to noise interference
Transient detection	Leakage allocation	Computational and requires system modelling

2.6 Residential water leakage detection background

The previous section broadly reviewed leakage detection methods used in water networks. It is summarised that such approaches require multiple monitoring points which could be inappropriate for household applications. This section however reviews water leakage detection methods suitable for residential applications.

That is because it is estimated that more than 45 million m^3 of water are lost globally through water leakage in the distribution network [86]. Whereas in the United Kingdom and the United States leakage ranges from 10 to 30% of the water supply, in developing countries leakage accounts for up to 70% of the supply [87]. In the case of the Middle East and North Africa region, water leakage is more than 30% [88]. Thus, in the process of bridging the gap between the water supply threatened by scarcity and the high demand, improving water management technologies has become an urgent matter. Evidently, much research effort has been devoted to improving water leakage detection methods for water distribution networks, however, studies on water leakage at the domestic level have been limited.

It is evident from the reported literature, that water losses in residences could account for a significant portion of the water supply [89]. This is exemplified by the investigation of residential end-use of water which reported that nearly two-thirds of the investigated households leaked on average 45 liters per day [90]. The extent of this is signified by findings of the study in [91] which concluded that around 38% of the studied leaking households were responsible for 90% of the total leakage per capita.

Indeed, identification of large flow rates in residences (i.e. liters per minute (L/ min.) with floods or bursts through the analysis of household water consumption is highly fea-

sible. Unlike micro leaks, large leaks do not inevitably initiate the greatest volume of water loss, particularly if the water leak is apparent. In contrast, micro leak losses (i.e. milliliters per minute) might seem insignificant but temporal and geographical aggregation of leakage water ultimately leads to major water loss. A study in [92] suggested that three-quarters of the surveyed households were not aware of the existence of water leakage in their households. By inference, the inability to detect such unobtrusive leaks reduces detection likelihood pending evidence of its detrimental effects.

Most studies on the analysis of household water consumption are centralised at end-use water events classifications and water monitoring control as opposed to residential water leakage detection. In the study of categorising residential water end-use events, the effects of low flow rates were discarded [93]. Similarly, an internet based application in [94] to educate residents about efficient water usage features a means of automatic leakage detections. The web interface offers real time water flow monitoring and infers possible leakage is causing excessive water usage. Short message service (SMS) technology has also been incorporated into residential water leakage detectors [95, 96]. The system reported in [95] learns about the household water consumption patterns and interprets any unusual water flow pattern as a leakage. However, the reliability of such detectors is challenged by the erratic nature of household water consumption (i.e. having guests, absence from work, using water late at night). A review on features and limitations of studies that facilitated domestic water leakage is tabulated in Table (2.4).

Table 2.4: Comparative summary of the research on residential water leakage detection technologies.

Technology	Reference	Application	Parameters	Limitations
SMS & GSM*	[95]	Water leak detection	Pressure	Specific to consumption pattern
	[96]	Home automation system	Flow rate	Undefined detection range
	[97]	Remote monitoring	Flow rate	Undefined detection range
Pattern recognition	[93, 98]	Residential end-use classification	Flow rate	Undefined detection range
Statistical models	[99]	Domestic water leakage detection	Flow rate	Estimated detection threshold
	[100]	Irregularity detection	Flow rate	DMA measurements**
ANN	[101]	Pipeline leakage detection	Pressure & flow rate	Simulated domestic network
Internet of things	[94]	Water management	pH, flow rate & temperature	Specific to consumption pattern

* Global System for Mobile Communications
** Normalised pattern consumption

2.7 Conclusion

This chapter motivated the research presented in this thesis in terms of hydropower microgeneration and MPPT optimisation control. The literature reviewed in this chapter identified the lack of in-depth research on MPPT control issues appropriate for HPCSs. The limitations of existing methods were reported. The model dependency of the direct optimisation was the main drawback. The fact that the rotational speed at MPP of the whole hydropower system varies from that at maximum turbine power challenged its application. Indirect optimisation could be promising for simple control requirements. Considering the identified knowledge-gap influenced by the technological barriers of such systems, the emphasis of this thesis is towards investigating the electrical characteristics of such technology. Acquiring such knowledge could assist in realising an electrically based control scheme for MPPT hence allowing significant simplification in system design. The literature reviewed on water leakage detection, albeit non-exhaustive, identified an urgency for the means to enhance water micro-leakage detection.

The next chapters will report on an empirical investigation on the electrical characteristics impedance of hydro power generators. A model-independent MPPT for hydropower systems is presented which tracks the MPP regardless of the turbine model. An innovative micro-leakage detection system based on wavelet analysis is presented.

Chapter 3

Empirical Investigation and Modelling of Hydroelectric Power Generators Characteristics Impedance

3.1 Introduction

The previous chapter has identified the knowledge-gap in investigating hydropower generators electrical properties. Initial research efforts reviewed in the literature fall short of identifying key features, such as the characteristic impedance [4–6]. The lack of understanding of its electrical characteristics has limited its power control opportunities. As a result, the adoption of advanced power control mechanisms which rely on the system's electrical properties lags behind that of wind and solar systems.

Moreover, the variable and intermittent nature of hydropower alongside the associated difficulties in acquiring results from an integrated hydropower plant has challenged investigation of its operation. Early attempts on the concept of electronic simulation of hy-

dropower turbine envisioned its paramount role in facilitating the research of hydropower technology [102]. The renewed interest has necessitated the need for experimental evaluation, which utilises low-cost equipment within a controlled environment, for research. This has been made possible by the development of small hydropower generators. A number of hydropower emulators are reported in the literature [103–105]. The example in [103] uses pre-programmed characteristics curves to emulate the turbine behaviour. The use of manufacturer specification-based models as a substitute for the turbine optimises the operation. Similarly, the case with the software simulation based emulators is reported in [104, 105].

This chapter begins by detailing the construction of an intelligent low-cost hardware-oriented micro-hydropower emulator which facilitated the laboratory investigation. It then proceeds to briefly describe the principles of current-voltage I-V characteristics measurements. It reports on experimental investigations of the electrical characteristics of three different models of micro-hydroelectric power generators (MHPGs). Following the empirical validations, the characteristics of MHPGs are compared to the well-known solar and wind characteristics. In the light of the experimental results, an analysis is conducted to model the characteristics of a MHPG. This begins by introducing a new heuristic analysis on the modelling of a hydroelectric power generator. It further proposes a Simulink-Simulation model developed from the heuristic analysis. Finally, the chapter concludes with an outline and discussion of the main findings.

3.2 DC characteristic analysis of MHPGs

As shown in Figure(3.1), the DC equivalent circuit for a MHPG is represented here by a current source and a parallel resistor R_s. The current source models electron injection from a water flow. The source resistance R_s, also known as characteristic impedance, represents the internal impedance of the MHPG. The I-V characterisation provides a

means to evaluate the power system efficiency. The parameters used to characterize the performance of the power system are listed in Table (3.1).

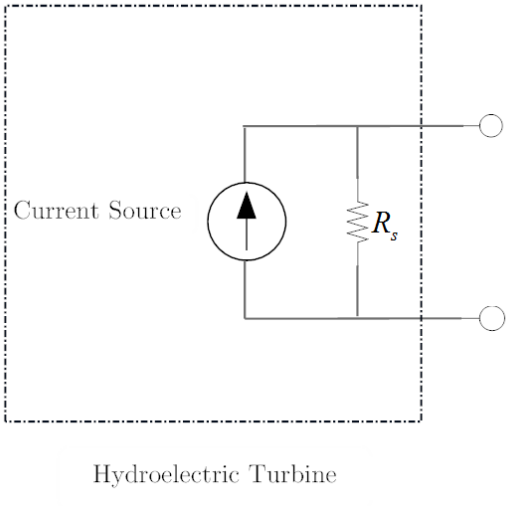

Figure 3.1: The DC equivalent electrical circuit of a MHPG.

Table 3.1: I-V characteristic measurement parameters.

Parameter	**Symbol**	**Unit**
Short Circuit Current	I_{sc}	A
Open Circuit Voltage	V_{oc}	V
Maximum Power Point	P_{max}	W
Current at Maximum Power Point	I_{mpp}	A
Voltage at Maximum Power Point	V_{mpp}	V
Characteristic Impedance	R_s	Ω

The term short circuit current I_{sc} specifies the highest electrical current that can pass through the generator under short-circuit conditions (i.e. zero load impedance and zero voltage drop, ideally), the open circuit voltage V_{oc} defines the maximum available voltage from the generator (infinite load impedance). The maximum power P_{max} describes the maximum electrical output power available from the generator at current and voltage I_{mpp} and V_{mpp} respectively.

3.2.1 Characteristic impedance matching

The characteristic impedance R_s represents the internal power losses of the generator. Ideally, the system should have no such losses. However, depending on the dynamics of the system, R_s can be determined with reference to the open circuit voltage V_{oc} and short circuit current I_{sc} as in Equation (3.1), where the terms k_V and k_I are the constants of proportionality.

$$R_s = \frac{k_V V_{oc}}{k_I I_{sc}} \tag{3.1}$$

The characteristic impedance has a significant role in maximising the harvested output power. This is because maximum power is transferred to the load when its impedance matches that of the source, a well-known result from the Maximum Power Transfer Theorem. This theorem is the core of today's advanced power conversion controllers. The voltage V_{mpp} and current I_{mpp} at the MPP are therefore proportional to V_{oc} and I_{sc} respectively. Under such conditions the characteristic impedance can be generally expressed as in Equation (3.2).

$$R_s = \frac{k_V V_{oc}}{k_I I_{sc}} = \frac{V_{mpp}}{I_{mpp}} \tag{3.2}$$

3.2.2 Characteristic impedance measurement

The fundamental principle in measuring the characteristic impedance is based on the control of the current supplied by the turbine module between the zero current point (at V_{oc}) and the maximum supplied current point (I_{sc}). Ohmic measurements were carried out using a variable resistive load, which was controlled to capture the system response between I_{sc} and V_{oc}. The change of the voltage with respect to the current represents the I-V characteristics of the generator module as given in Equation(3.3).

$$V(I)|_{I=I_{sc}\to 0} = [0,\ V_n(I_n),\ V_{n+1}(I_{n+1})\ .....,V_{oc}] \tag{3.3}$$

$$(I_x(\mathrm{R}), V_y(\mathrm{R}))|_{R=0\to\infty} = \begin{pmatrix} (I_{x1}(\mathrm{R})\,, V_{y1}(\mathrm{R})) \\ (I_{x2}(\mathrm{R})\,, V_{y2}(\mathrm{R})) \\ \vdots \\ (I_{xn}(\mathrm{R})\,, V_{yn}(\mathrm{R})) \end{pmatrix} = \begin{pmatrix} (I_{sc}\,, 0) \\ (k_{x1}I_{sc}\,, k_{y1}V_{oc}) \\ \vdots \\ (0\,, V_{oc}) \end{pmatrix} \tag{3.4}$$

The pros and cons of various I-V characteristic measurement methods are reviewed in the literature [106]. The ohmic measurements are an inexpensive means of approximating a system performance. The advance in intelligent automated digital multimeters has made such a method highly reliable and flexible.

3.3 The overall design and implementation of the characteristic impedance investigation

The intelligent, indoor, built-in-house, hydroelectric power emulator was the core of the test-rig. The hydroelectric power emulator incorporated three different configurations of MHPGs. As a load impedance, a high power rating variable resistance box was used to investigate the characteristic impedance of the MHPG. A USB digital current meter was used to capture the current through the resistive load. Similarly, a USB voltmeter was used to monitor the voltage drop across the resistive load. The use of a USB digital multimeter offers fast and accurate measurements and allows the data to be further processed in MATLAB. This section details the design of the hydropower emulator published in [23] and reports on the empirical investigations of the electrical characteristics of a range MHPGs.

3.3.1 Hydropower emulator design and construction

Mechanically, the complete system of the hydropower emulator consists of two lightweight wooden frames and a plastic water tank. The 20 litre plastic water tank is placed on a wooden frame base with four castors making it easy to move the emulator. A square wooden frame is placed on the mobile wooden base and surrounds the base of the water tank, to secure the water tank to the wooden base. A Gardena high power speed-controlled submersible pressure pump is placed inside the water tank (up to 5 bar pressure at 2000L/Hour). The pressure pump emulates domestic water flow and drives the water flow to and from the water tank. A light weight wooden frame which has a truncated pyramid shape is mounted on top of the water tank. The truncated body is secured to the tank using a wooden strip on both sides of the frame. Two opposite sides of the truncated body are left open, for ventilation and allowing space for a measurement desk. A cross section diagram of the emulator is shown in Figure (3.2).

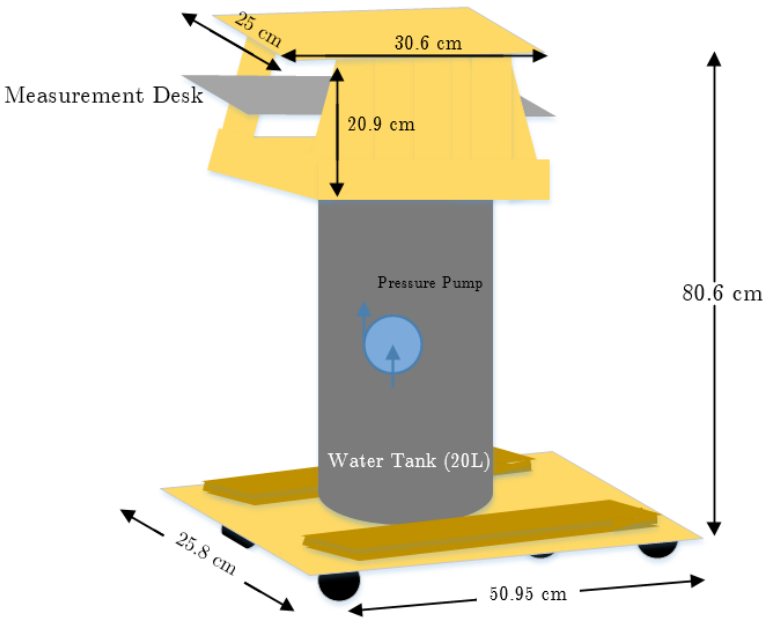

Figure 3.2: A schematic of the hydropower emulator mechanical construction.

The control circuit is placed on the top of the truncated pyramid body. It includes a power speed controller and electronic switch. A power speed controller provides control of the water flow by adjusting the speed of the pressure pump. The high power speed controller is made up of a 1500 W sliding dimmer connected to the pressure pump placed inside the tank. This allows the study of the characteristics of the turbines at various flow rates. The electronic switch acts as a phase shifter and is digitally controlled to emulate different loads (i.e. household, hotel or university residence). The hydraulic emulator is completely automated as it employs USB-powered voltmeters and USB-powered switches. An elegant feature is that the system can be remotely controlled, through OpenVPN software, across the globe allowing large data-collection and system control.

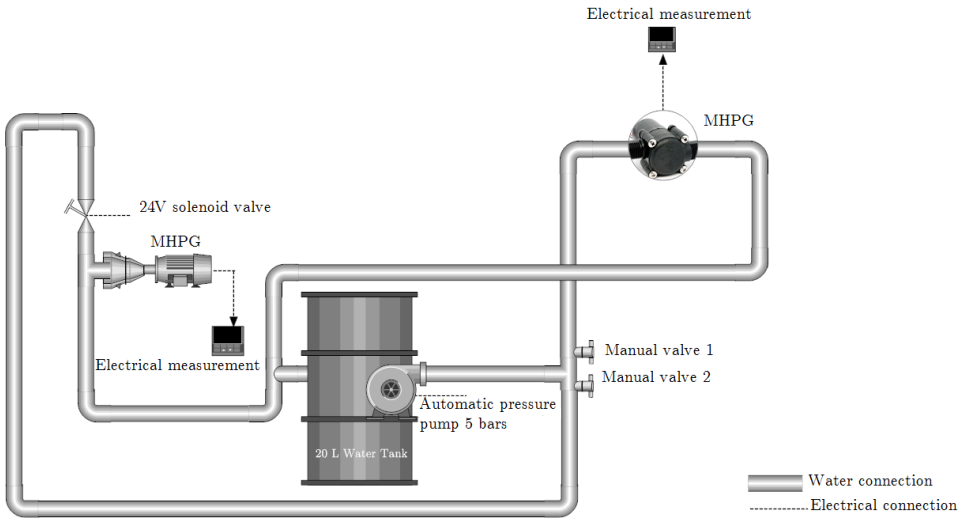

Figure 3.3: A schematic of the hydraulic construction of the hydropower emulator.

The hydraulic construction of the intelligent hydropower emulator is shown in Figure (3.3). Manual valves are used to control the water flow through the two water flow circuits as shown in Figures (3.4) and (3.6). The emulator is fitted with U.K. certified 15 mm water pipes. A turbine circuit is connected to each side of the truncated shape frame of the emulator. When valve 1 is switched ON, the water is pumped from the closed tank through the pipes to the MHPG. As the water flows through MHPGs, the blades start

to rotate generating power. The output power is then connected to the system's output terminal to be further processed. Given the laboratory's constraints, the water is recycled back to the plastic water tank as in Figure (3.4). The circuit for the MHPG allows the operation of two different configurations. A low-cost 50 V, 1.8W Impulse MHPG and a set of 15 V, 1 W reaction MHPGs. The commercial-off-the-shelf micro-hydros with 1/2 inches water inlet/outlets, are suitable for domestic water pipes are shown in Figure (3.5).

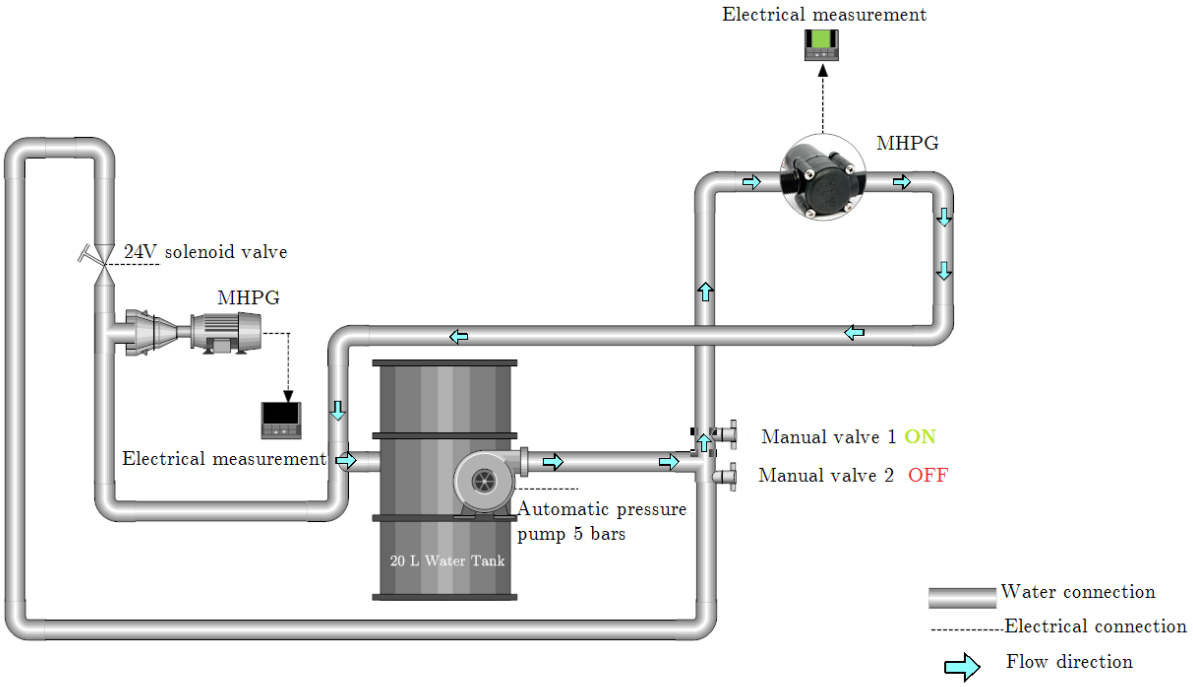

Figure 3.4: A schematic of the water flow through the MHPG, valve 1 ON and valve 2 OFF.

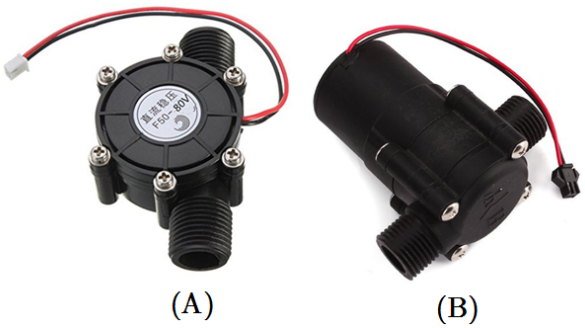

Figure 3.5: MHPGs, A)$\approx 80V, 1.5$ watts. B)$\approx 15V, 1$ watts.

Similarly, when valve 2 is ON and valve 1 is OFF, the water flows through valve 2 to travel through the pipes into the automated solenoid valve (Figure 3.6). The 12V,6W propeller hydroelectric power generator generates electricity from the flow of water. The water is then recycled back to the plastic tank.

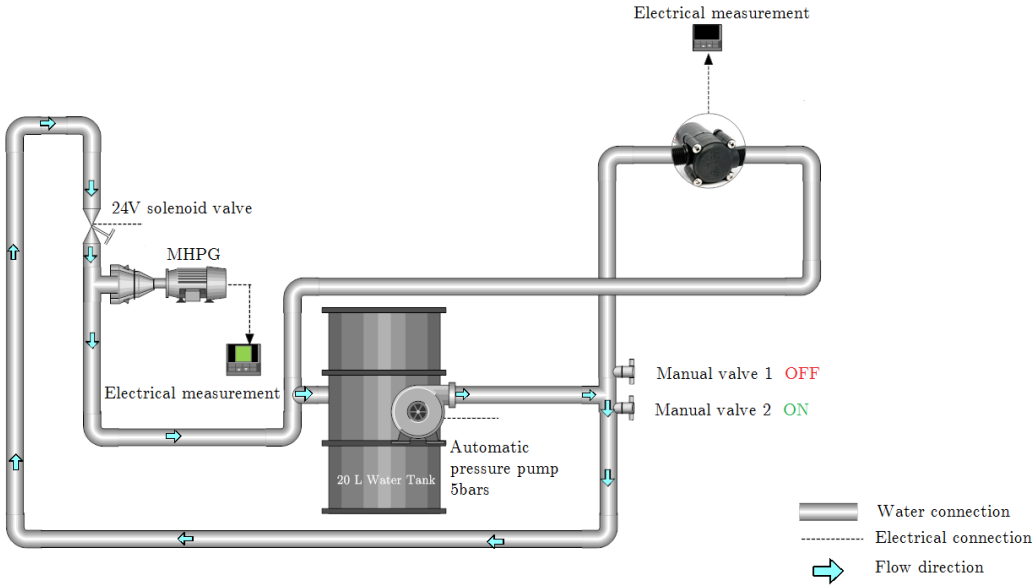

Figure 3.6: A schematic of the water flow through the mini 12V,6W propeller hydroelectric power generator, valve 2 ON and valve 1 OFF.

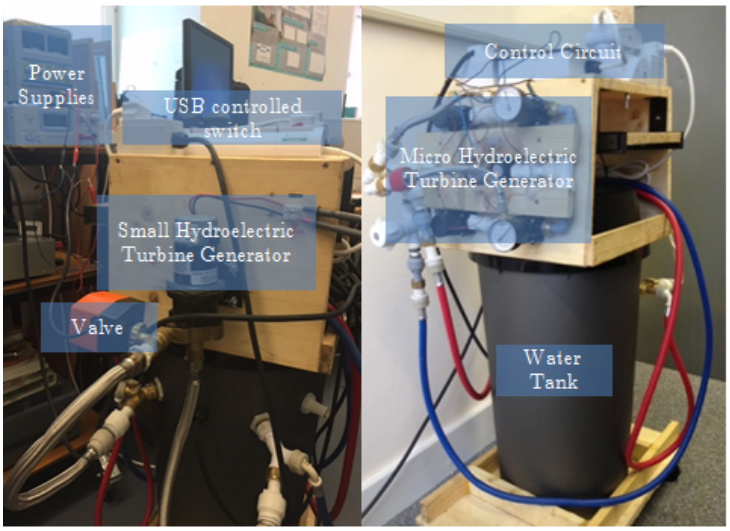

Figure 3.7: Pictures of the built-in-house, indoor, hydroelectric generator emulator prototype.

3.4 The experimental results of MHPG characteristics investigation

This section presents the experimental results of the current-voltage and power-resistance characteristics for three different configurations of MHPGs. These are a 50V, 1.8W impulse MHPG [107], a 1W reaction MHPGs [108] and 6W propeller MHPG [109].

3.4.1 A 50V, 1.8W impulse MHPG

The manufacture specifications of the MHPG studied in this section are listed in Table 3.2 below.

Table 3.2: The manufacture specification of the 50V, 1.8W impulse MHPG.

Parameter	**Information**
Start water pressure	0.05 Mpa
Maximum Water Pressure	0.6 Mpa
Generator single volume	90 g
Insulation resistance	10 M
Dimension	8.8x 5.8x3.9 cm (L x W x H)
Manufacture	Gaoxing Tech
Provider	Amazon [107]

The I-V characteristic curves for a commercial, off-the-shelf 1.8W crossflow MHPG at different flow rates Q_n are shown in Figure (3.8). The corresponding power-resistance (P-R) curves are shown in Figure (3.9).

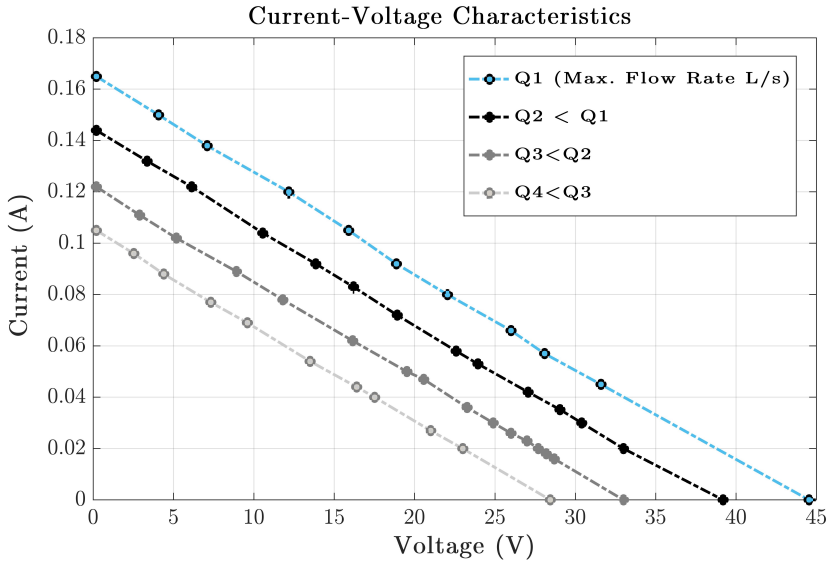

Figure 3.8: The I-V characteristics for a 1.8W MHPG at different flow rates Q ($Q_n > Q_{(n+1)}$).

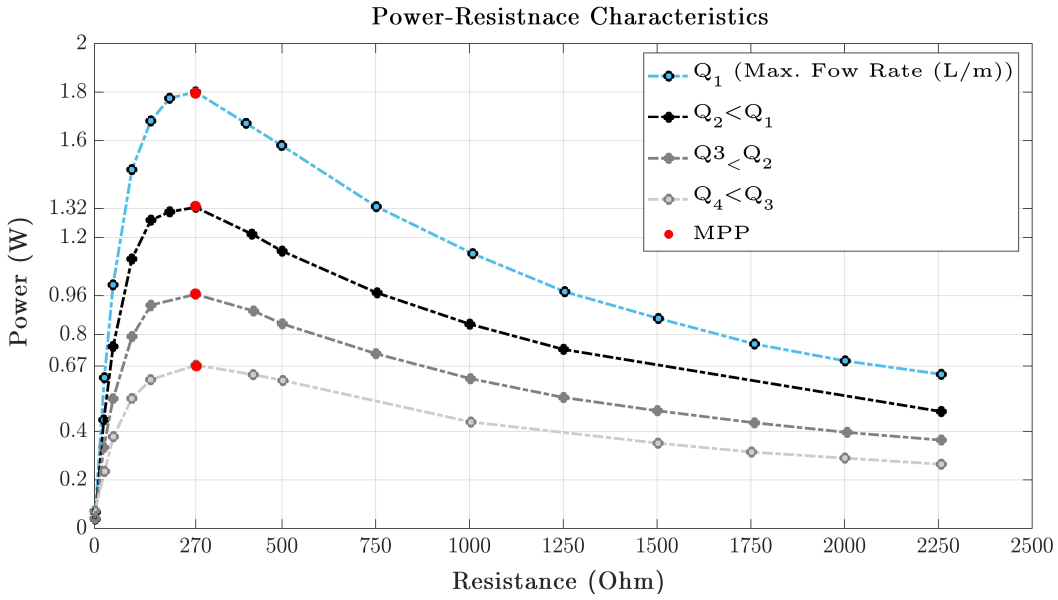

Figure 3.9: The P-R characteristics for a 1.8W MHPG at different flow rates Q ($Q_n > Q_{(n+1)}$).

The experimental findings indicate a constant linear relationship between MHPG voltage and current across various flow rates. These results obviously suggest constant characteristic impedance (i.e. 270Ω) regardless of the water flow.

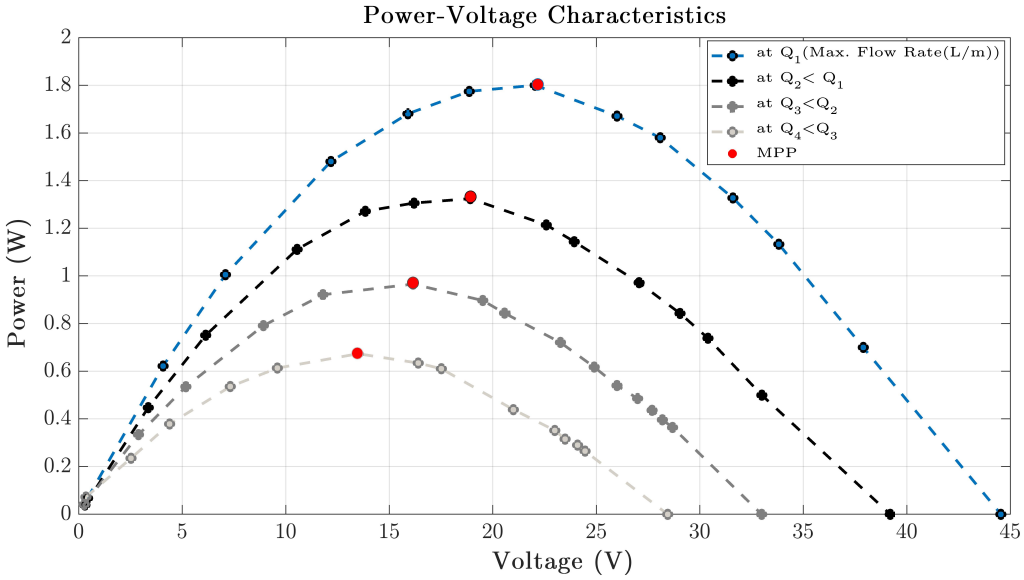

Figure 3.10: The P-V characteristics for a 1.8W MHPG at different flow rates Q ($Q_n > Q_{(n+1)}$).

Determination of the maximum power load is also possible through analysis of power-voltage (P-V) curves and is shown in Figure(3.10). Despite the variation in the water flow, the experimental results demonstrate a constant direct proportionality between (V_{mpp}) and (V_{oc}) as given in Equation(3.5), where $V_{mpp_{(Q_n)}}$ is the MPP voltage for flow rate Q_n and k_v is the constant proportionality.

$$V_{mpp_{(Q_n)}} = k_v V_{oc(Q_n)} \tag{3.5}$$

3.4.2 A 2X2 series parallel 15V,1W combination of reaction MHPGs

This section studies the power characteristics of a combination of reaction MHPGs. A set of commercial, off-the-shelf 15V, 1W MHPGs were optimised into a 2x2 series/parallel arrangement. The optimum 2x2 of four MHPGs for a U.K. domestic supply delivered through a 15mm pipe is shown in Figure (3.11). The optimised combination produces

4W into 300 ohms (35 VDC) which provides a means of power supply on an intermittent battery-backup basis for low-power applications. The manufacture specifications of each single unit of the MHPGs used in the results presented in this section is tabulated in Table 3.3.

Table 3.3: The manufacture specifications of each single unit used to make up the 2x2 arrangement of 4 MHPGs.

Parameter	**Information**
Starting water Pressure	0.08 MP
Maximum Water Pressure	0.55MP
Generator single volume	90g
Dimensions	14.7 x 12.7 x 4.572cm (L x W x H)
Water inlet/outlet	1/2 ”
Manufacture	Yosso
Provider	Amazon [108]

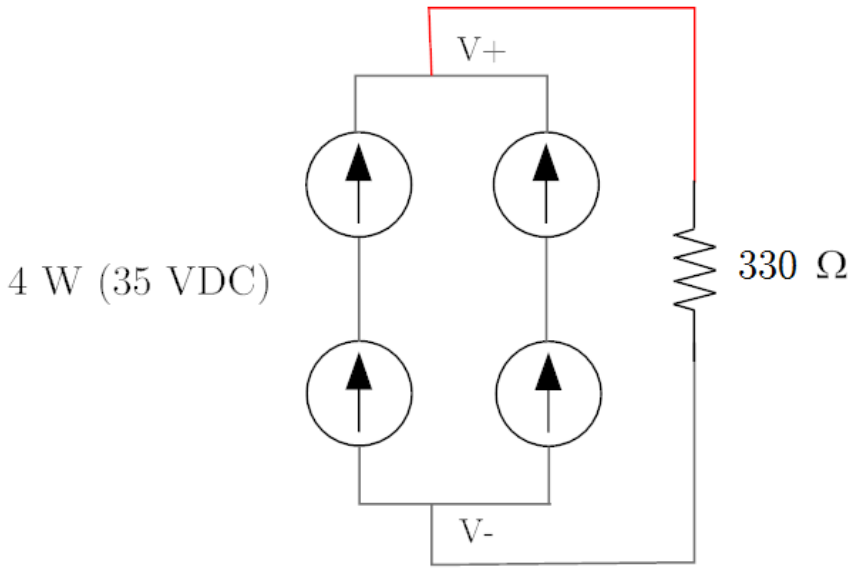

Figure 3.11: The 4W(35 VDC) optimised 2x2 serial/parallel arrangement of 4 MHPGs.

The electrical specifications of the 2x2 MHPGs combinations as measured in the laboratory are summarised in Table (3.4) and illustrated in Figures (3.12) and (3.13). Appropriate combinations can be optimised for a wide range of water flow rates and pressures.

Table 3.4: The characteristics of the optimised 2x2 serial/parallel arrangement of 4 MHPGs at the maximum flow rate.

Parameter	**Value**
Short Circuit Current I_{sc}	0.2 A
Open Circuit Voltage V_{oc}	70 V
Maximum Power Point P_{max}	4 W
Voltage at Maximum Power Point V_{MPP}	35 V
Characteristic Impedance R_s	330 Ω

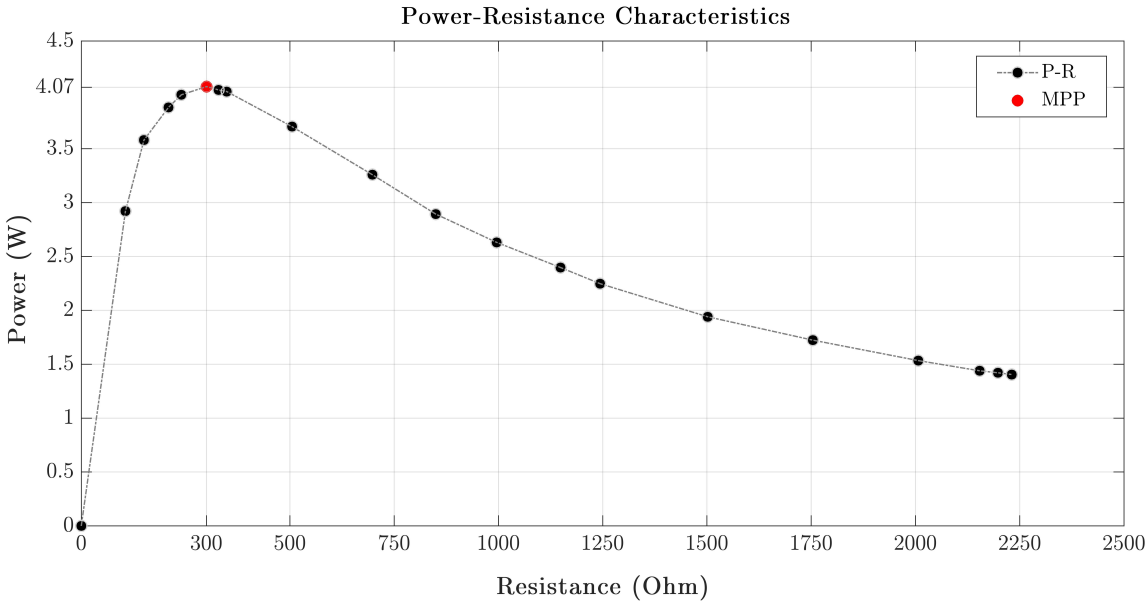

Figure 3.12: The P-R characteristic curve for the optimised 2x2 serial/parallel arrangement of 4 MHPGs at the maximum flow rate.

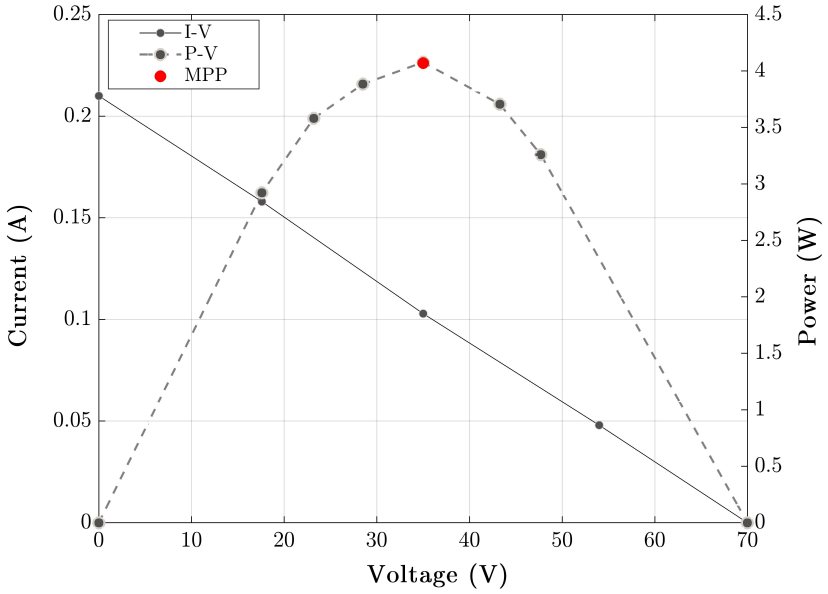

Figure 3.13: The I-V and P-V characteristics for the optimised 2x2 serial/parallel arrangement of 4 MHPGs at the maximum flow rate.

The family of the electrical characteristics curves P-R, I-V and P-V for the MHPGs at the maximum flow rate are shown in Figures (3.12) and (3.13) respectively. The results are in agreement with that of the single unit in section (3.4.1). This includes linear system characteristics which bear a close resemblance to that of an ohmic impedance. Findings indicated in Figure (3.13) further reinforce the direct relationship between V_{mpp} and V_{oc} analysed as previously observed in section (3.4.1). The electrical operational performance of the combined MHPGs was further examined under various water flow rates. The I-V characteristic curves for the 2x2 MHPGs are shown in Figure (3.14). Figure (3.15) shows the corresponding P-R characteristic curves.

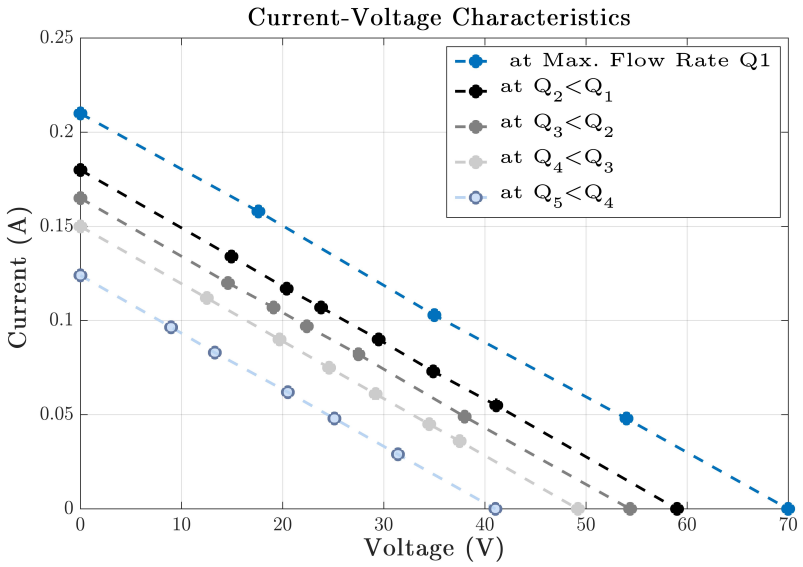

Figure 3.14: The I-V characteristics for the 2x2 MHPGs at different flow rates Q ($Q_n > Q_{(n+1)}$).

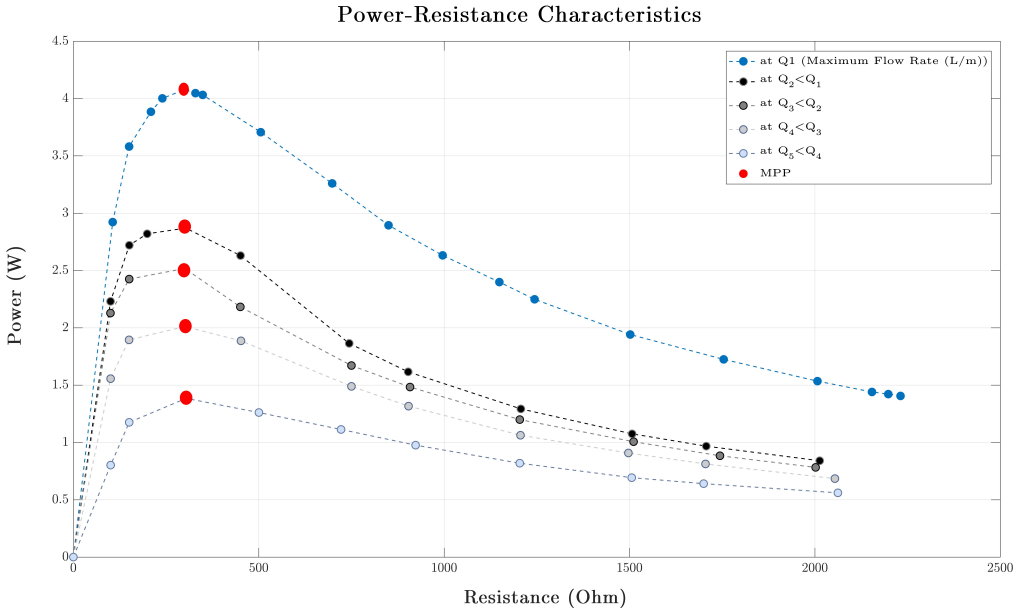

Figure 3.15: The P-R characteristic curves for the 2x2 MHPGs at different flow rates Q ($Q_n > Q_{(n+1)}$).

The experimental findings as captured in Figure (3.14) again suggest a linear I-V characteristic and a constant source impedance of the hydro generators, despite varying water

flow. This is further substantiated by the P-R curves in Figure (3.15) whereby maximum power is always generated at constant load (330Ω in this case). This demonstration proves a constant source impedance for the combined MHPGs as well as single units. The characteristic impedance can be interpreted by the inverse of the I-V lines gradient as expressed in Equation(3.6) where Q is the flow rate (in L/min.) and $Q_n > Q_{n+1} > Q_m$.

$$R_s = \frac{V_{oc_{Qn}}}{Isc_{Qn}} = \frac{V_{oc_{Q(n+1)}}}{Isc_{Q(n+1)}} = ... = \frac{V_{oc_{Q_m}}}{Isc_{Q_m}} \tag{3.6}$$

3.4.3 A 12V,6W propeller MHPG

This section reports further examination carried out on a MHPG of a different design. The manufacturer specification of the propeller MHPG examined is section are listed in Table 3.5. The I-V characteristic curves of this commercial, off-the-shelf DCPAT-20 propeller MHPG at the highest maximum and lowest minimum water flows are shown in Figure (3.16).

Table 3.5: The manufacture specifications of each single unit used to make up the 2x2 arrangement of 4 MHPGs.

Parameter	**Information**
Starting water Pressure	0.08 MP
Maximum Water Pressure	1.03 MP
Generator single volume	2.5 Kg
Dimensions	21.15 x 11.437 x 11.9cm (L x W x H)
Water outlet	3/4”
Water inlet/outlet	1/2 ”
Manufacture and provider	NoOutage [109]

The experimental observations captured in Figure (3.16) confirm approximate linearity of the I-V characteristics for the 6W MHPG unit whereby the characteristic impedance

obeys the expression in Equation (3.6). Implications from Figure (3.16), with reference to (3.6), reinforce the empirical conclusion about MHPG constant source impedance despite varying water flow.

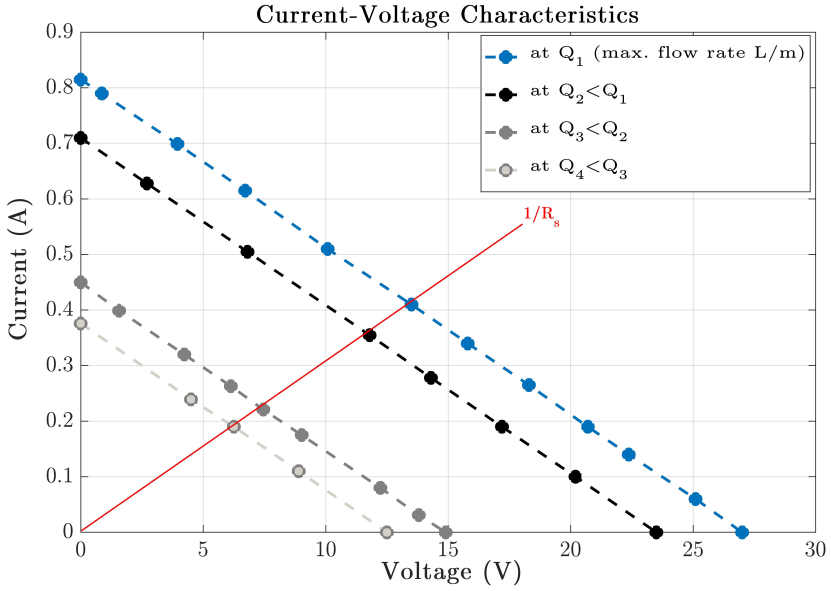

Figure 3.16: The I-V characteristics for the DCPAT-20 MHPG at the highest and lowest water flow rates Q ($Q_n > Q_{(n+1)}$).

3.5 Electric-hydraulic impedance analogy

The analysis of MHPG electrical characteristics is best achieved through the analogies between current flow and water flow. Whereas the electric current flow (A) is analogous to the fluid flow rate of the rate Q (in m^3/s), in electrical analogies, the voltage (V) is analogous to the pressure $\boldsymbol{p}$ (in J/m^3). The hydraulic impedance of fluid flow Z_{hydro} is given in Equation (3.7) [110]. This is dependent on the physical properties of the fluid, fluid velocity in particular. This bears a strong similarity to the principles of electrical impedance demonstrated earlier.

$$Z_{hydro} = \frac{\Delta \boldsymbol{p}}{Q} \tag{3.7}$$

Given the kinetic KE_{fluid} and potential energy PE_{fluid} of a moving fluid in Equations (3.8) and (3.9) respectively, analogies between the electrical and hydraulic potential power can be made. Where the energy density is expressed by the fluid pressure, the power available at any one point in a fluid power system is defined by the pressure and the flow at that point as shown in Equation (3.10) [111].

$$\frac{KE_{fluid}}{Volume} = \frac{1}{2}\rho v^2 \tag{3.8}$$

$$\frac{PE_{fluid}}{Volume} = \rho g h \tag{3.9}$$

$$P_{fluid} = \boldsymbol{p}Q \tag{3.10}$$

Where P_{fluid} is the power in watts available from fluid (density ρ) kg/m^3 flow Q (m^3/sec) with head (h)(meters), gravitation acceleration $(g)(m/s^2)$.

Therefore, the electrical power generated from a hydropower system is conceptually analogous to hydraulic principles. This explains the interconnections between MHPG electrical properties and flow dynamics in relation to impedance.

3.6 Comparison of I-V characteristics of hydro, solar PV and wind power systems

The empirical findings reported in section 3.4 demonstrate the unique traits of MHPGs. The significance of the experimental results is summarised in Figure (3.17). Comparisons between the well-known I-V characteristics for solar photovoltaic and wind power systems, against the empirically investigated characteristics for MHPG are tabulated in Table (3.6). An overview of solar photovoltaic and wind power systems characteristics is revisited, by

way of illustration, in Figure (3.18) and Figure (3.19), respectively.

Table 3.6: Comparative summary of the key characteristics for hydroelectric power generator, solar photovoltaic and wind power generator.

Characteristic	**Hydroelectric power generator**	**Solar photovoltaic**	**Wind power generator**
Current-Voltage (I-V)	Linear	Non-linear	Non-linear
Short Circuit Current I_{sc}	$2I_{mpp}$	Greater than I_{mpp}*	Less than I_{mpp}
Open Circuit Voltage V_{oc}	$2V_{mpp}$	Greater than V_{mpp} **	Greater than V_{mpp}
Characteristic Impedance R_s	Constant	Insolation-dependent	Wind-speed-dependent
Maximum Power Point	Directly related to flow rate	Directly related to insolation level	Directly related to wind speed

* I_{mpp} is typically between 72-92% of I_{sc} [112]

** V_{mpp} is typically between 70-80% of V_{oc} [113]

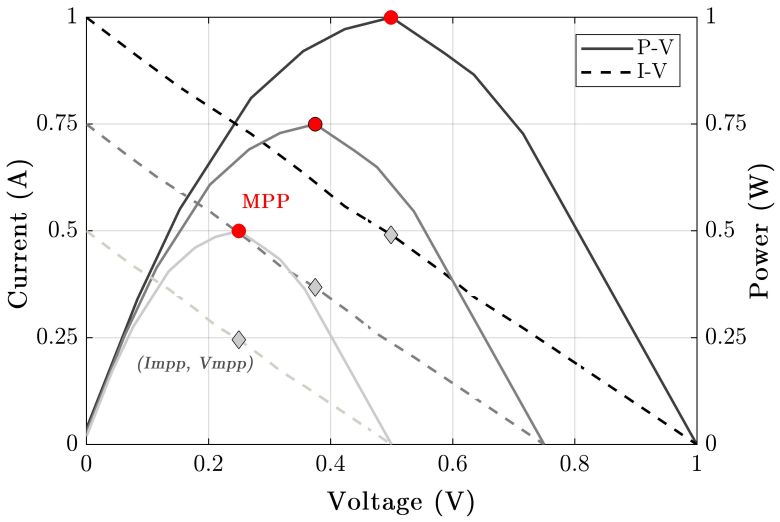

Figure 3.17: Normalised I-V and P-V characteristics for a hydroelectric power generator at different water flow rates.

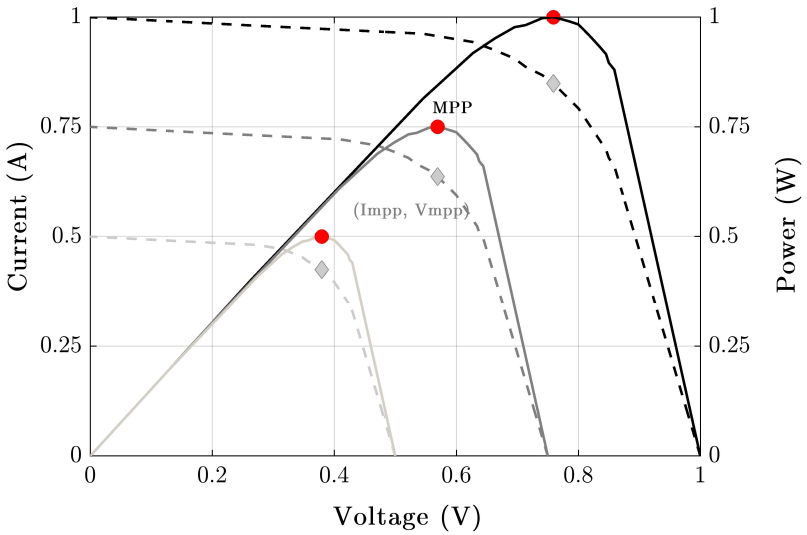

Figure 3.18: Normalised overview of I-V and P-V characteristic curves for a solar PV at different insolation levels.

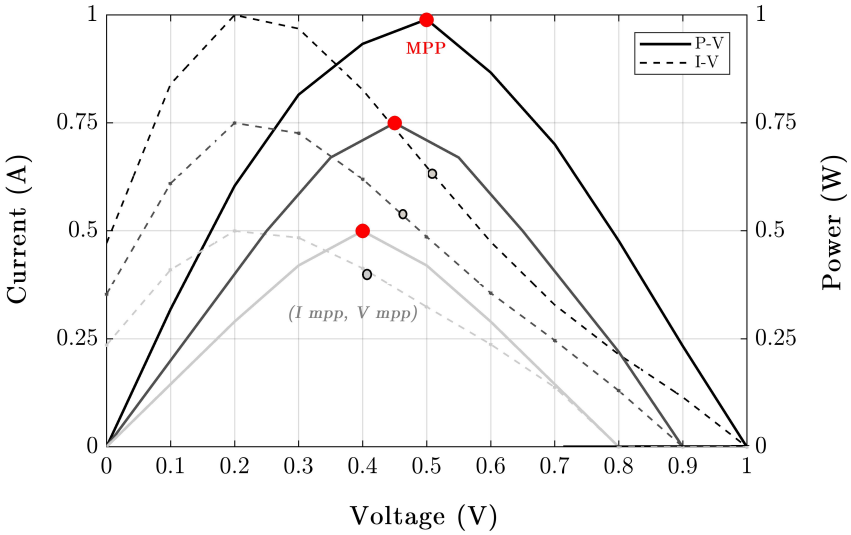

Figure 3.19: Normalised overview of I-V and P-V characteristic curves for a wind power generator at different wind speeds.

3.7 Modelling of a hydropower turbine generator characteristics

Based on the empirical validations of the characteristics of a hydropower generator, this section presents an electrical model for a hydropower generator. Heuristic analysis on the output hydropower as a function of the current and voltage is presented. The heuristic model was validated through MATLAB-Simulink simulations.

3.7.1 Heuristic analysis of hydroelectric power

The experimental findings are normalised to be within the range 0 to 1 (i.e. I_{sc}, V_{oc} =1) to allow a generic solution to be found. The evidently reported system linearity defeats the multi-flow investigation argument. The analysis of $P(I)$ is reinforced, by way of illustration, through the findings captured in Figure (3.20). Likewise, indications highlighted in Figure (3.21) aids in the derivation of $P(V)$.

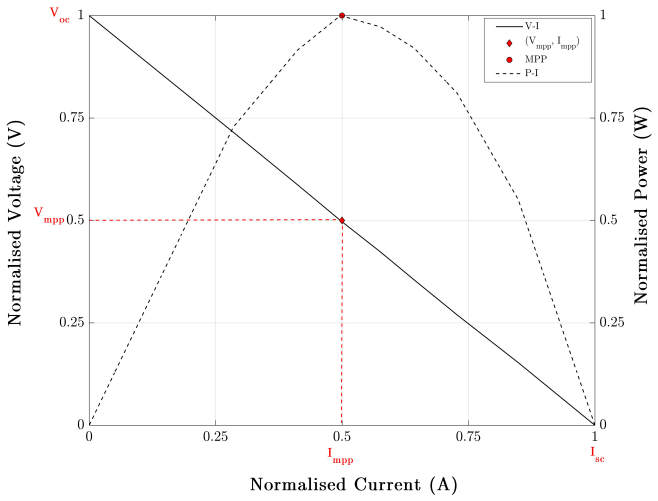

Figure 3.20: Normalised V-I and P-I characteristics.

The generator's voltage as a function of the current (I) can be mathematically expressed by an equation of a straight line with a gradient $-\frac{V_{oc}}{I_{sc}}$ and intercept V_{oc} on the y-axis as in Equation (3.11). The source impedance can therefore be determined by the magnitude of the slope (i.e. Equation (3.12)). Substituting for the voltage $V(I)$ into the transferable power definition Equation (3.13), the power (in watts) as a function of the current $P(I)$ is expressed in Equation (3.14), where, V_{oc} is the open circuit voltage, I_{sc} is the short circuit current, R is the load.

$$V(I) = -\frac{V_{oc}}{I_{sc}}(I) + V_{oc} \tag{3.11}$$

$$R_s = \frac{V_{oc}}{I_{sc}} \tag{3.12}$$

$$P(I) = \frac{V(I)^2}{R} \tag{3.13}$$

$$P(I) = \frac{{V_{oc}}^2(1 - \frac{I}{I_{sc}})^2}{R} \tag{3.14}$$

Alternatively, the power in terms of voltage $P(V)$ can be revised, with knowledge of the source impedance R_s highlighted in Equation(3.12), as outlined in Equation (3.15).

$$P(V) = \frac{{V_{oc}}^2(1 - \frac{V}{V_{oc}}(\frac{R_s}{R}))^2}{R} \tag{3.15}$$

In relation to Equations (3.14) and (3.15), with reference to Figures (3.20) and (3.21), the MPP can be deduced from Equation (3.16), where the load impedance R matches that of the source R_s at an approximate of $50\%I_{sc}$ and $50\%V_{oc}$.

$$P_{max} = \frac{0.25{V_{oc}}^2}{R_s} \tag{3.16}$$

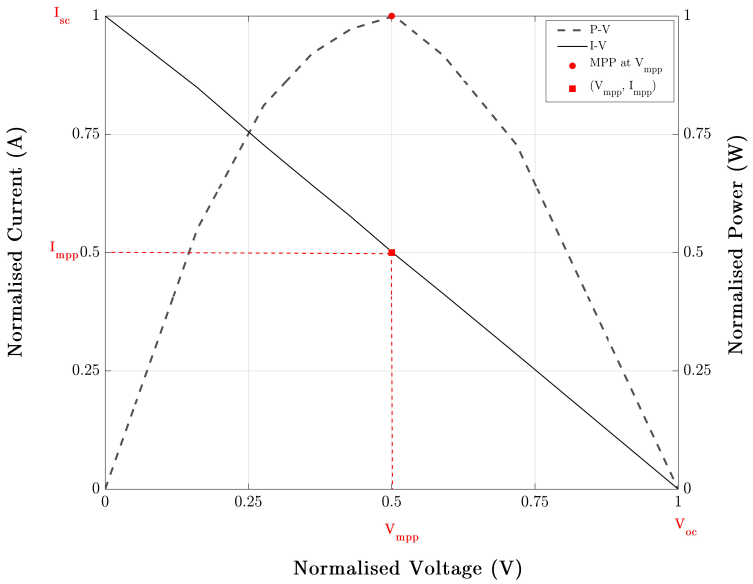

Figure 3.21: Normalised I-V and P-V characteristics.

The definition of the power can be further simplified into Equation (3.17) where $\frac{R_s}{R} = x$, $0 \leq x \leq \infty$ and $\frac{V}{V_{oc}} = y$ where $0 \leq y \leq 1$, hence $0 \leq xy \leq 1$. Regression analysis of the empirical results carried out in MATLAB implies that the relation between the voltage ratio y (i.e. $\frac{V}{V_{oc}}$) as a function of the impedance ratio x (i.e. $\frac{R_s}{R}$) is best expressed by a decaying exponential of first degree as given in Equation (3.18) and illustrated in Figure (3.22), where $0 \leq x \leq \infty$.

$$P(x) = V_{oc} I_{sc} x(1 - xy)^2 \tag{3.17}$$

$$y(x) = \frac{1}{(1+x)} \tag{3.18}$$

The output range of the positive index $y(x)$ in relation to the load impedance R is outlined in Equation (3.19). Whereby $y(x)$ is 1 at open circuit conditions (V_{oc}, $x = 0$) but decays exponentially with decreasing load impedance towards the MPP at 0.5 (i.e. $R_s = R$, $x = 1$), or converges to null below the MPP (i.e. $R << R_s$) towards the short circuit conditions($x \to \infty$).

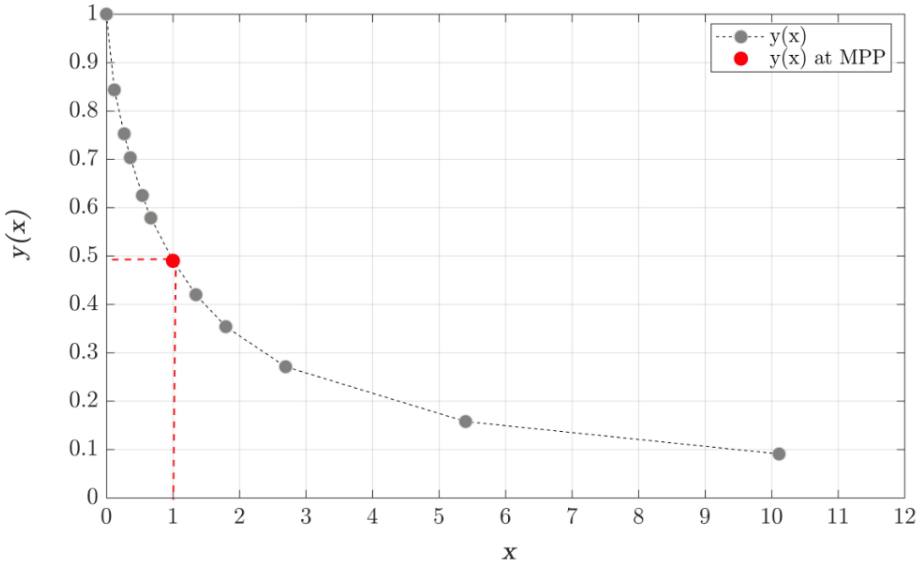

Figure 3.22: The experimental results of y (i.e. $\frac{V}{V_{oc}}$) as a function of x (i.e. $\frac{R_s}{R}$), indicating $y(x)$ at MPP.

$$y(x) = \begin{cases} 0.5, & \text{if } R = R_s \text{ at MPP} \\ 0.5 < y(x) \leq 1, & \text{if } R > R_s \\ 0.5 > y(x) \geq 0, & \text{if } R < R_s \end{cases} \tag{3.19}$$

Given the obvious $\frac{d}{dx}(P(x)) = 0$ at MPP, the value of x at MPP can be defined in terms of y. Thus, applying first derivative with respect to x into Equation (3.17) leads to Equation (3.20).

$$\frac{d}{dx}P(x) = 3V_{oc}I_{sc}y^2\ x^2 - 4V_{oc}I_{sc}y\ x + V_{oc}I_{sc} \tag{3.20}$$

Solving the quadratic equation in Equation(3.20) for x defines x at MPP with respect to y as in Equation (3.21).

$$x = \frac{1}{3y} \tag{3.21}$$

Given $y = 0.5$ at the MPP by substituting for x into Equation (3.17), the maximum power available for harvesting $P(x)_{mpp}$ can therefore be determined from Equation (3.22).

$$P(x)_{mpp} \simeq 0.25 V_{oc} I_{sc} \tag{3.22}$$

Thus, based on the conclusions mathematically derived above along with the empirical observations, the output power of the heuristic model for hydroelectric generator $P(x)$ below, beyond and at the MPP is defined in Equation (3.23) and highlighted in Figure (3.23).

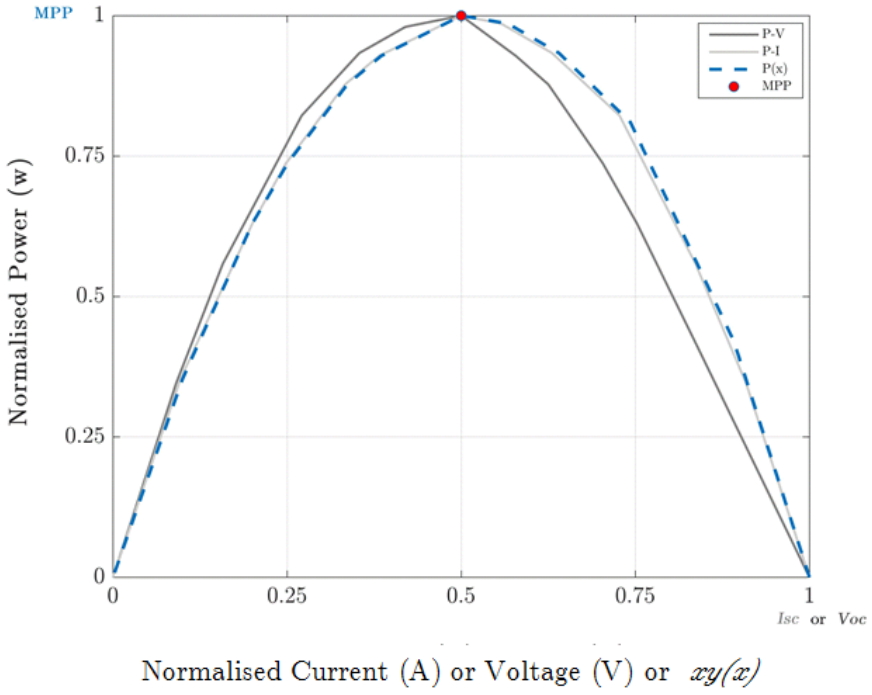

Figure 3.23: The output of $P(x)$ against current, voltage or xy calculated from normalised empirical results.

$$P(x) = \begin{cases} 0.25 V_{oc} I_{sc}, & \text{at MPP} \\ 0 \leq P(x) < 0.25 V_{oc} I_{sc}, & \text{otherwise} \end{cases} \tag{3.23}$$

3.7.2 MATLAB-Simulink simulation model of a MHPG

MATLAB-Simulink simulations which validates the heuristic model are presented in this section. Through the use of Simulink, the simulation model was developed systematically by means of function blocks. A generic block diagram of the hydroelectric turbine generator in the GUI environment for Simulink software of MATLAB is given in Figure (3.24). This block was made up of subsystems that are interconnected to simulate the performance of a hydroelectric generator. The main inputs are the open circuit voltage V_{oc} and short circuit current I_{sc}. The output power of the simulation model was monitored on the scope (XY Graph) relative to x and xy. Similarly, the current-voltage characteristic (I-V) was observed. Figure (3.25) illustrates a block diagram of the simulation model subsystems. The realisation of the subsystem y(x) as defined by Equation (3.18) is shown in Figure (3.26).

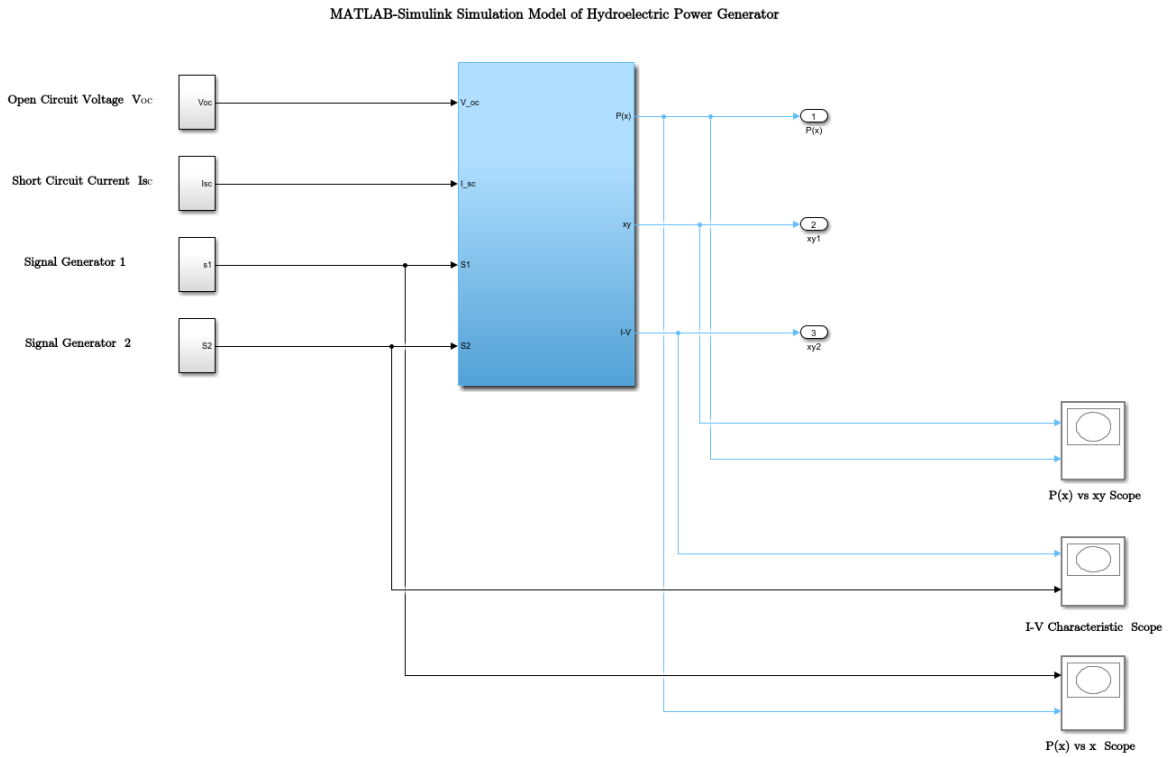

Figure 3.24: Block diagram of a MHPG MATLAB-Simulink simulation model.

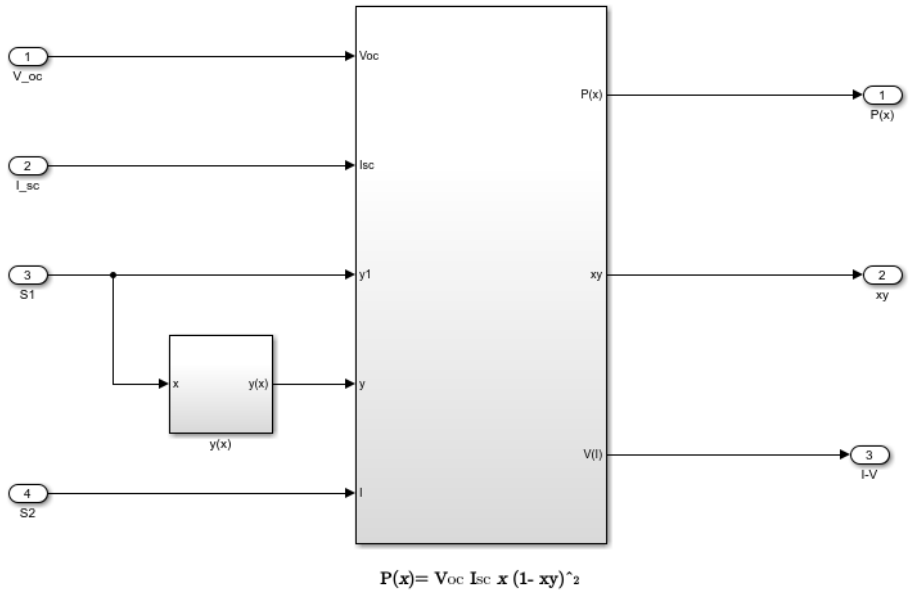

Figure 3.25: The subsystems of a MHPG MATLAB-Simulink simulation model.

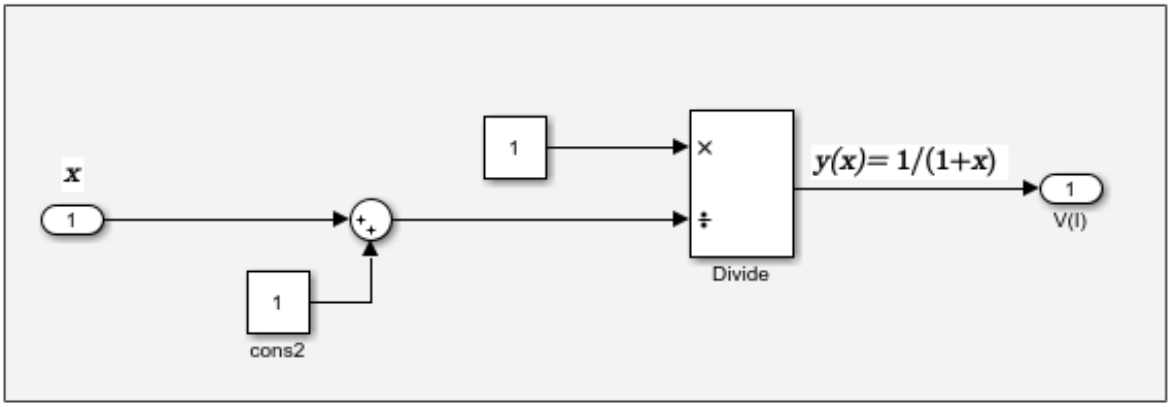

Figure 3.26: The internal subsystem of y(x) composed of mathematical function blocks in MATLAB-Simulink.

The implementation of the hydroelectric MHPG model output power $P(x)$, which is defined in Equation (3.17), is shown in Figure (3.27). Likewise, Figure (3.28) indicates the realisation of the I-V characteristics for the MATLAB-Simulink simulation model of MHPG, interpreted in Equation (3.11).

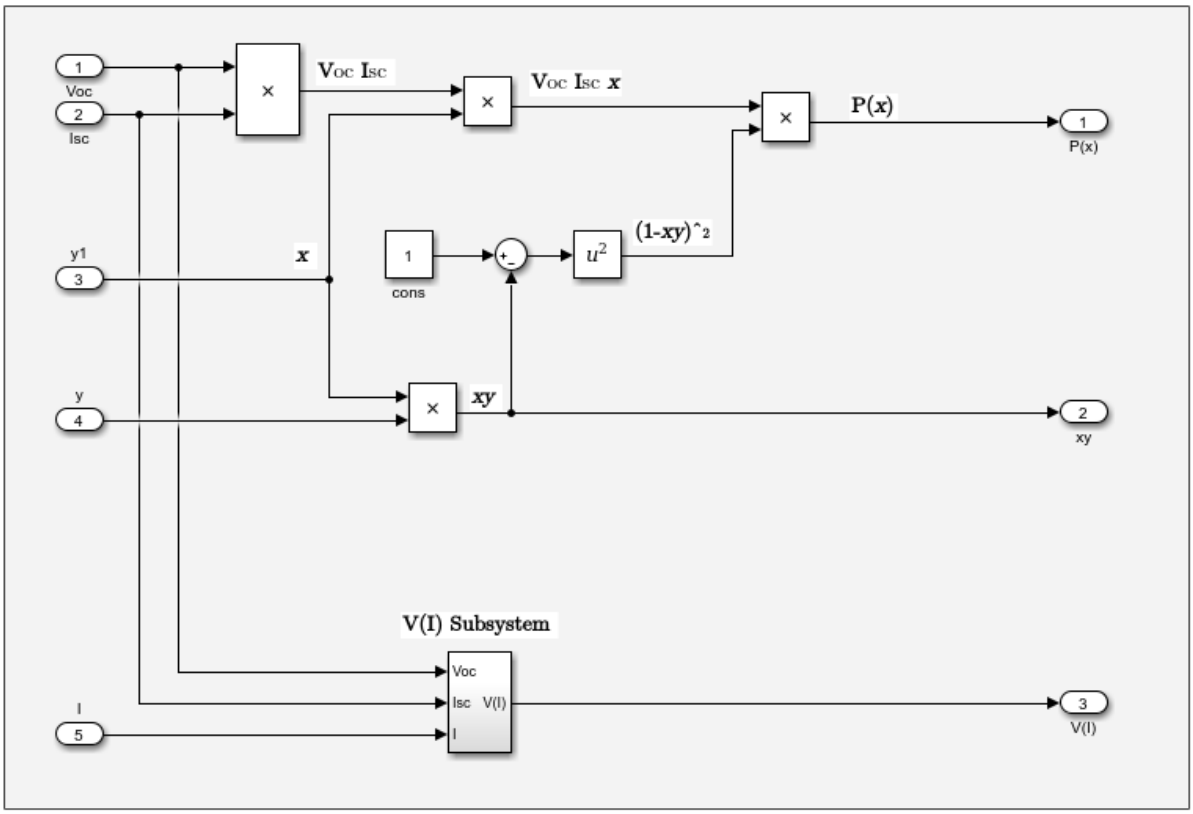

Figure 3.27: The MATLAB-Simulink simulation model of a MHPG output power $P(x)$.

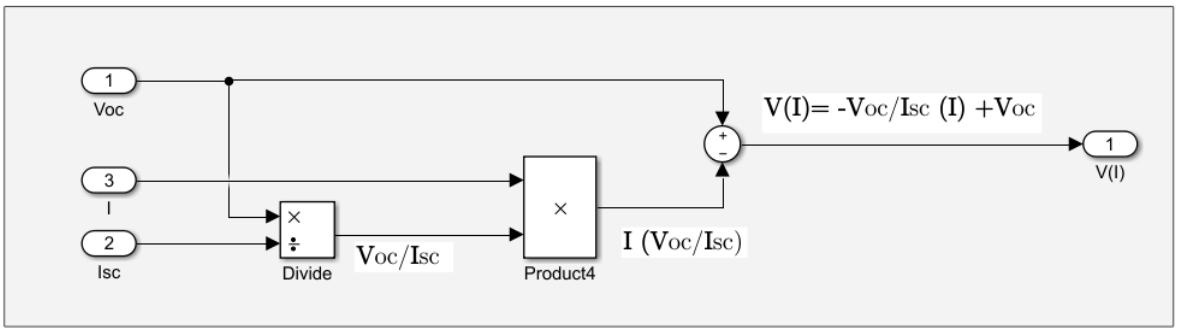

Figure 3.28: The MATLAB-Simulink simulation model of a MHPG I-V characteristics.

3.7.2.1 Modelling the characteristics of a 1.8W MHPG

The simulation results based on the characteristics parameters of the 1.8W micro-hydro generator examined in Section (3.4.1) are illustrated in Figure (3.29)and Figure (3.30). Figure (3.29) is a great indication of the satisfactory modelling of the output power of

the hydroelectric generator whereby, as outlined in Equation(3.23), the MPP is $\simeq 25\%$ of the product V_oc and I_{sc} (i.e. 0.25(44.99V)(0.165A) in this case) which coincides with 50% of xy. It is worth noting that the results in Figure (3.30) further validate the simulation model, confirming that maximum power is available when the load impedance matches that of the source, defined mainly from its characteristic parameters I_{sc}, V_{oc}.

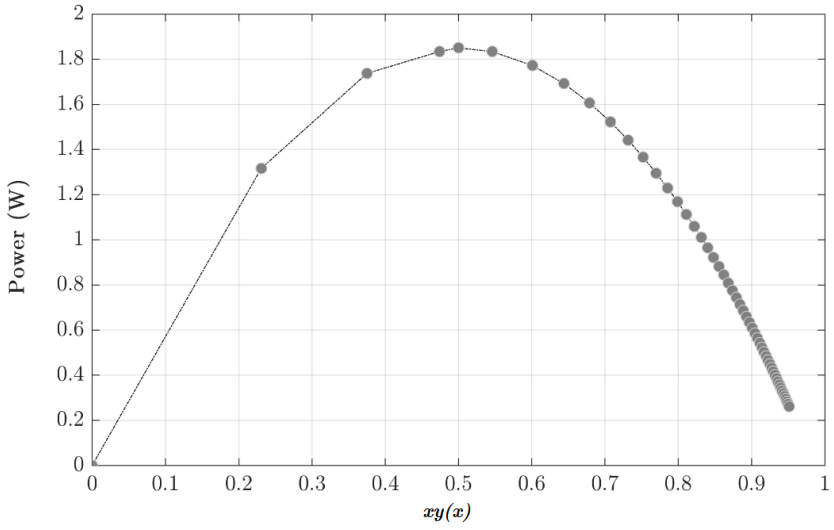

Figure 3.29: The output power of the MATLAB-Simulink simulation modelling of the 1.8W MHPG at the maximum flow rate against $xy(x)$, where $xy(x) = \frac{x}{1+x}$ and $x = \frac{R_s}{R}$.

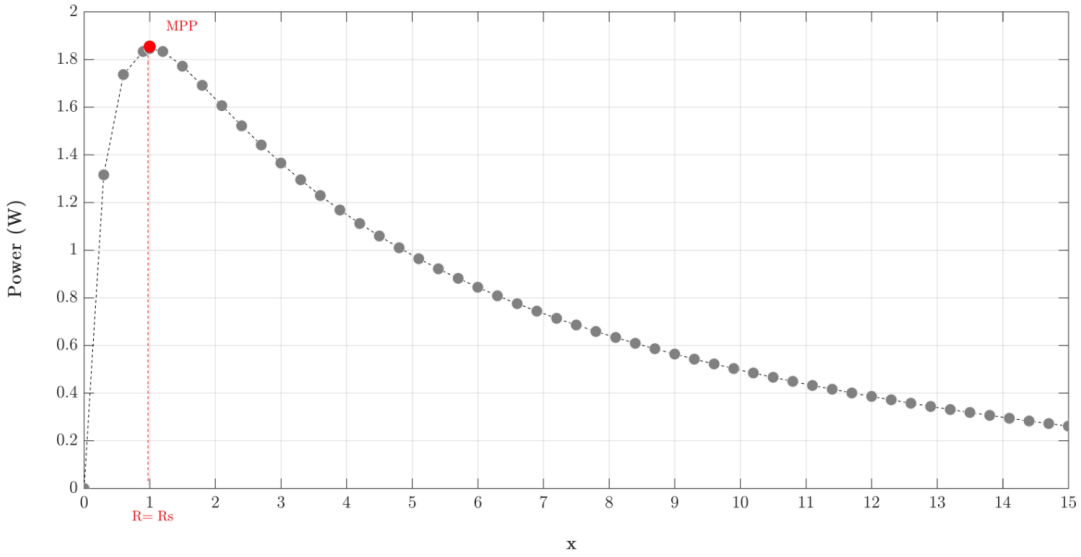

Figure 3.30: The output power of the MATLAB-Simulink simulation modelling of the 1.8W MHPG at the maximum flow rate against x, , where $x = \frac{R_s}{R}$

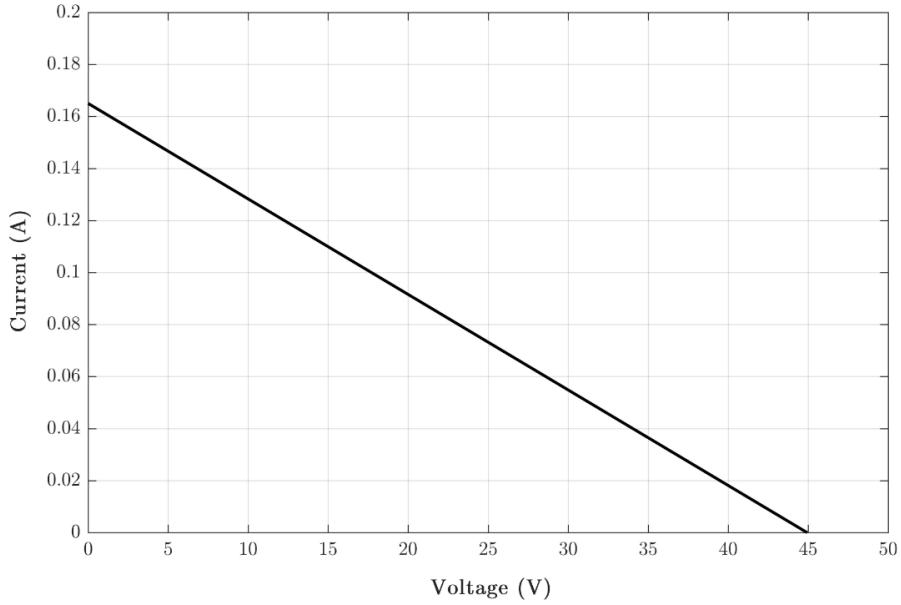

Figure 3.31: The I-V characteristic of the MATLAB-Simulink simulation modelling of the 1.8W MHPG at the maximum flow rate.

3.7.2.2 Modelling the characteristics of the 4W optimised 2x2 serial/parallel arrangement of 4 MHPGs

In addition, the simulation was replicated using the characteristic parameters of the optimised 2x2 serial/parallel arrangement of 4 MHPGs investigated in Section(3.4.2) in two scenarios: maximum and minimum flow rate. As expected the results were in complete agreement with the empirical observations reported in Section (3.4.2). This is evident through the illustrations of the linear I-V characteristics of the modelled hydro generator at different flow rates presented in Figure (3.32) and Figure (3.33). These simulations highlight a great illustration of the hydro generator's ohmic characteristic impedance. In validating the proposed hydropower generator model, the parabolic power-resistance (P-R) characteristic curve is pronounced in the simulation results of P(x) in relation to the resistive ratio x captured in Figure (3.34) and Figure (3.35). The fact that the model simulates the maximum power available for harvesting when the load impedance coincides with that of the source strongly validates the proposed model.

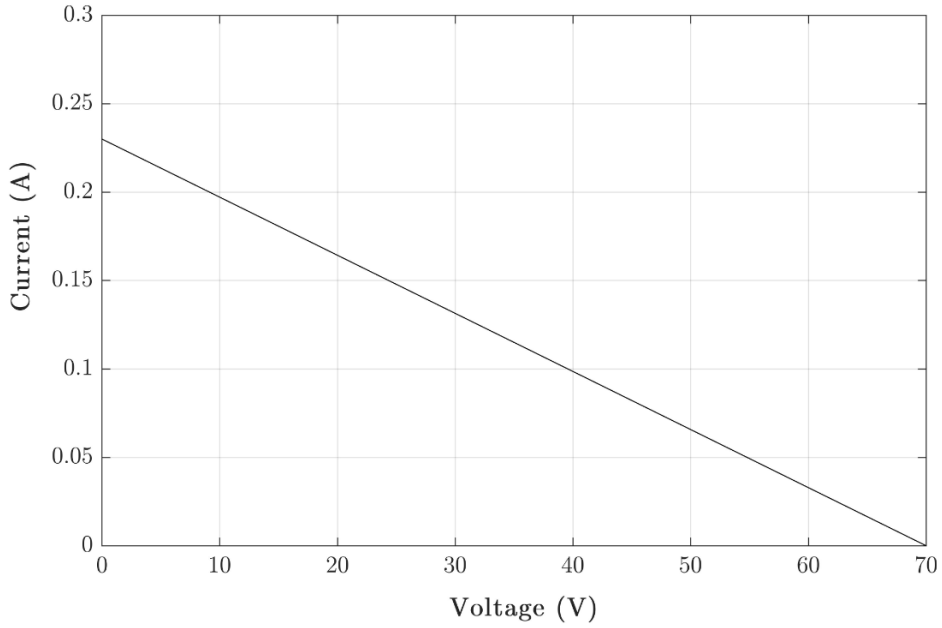

Figure 3.32: The I-V characteristics of the MATLAB-Simulink simulation modelling of the 4W optimised 2x2 serial/parallel arrangement of 4 MHPGs at the maximum flow rate.

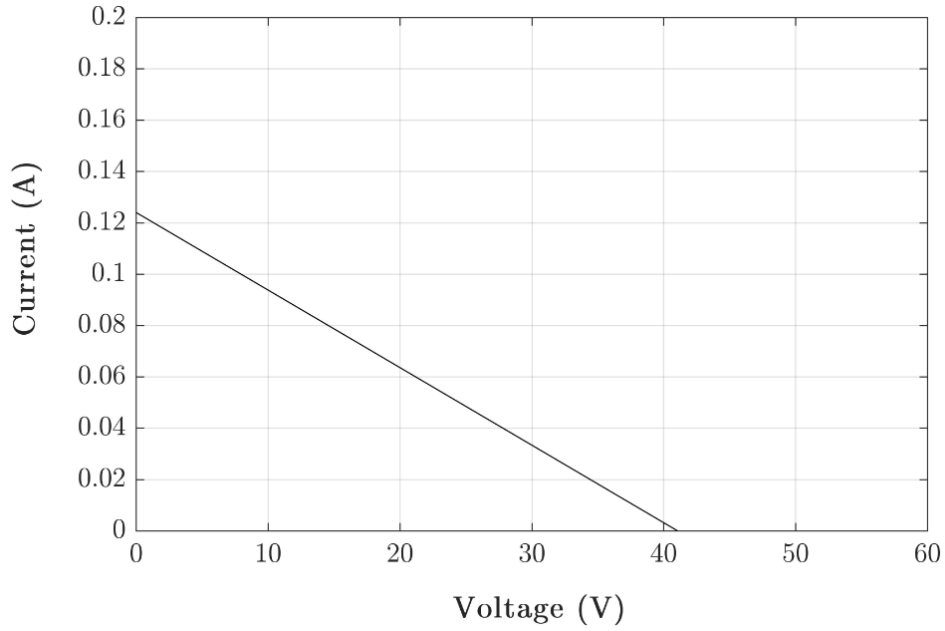

Figure 3.33: The I-V characteristic of the MATLAB-Simulink simulation modelling of the 4W optimised 2x2 serial/parallel arrangement of 4 MHPGs at the minimum flow rate.

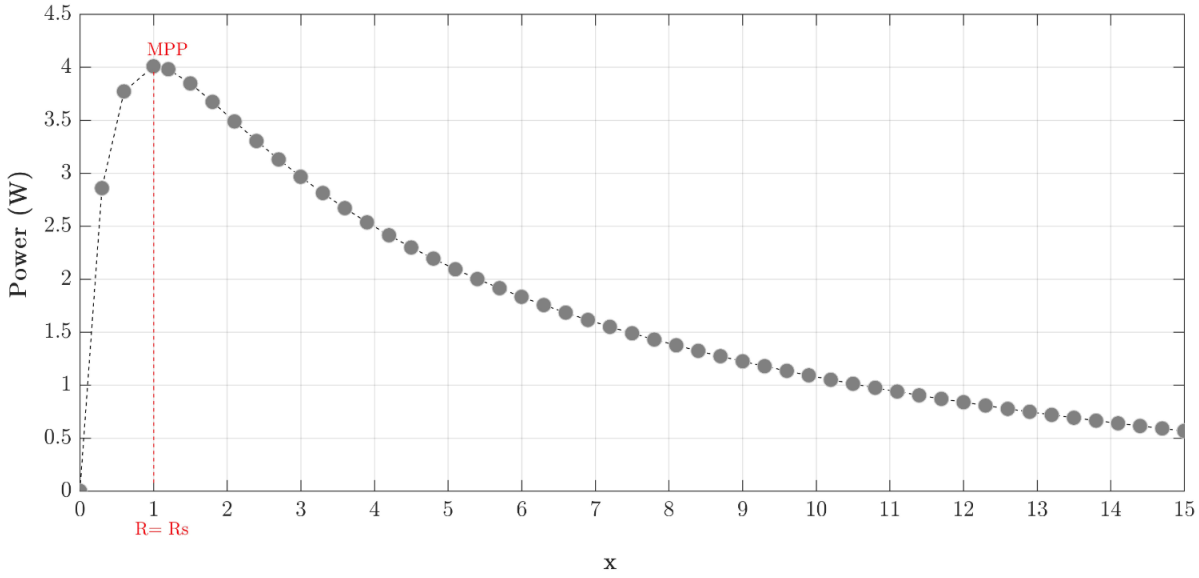

Figure 3.34: The output power of the MATLAB-Simulink simulation modelling of the 4W optimised 2x2 serial/parallel arrangement of 4 MHPGs at the maximum flow rate against x , where $x = \frac{R_s}{R}$.

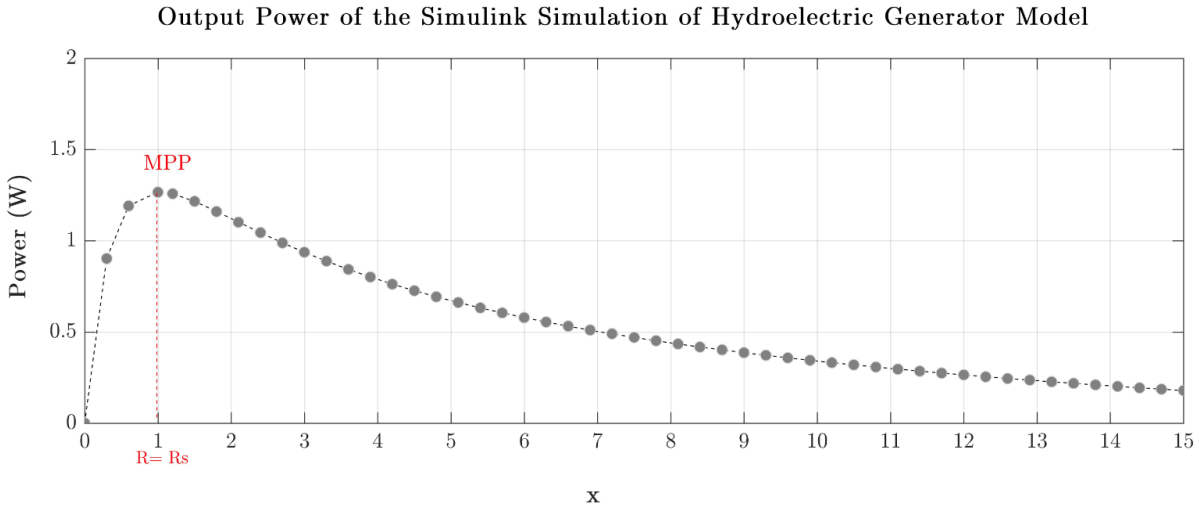

Figure 3.35: The output power of the MATLAB-Simulink simulation modelling of the 4W optimised 2x2 serial/parallel arrangement of 4 MHPGs against x at the minimum flow rate, where $x = \frac{R_s}{R}$.

Also, the illustrations in Figure (3.36) and Figure (3.37) show a satisfactory approximate to the relation between the MPP and R_s, V_{oc} and I_{sc} (defined by xy), which simulates the generation of the maximum power at $R = R_s$, $V = 50\%V_{oc}$ and $I = 50\%I_{sc}$.

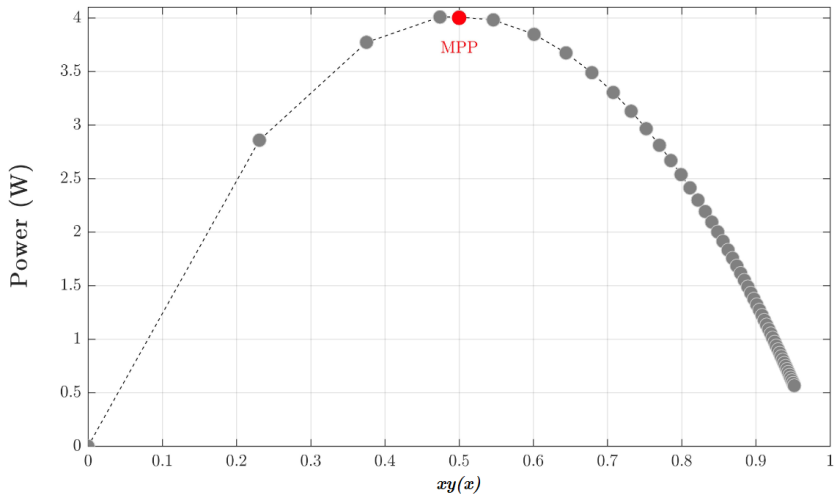

Figure 3.36: The output power of the MATLAB-Simulink simulation modelling of the 4W optimised 2x2 serial/parallel arrangement of 4 MHPGs at the maximum flow rate against $xy(x)$,where $xy(x) = \frac{x}{1+x}$ and $x = \frac{R_s}{R}$.

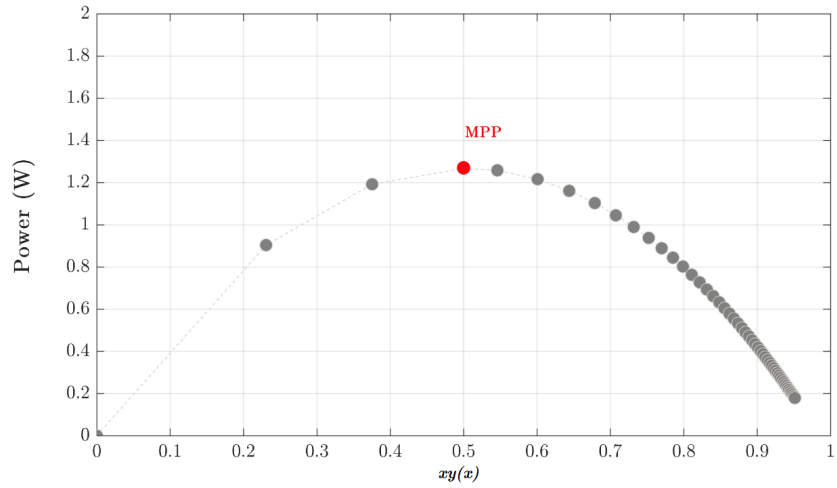

Figure 3.37: The output power of the MATLAB-Simulink simulation modelling of the 4W optimised 2x2 serial/parallel arrangement of 4 MHPGs at the minimum flow rate against $xy(x)$, where $xy(x) = \frac{x}{1+x}$ and $x = \frac{R_s}{R}$.

In general, the simulation results of the hydroelectric power generator are well substantiated by the empirical findings reported in this chapter. The noteworthy alignment between the empirical and the simulation outcomes emphasizes the validity of the novel hydroelectric generator model. Further, this could have an great role in hydropower systems simulation analysis.

3.8 Conclusion

In this chapter insight into the electrical characteristics of MHPGs has been demonstrated. The design of an intelligent low-cost, with high power, speed-controlled pump hydropower emulator prototype was detailed in section (3.3.1). The indoor, built-in-house, hydroelectric power emulator facilitated the investigation of MHPGs within an autonomously-controlled test environment.

Empirical results reported for the first time in this chapter introduced a new understanding of MHPG properties. Arguably, the most useful is the observation of constant ohmic source impedance in these generators. A second major finding concerned the variable multi-flow correlation between the voltage and current at the MPP, which coincides with 50% V_{oc} and 50% I_{sc}. The MATLAB-Simulink simulation carried out validated the proposed heuristic model and concurred very well with the experimental observations. These novel heuristic MHPG models are expected to assist with emerging hydropower generation strategies.

Chapter 4

The Seesaw Maximum Power Point Optimisation for Hydropower Systems

4.1 Introduction

It was demonstrated in Chapter 3 that a MHPG has a constant characteristic impedance which exhibits linear I-V characteristics, despite varying water flow. However, its MPP and corresponding V_{mpp} and I_{mpp}, vary with water flow rate. While the flow rate sets the limits of the maximum power available from the MHPG, the loaded voltage determines the actual amount of power delivered. Thus for maximum utilisation efficiency, it is important to match the hydro generator to the load such that the equilibrium operating point coincides with the MPP of the generator source under various atmospheric conditions.

The literature reviewed in Chapter 2 highlighted the need to improve MPPT control for hydropower systems [44]. The demonstrated system linearity offers promising opportunities for improved, more efficient MPPT. That is because the matching between hydro

generated power and rated hydropower is a function of the generator voltage only. The fact that good quality measurement of the voltage signal is more feasible compared to the current measurement [114], makes the former a prominent feature of HPCSs. Obviously, the changing water flow causes the hydro generator current to vary dramatically. Thus, using the current as a reference would require the controller to rapidly track the operation from zero to the short-circuit current point. As a result, the transient response of the MPPT controller in relation to the rapidly changing current can drive the generator towards its saturation point (i.e. I_{sc}). This could result into a sudden voltage drop, hence power loss, and could eventually damage the generator.

The linear dependency between the MHPG V_{mpp} and V_{oc} (i.e. $V_{mpp} = 50\%V_{oc}$) highlights the potential in maximising HPC extraction through means of a constant voltage optimisation mechanism. However, positive feedback constant voltage MPPTs have been considered previously [115–119]. The examples in [116,117] require prior knowledge of the open circuit voltage obtained from pilot measurement. Improved versions in [118, 119], employ microprocessors-controlled MPPT, adding to the system cost and complexity and are only feasible at high power levels.

Conventionally, direct, indirect, or classical numerical MPPT methods are based on the generator power characteristics. This requires additional mathematical operation, prior knowledge of the initial conditions and involves iterative calculations. These control conditions are not usually satisfied in practice which causes the system to oscillate around the MPP leading to significant power loss. Current-voltage MPPT was introduced in [120] to enhance the controller complexity only estimated the MPP. Similarly, the example in [121] failed to deliver maximum extracted power to the load.

This chapter presents a low-cost, simple analogue MPPT controller independent of the system model which continuously tracks the MPP under varying operational conditions (i.e. flow rate). The innovative controller is based on the I-V characteristics of the power

system. It utilises a buck-boost converter to transform the load impedance to that of the source through a positive feedback mechanism on the load-side to achieve maximum power operation. The subsequent sections detail the principles of the operation, implementations and experimental results.

4.2 The Seesaw MPPT operation principles

This section describes the operation of the proposed MPPT controller. In its basic form, the controller incorporates positive feedback in conjunction with current-mode control. The theory proposed here renews interest in the applications of the well-known feed-forward control mechanism. The name Seesaw is given by the author of this thesis which reflects on the mechanism of the controller as being similar to that of the seesaw fun game (also known as a teeter-totter or teeterboard).

The advantages of using current-mode controlled DC-DC converter, whereby the converter is controlled to perform as a current source with a single-pole transfer function and output current control, are well known [122]. Positive-feedback control for MPPT optimisers have been considered for PV systems [123–125]. The control proposed in [124] requires the measurement of the input voltage and output current parameters. It controls the current of a current-mode controller to maintain the output voltage at a prescribed value, involving lengthy computation. A simplified version in [125] introduced feedback control of the output current only but does not overcome the control dependency on the generator module. That, alongside the controller response to rapid atmospheric variations, are major drawbacks.

The low-cost Seesaw MPPT controller presented here is independent of the generator module. The control of the MPPT optimiser is based on sensing a single output parameter (i.e. voltage). Considering a battery backup system whereby the MPPT output power is monitored for charge control and protection purposes, this is achieved at no

additional cost. This along with the utilisation of the I-V characteristics instead of power-characteristics reduces the control requirements for mathematical operation functions (e.g. multipliers). The impedance transformation is established through a buck-boost converter which maximises the power into any given load above or below the MPP.

4.2.1 The Seesaw MPPT control mechanism

In its basic form, the Seesaw controller combines a current-mode-controlled buck-boost converter with feed-forward of the output voltage to maximise the voltage into the load. As shown in Figure (4.1) the output voltage V_o is fed forward in a positive feedback mechanism. A feedback control parameter Δ is obtained from the difference between the current-mode controller voltage and the load voltage.

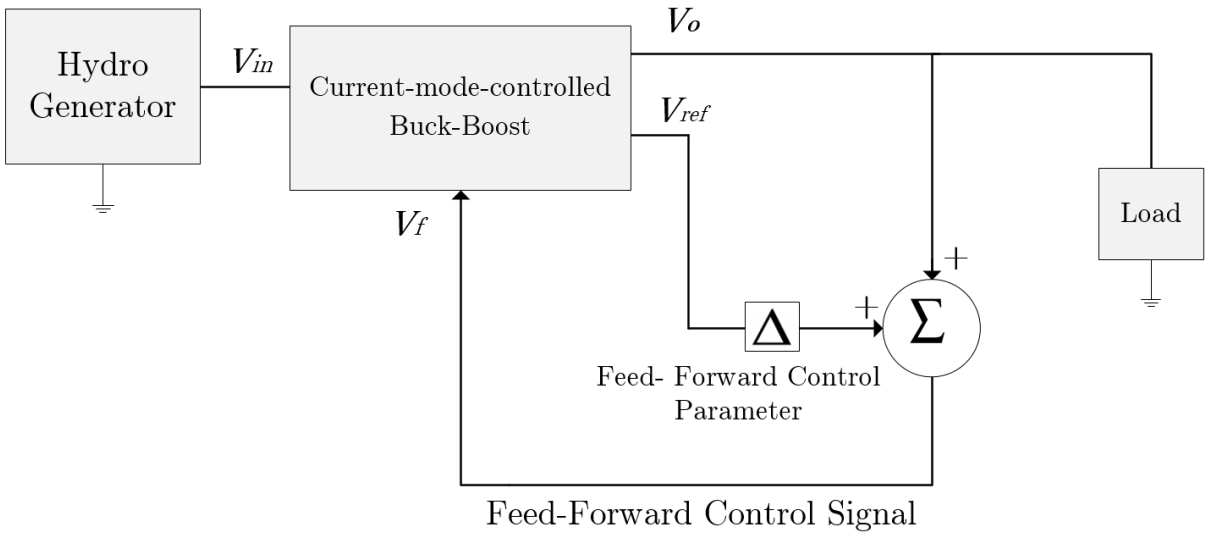

Figure 4.1: Block diagram showing the working principles of the proposed Seesaw MPPT controller.

The offset voltage initiates the start-up when the input power is applied. The output voltage (which is a portion of the buck-boost input voltage) increases as a result of feeding the output voltage forward by means of geometric progression (i.e. Equation (4.1)). The n-th term of the geometric sequence with an initial value V_{out} and a common ratio of r,

where $r \neq 0$, is defined in Equation (4.2).

$$\sum_{k=1}^{n} V_{out}\, r^{k-1} = V_{out}r^0 + V_{out}r^1 + V_{out}r^2 + ... + V_{out}r^{n-1} \tag{4.1}$$

$$V_{out_n} = V_{out}r^{n-1} \tag{4.2}$$

As n approaches ∞, when the absolute value of r is less than one for the series to converge, the sum of the sequence becomes:

$$\sum_{k=1}^{\infty} V_{out}\, r^{k-1} = \frac{V_{out}}{1-r}, \text{ for} |r| < 1 \tag{4.3}$$

It can be seen from Equation (4.3), that the summation of feeding the voltage forward could be as much as $10^2(V_{out})$ for $r = 0.99$. A block diagram of the control system mechanism is shown in Figure (4.2), where a buffer amplifier is used to feed the output forward. The voltage gain is given by Equation (4.4) where, the buffer amplifier gain A is unity and B is the fed-forward voltage.

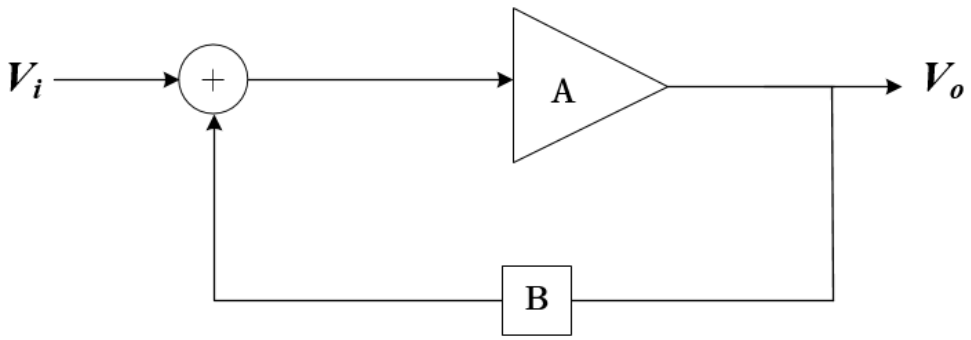

Figure 4.2: Block diagram of the proposed Seesaw MPPT control system mechanism

$$G = \frac{V_o}{V_i} = \frac{A}{1-AB} \tag{4.4}$$

From Equation (4.4),where, V_i and V_o represent the Seesaw input and output voltages, respectively, the controller gain is infinite when $AB > 1$. Given that the output of positive

feedback is to augment changes, even small perturbations result in great change.

As the output voltage V_{out} increases towards V_{mpp}, the current-mode controller input voltage V_{in} reduces as a result. Beyond V_{mpp}, the controller cannot draw any more voltage into the load (i.e. $V_{in} << V_{out}$), so the operation point settles at the maximum voltage V_{mpp}.

An outline of the proposed Seesaw controller circuit diagram is shown in Figure (4.3). A buffer amplifier with unity gain is used to feed the output voltage forward. The Zener diode introduces the offset voltage to initiate the operation. As the controller output voltage increases with respect to the offset voltage, the load voltage rises accordingly. The voltage is controlled towards V_{mpp} beyond which the controller cannot supply any more voltage. The closed-loop configuration, with the effect of the control parameter Δ, controls the feed-forward operation. The control parameter changes polarity and forces the operation point back to V_{mpp}. This is achieved by means of managed unstable feedback.

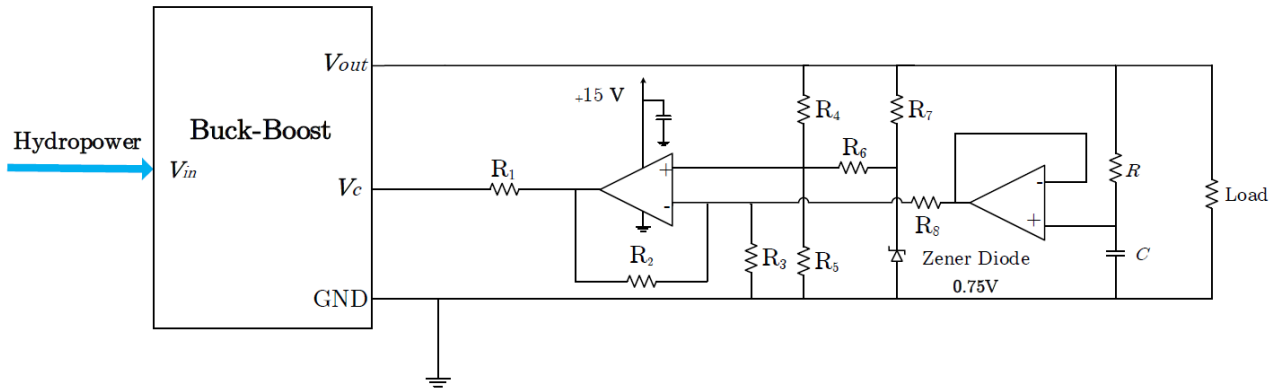

Figure 4.3: Outlines of the proposed Seesaw MPPT controller using a buffer amplifier to feed the output voltage forward.

The voltage response of the feed-forward can be written as in Equation (4.5), where v_f is the fed-forward voltage, Δ is the positive feedback control parameter and RC is the time constant for the positive feedback.

$$v_f(t) = (v_f(t) + \Delta)(1 - e^{\frac{-t}{RC}}) \tag{4.5}$$

The voltage response as A function of time can be further simplified into Equation (4.6). The controller response to an impulse function is shown in Figure (4.4). Evidently the controller response increases rapidly with time, without bound from a finite initial condition for $\pm\Delta$.

$$v_f(t) = \Delta(e^{\frac{t}{RC}} - 1) \tag{4.6}$$

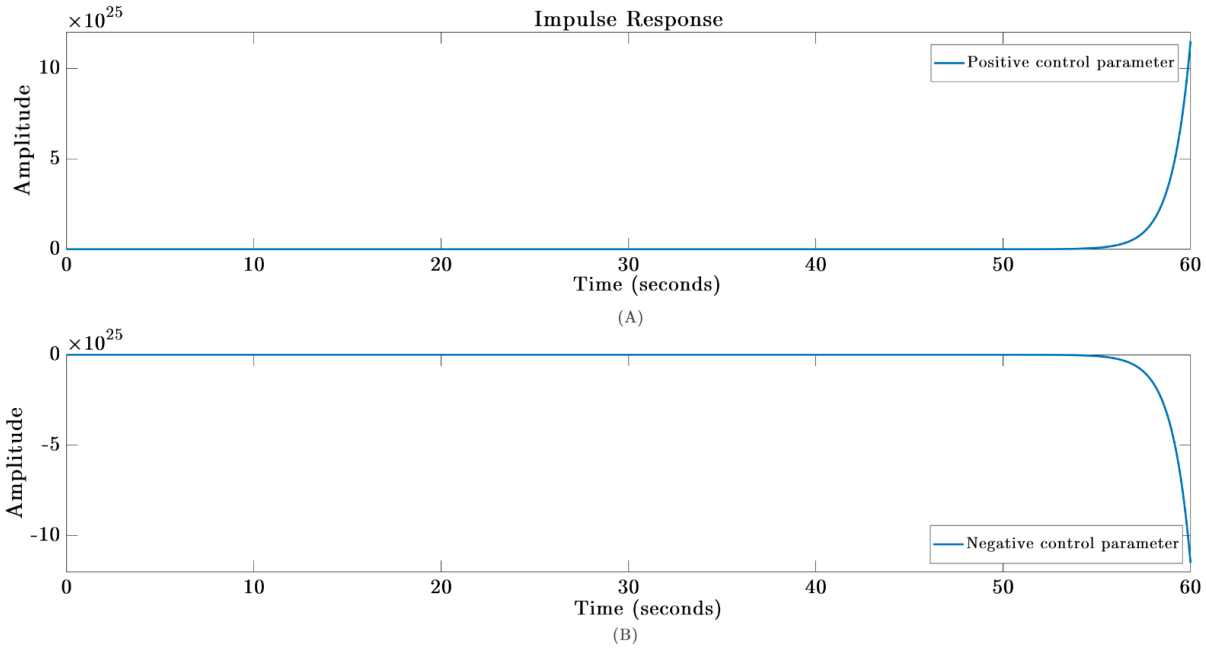

Figure 4.4: The proposed Seesaw MPPT control system impulse responses over time, A) positive control parameter ($+\Delta$). B) non-positive control parameter ($-\Delta$).

4.2.2 The utilisation of a buck-boost converter for impedance transformation

To ensure maximum power is harvested from the generator, the load impedance is transformed to reflect that of the generator by using an intermediate DC-DC converter. A buck-boost DC-DC converter is selected because it maximizes the power into any given load above or below the MPP.

At a steady-state continuous mode operation, the relationship between the converter equivalent input impedance R_{in} as seen by the MHPG and the load impedance R_L with respect to the buck-boost input V_{in} and output voltage V_{out} is given in Equation (4.7), whereby the relation between the generator voltage V_{in} and the converter output voltage V_{out}, governed by the duty cycle D, is given in Equation (4.8).

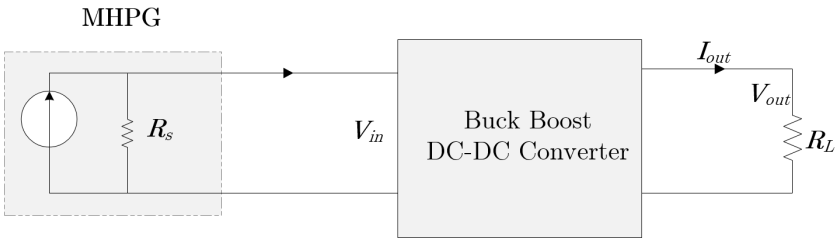

Figure 4.5: Outlines of the impedance transformation through a buck-boost converter.

$$R_{in} = \left(\frac{V_{in}}{V_{out}}\right)^2 R_L \tag{4.7}$$

$$\frac{V_{out}}{V_{in}} = \frac{D}{(1-D)} \tag{4.8}$$

Equation (4.7) shows that for a given load resistance, the equivalent impedance depends greatly on the converter output voltage. Thus, by controlling the output voltage V_{out}, and hence R_{in}, the load impedance can be transformed to reflect that of the source. The process of the load impedance transformation R_L is defined in Equation (4.9).

$$R_L = \begin{cases} R_s, & \text{at MPP} \\ 0 \leq R_L < R_s, & V_{out} >> V_{in} \\ R_s < R_L \leq \infty, & V_{out} << V_{in} \end{cases} \tag{4.9}$$

The equivalent impedance is therefore a continuous function of the duty cycle D ranging from 0 to ∞. The load impedance R_L can then be transformed from either low

or high impedance to R_s. This guarantees that under any operational conditions the controller coincides with the MPP. The control range of the equivalent impedance R_{in} for the load impedance transformation is shown in Figure (4.6).

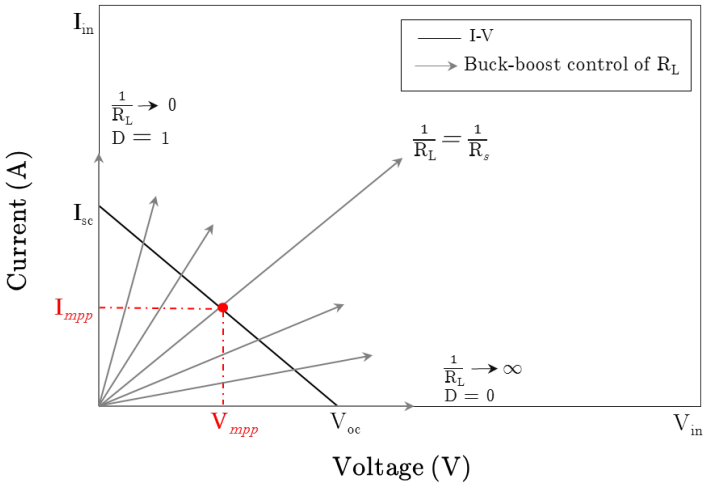

Figure 4.6: The buck-boost converter load impedance transformation control range of the equivalent impedance R_{in} in relation to the generator I-V characteristics.

4.2.3 Principles of the output parameters control method

MPPT controllers that optimise the generated power on the supply side (as shown in Figure 4.7) fail in delivering maximum harvested power to the load. This is due to power losses at the power conversion stage. For maximum utilisation efficiency, it is therefore important to ensure that most power extracted from the supply is delivered to the load. This has made it important to investigate the use of load parameters instead, whereby the power is optimised into the load. A study on using single output parameter MPPT control reported improved efficiency [19]. The major drawback of the load-side MPPT developed in [16] was that the load power was proportional to its current. That led to maximising the load current rather than the generator power. Similarly load-voltage MPPTs presented in [21,22] were based on the power characteristics, involving an iterative process to calculate the instantaneous power, increasing the controller complexity and

tracking time.

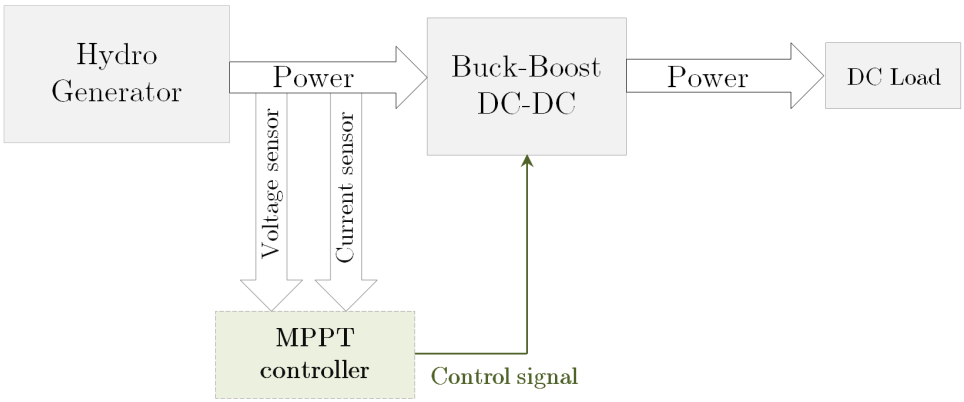

Figure 4.7: Block diagram of the conventional source-side MPPT method.

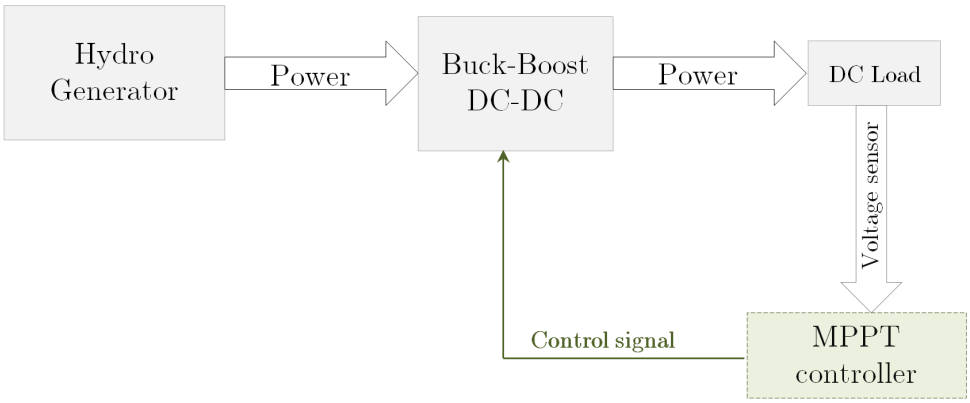

Figure 4.8: Block diagram of the proposed load-side MPPT method.

The MPPT proposed here is based on load-side MPP optimisation as shown in Figure (4.8), whereby power of the intermediate stage (DC to DC converter) is maximised into any given load. This approach enhances the system efficiency because optimum power delivery from the supply through the intermediate power converter stage to the load is guaranteed. Only a single sensor is therefore required to monitor the load voltage. The utilisation of the generator I-V characteristic eliminates the need for additional operational circuitry to calculate the power, which improves the controller tracking response.

4.3 Experimental implementation of the Seesaw MPPT

4.3.1 The overall layout of the Seesaw implementation

Figure (4.9) shows the implementation of the controller. The main components of the experimental set-up are the off-the-shelf 4-32 to 0.8-32V, DC-to-DC buck-boost non-inverting converter and the indoor automated hydropower emulator. A buck-boost was used in a current-mode control with the current set at its maximum. That matches the hydro generator module internal impedance to any given load. To maximise the voltage into the load, the output of the current-mode-controlled buck-boost converter was controlled by the Seesaw MPPT controller. A USB-voltmeter was used to observe the load and the converter input voltages. Here, a 50 V, 1.8 W MHPG was incorporated into the hydropower emulator (detailed previously in section 3.3.1).

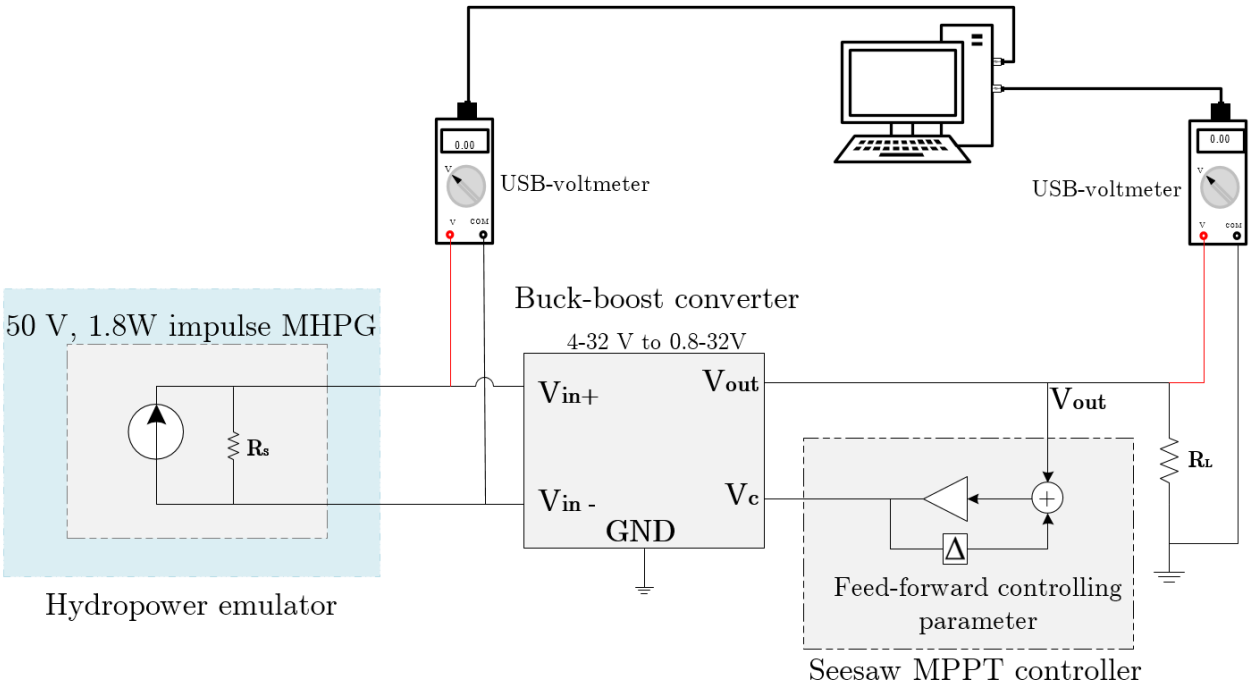

Figure 4.9: The layout of the Seesaw MPPT controller implementation.

4.3.2 Main components specifications

This section reports on the specifications of the main components. These are gathered from practical testing carried out in the laboratory and incorporated into the hydropower emulator introduced previously in section (3.3.1).

4.3.2.1 A 1.8 W impulse MHPG

The specifications of the MHPG used in this experiment are tabulated in Table (4.1). The I-V and P-V characteristics incorporated in the hydropower emulator at the maximum flow are shown in Figure (4.10).

Table 4.1: The characteristics of the 1.8W MHPGs at the maximum flow rate.

Parameter	**Value**
Short Circuit Current I_{sc}	0.165 A
Open Circuit Voltage V_{oc}	44.5 V
Maximum Power Point P_{max}	1.8 W
Voltage at Maximum Power Point V_{MPP}	22 V
Characteristic Impedance R_s	270 Ω

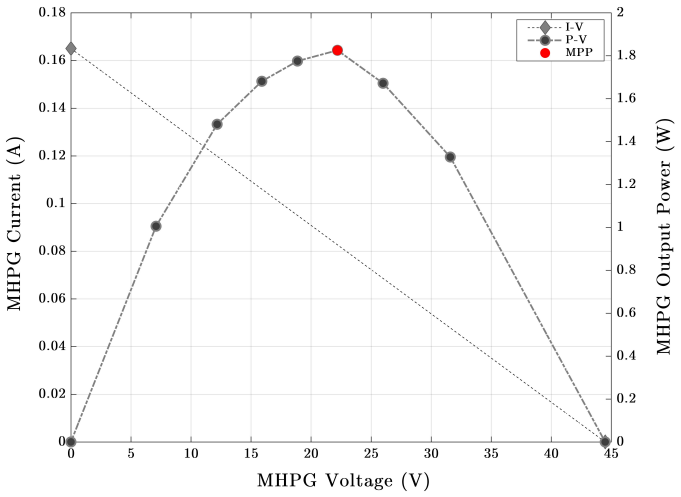

Figure 4.10: The MHPG I-V and P-V characteristics at the maximum water flow.

4.3.2.2 8A automatic buck-boost converter

The buck-boost converter transfers the power to the load above and below the supplied source voltage. It provides control of the current as well as voltage through built-in potentiometers. By adjusting the current potentiometer, the current was set at a maximum for current-mode operation. The power characteristic curve as a function of the duty cycle of the converter incorporated into the hydro power emulator at a resistive load of 25 Ω was obtained at the maximum flow rate as in Figure (4.11). The output power of the converters in relation to its input and output voltages was also found as captured in Figure (4.12). The MPP measured is indicated in red. It is worth mentioning that a portion of the generated hydropower is dissipated through the conversion stage.

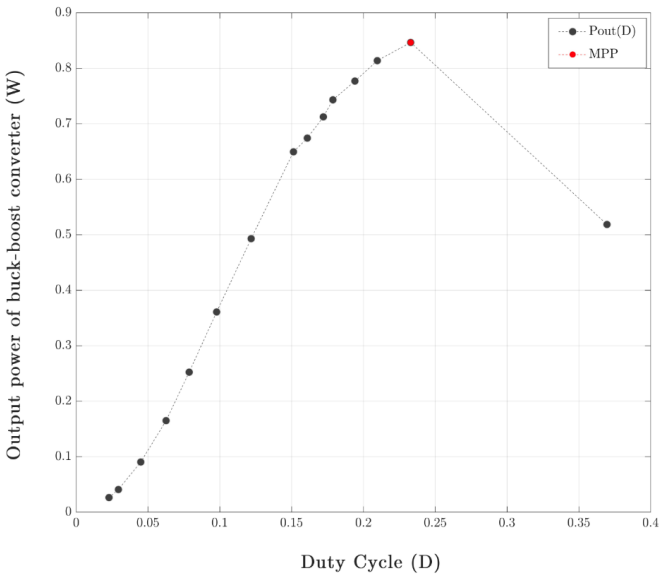

Figure 4.11: The buck-boost output power against the duty cycle at the maximum water flow.

From Figures (4.11) and (4.12), it can be seen that the output power of the buck-boost converter increased with decreasing input voltage, towards the MPP. It is noticeable that below the MPP the converter's input to output voltage ratio dropped towards zero. That indicates that the converter has supplied most of the available voltage from the source.

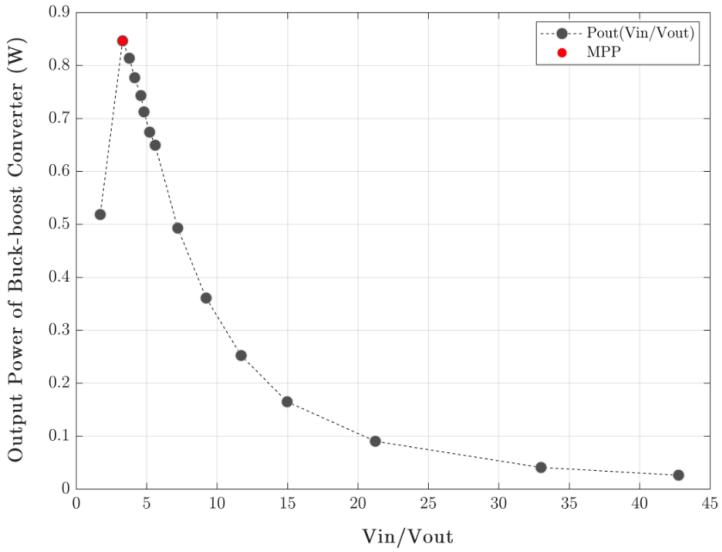

Figure 4.12: The experimental output power of the buck-boost in relation to the converter input V_{in} and output voltage V_{out} at the maximum water flow.

The MHPG's equivalent resistance in ohms (given by Equation 4.7) in relation to the converter output power, measured at the load, and $\frac{V_{in}}{V_{out}}$ is shown in Figure (4.13). The MPP transferred to the load is indicated in red.

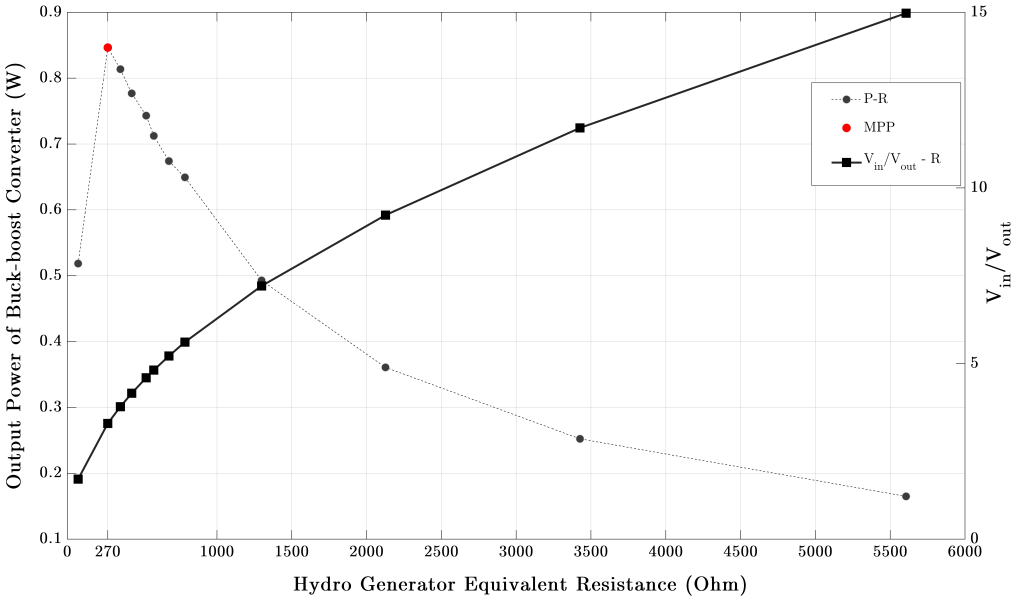

Figure 4.13: The buck-boost output power in relation to the converter input V_{in} and output voltage V_{out} at the maximum water flow.

From these findings shown in Figure (4.13) considering the P-R curve, the buck-boost converter transformed the load impedance (25 Ω) to that of the MHPG (270 Ω) at the MPP. Increasing the output voltage has transformed the operation point towards the equilibrium point. That indicates a decrease in the input voltage so that the converter can no longer supply any more voltage beyond V_{mpp}. Thus, the operational point converged to the neighbouring point around the MPP. That is the main feature of using a buck-boost converter in current-mode configuration for the proposed Seesaw MPPT optimiser.

4.3.3 Empirical results of the Seesaw MPPT optimiser

This section reports the empirical findings of the Seesaw controllers conducted on the laboratory hydraulic emulator. A resistive load of (50Ω) was used as a load. Figure (4.14) shows the measurement of the overall operation of the load impedance transformation to R_s in relation to the Seesaw input-to-output voltage at the maximum flow rate. The output power at the load in corresponding to the load impedance transformation was calculated and is shown in Figure (4.15) against time. The main control parameters measurements that govern the impedance transformation, V_{in} and V_{out} are captured against time in Figure (4.16). It is worth mentioning that the time steps are used as to illustrate the operation process. The measurements were collected through USB multi-meters.

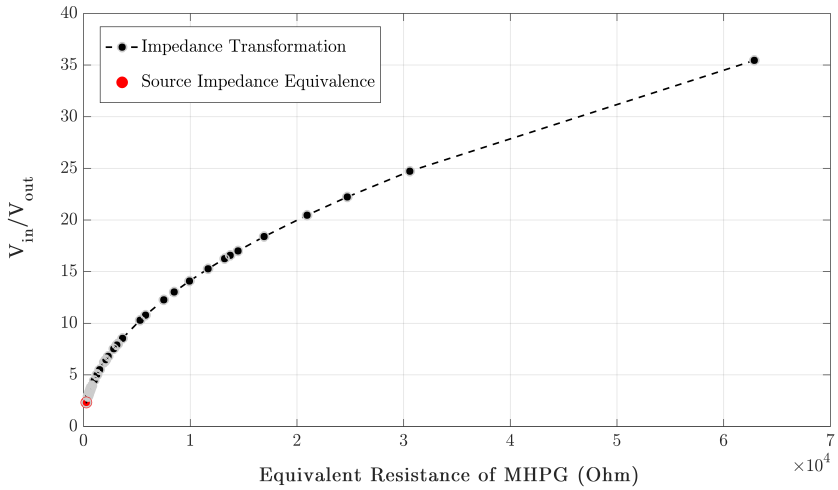

Figure 4.14: The experimental results of the equivalent impedance transformation in relation to the Seesaw controller input-to-output voltage $\frac{V_{in}}{V_{out}}$ at the maximum flow rate.

4.3.3.1 Load impedance transformations at different flow rates

This section reports the results of the load impedance transformation and MPPT control at various flow rates. From Figure (4.14) it can be seen that the equivalent impedance seen by the MHPG was transformed to R_s by controlling the buck-boost's output voltage in relation to the MHPG output power. Figures (4.15) and (4.16) provide more insight into the controlling process. The load transformation and the resulted load power over time were measured and captured in Figure (4.15). Similarly, Figure (4.16) shows the Seesaw control of the operational point from the maximum available voltage V_{oc} towards V_{mpp} as a function of time. That was achieved by feeding the output voltage forward which in turn increased the load voltage. As the load voltage approached V_{mpp} at the MPP, the load impedance was then transformed towards that of the MHPG (270Ω), at which the generator had supplied most of its available voltage. The load voltage dropped by $5mV$ below V_{mpp}. The operation was then automatically corrected back to V_{mpp} at MPP. The principles were proved at different flow rates as shown in Figures (4.17) , (4.18) ,(4.19) and (4.20).

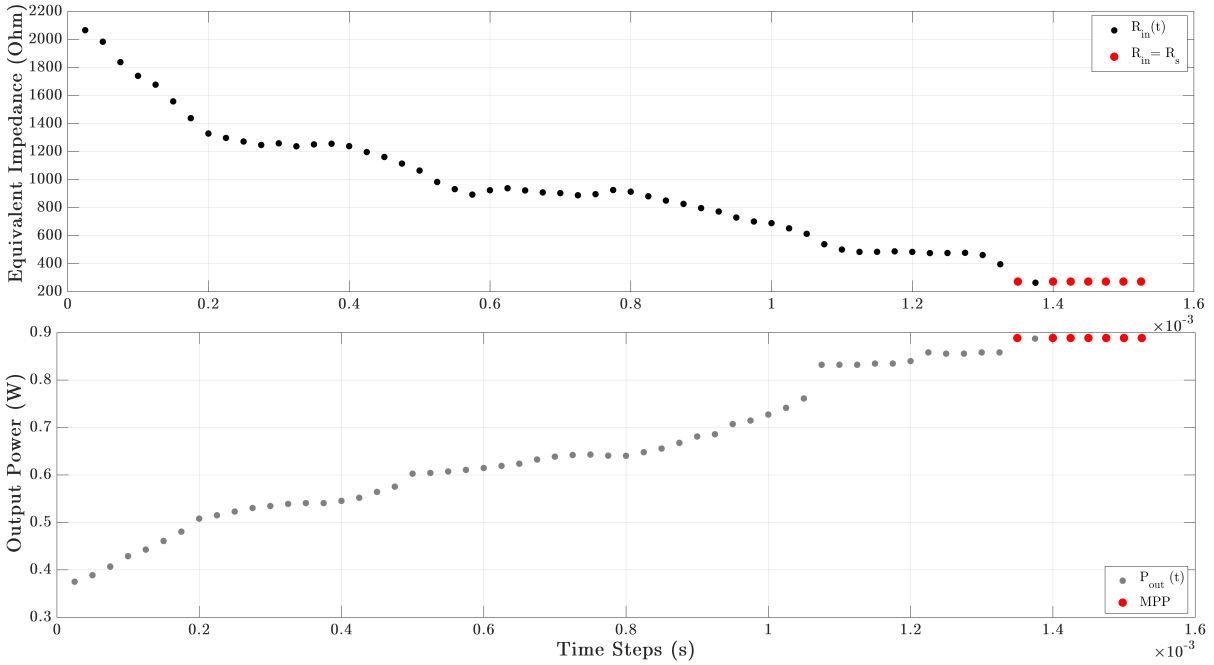

Figure 4.15: The experimental results of transforming the load equivalent impedance and the corresponding output power against time at the maximum flow rate Q_1.

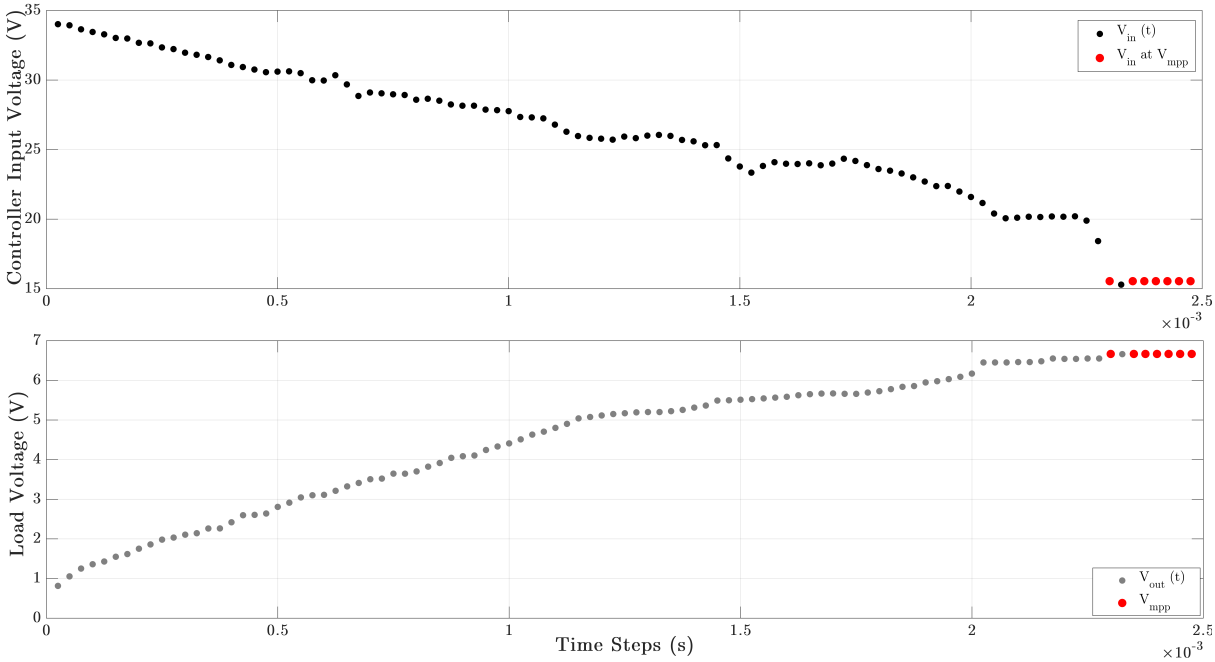

Figure 4.16: The experimental results of the Seesaw MPPT controller input and output voltages against time at the maximum flow rate Q_1.

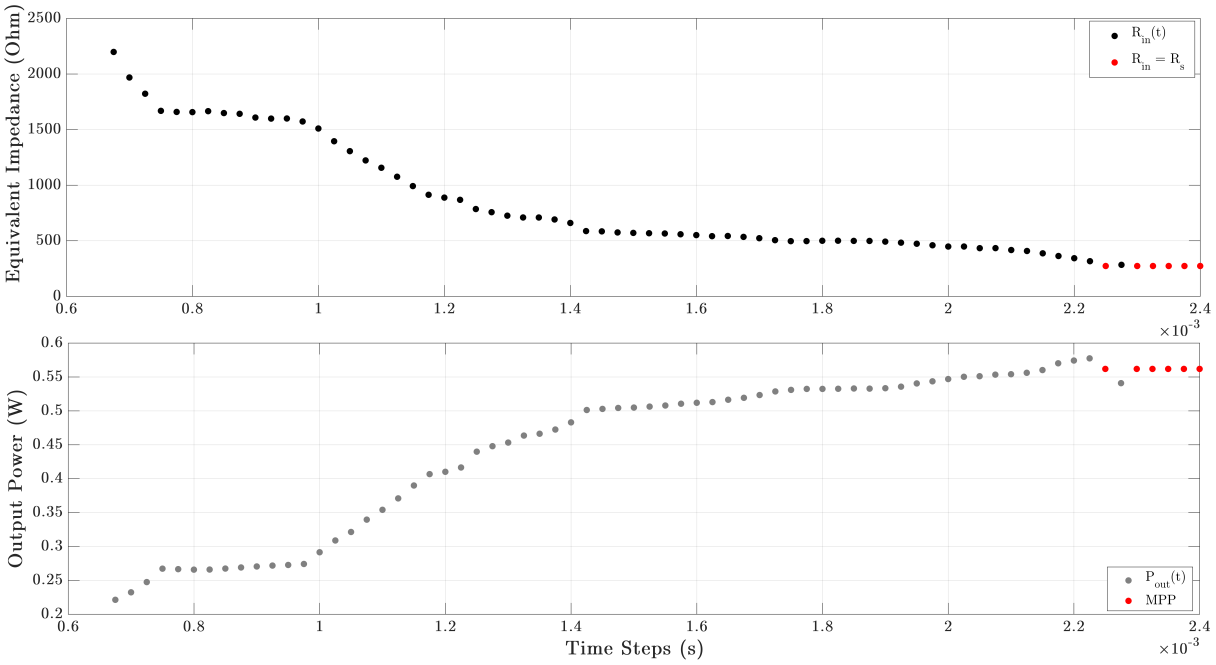

Figure 4.17: The experimental results of transforming the load equivalent impedance and the corresponding output power against time at a flow rate of Q_2, $Q_2 < Q_1$.

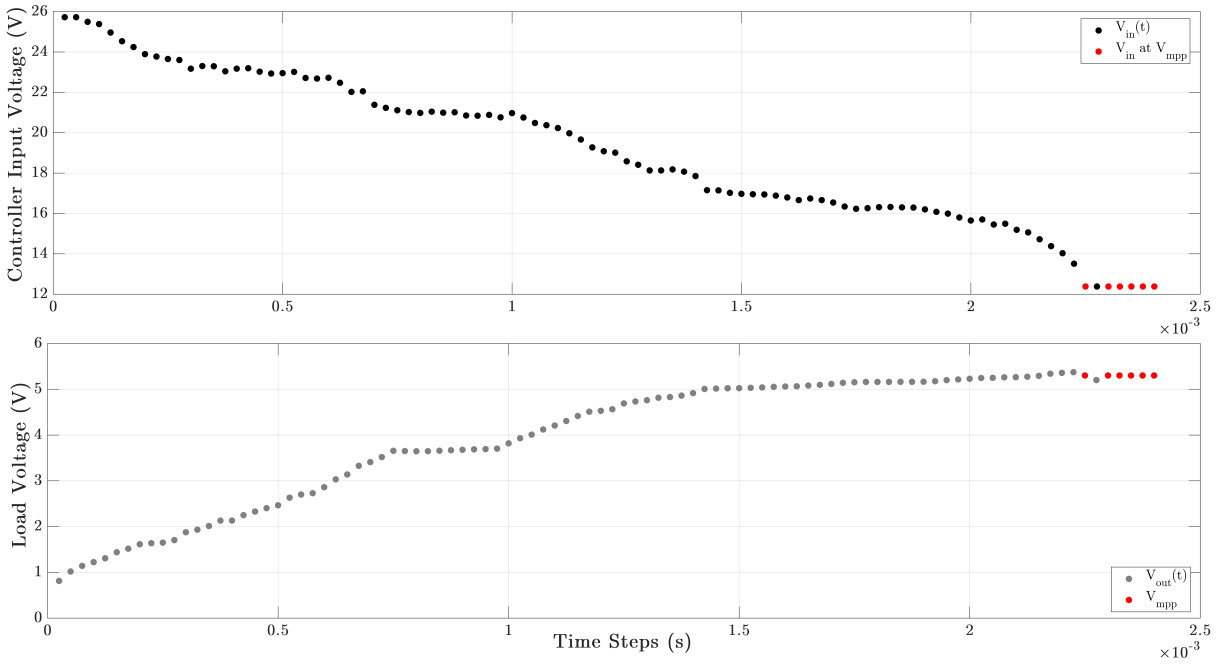

Figure 4.18: The experimental results of the Seesaw MPPT controller input and output voltages against time at a flow rate of Q_2, $Q_2 < Q_1$.

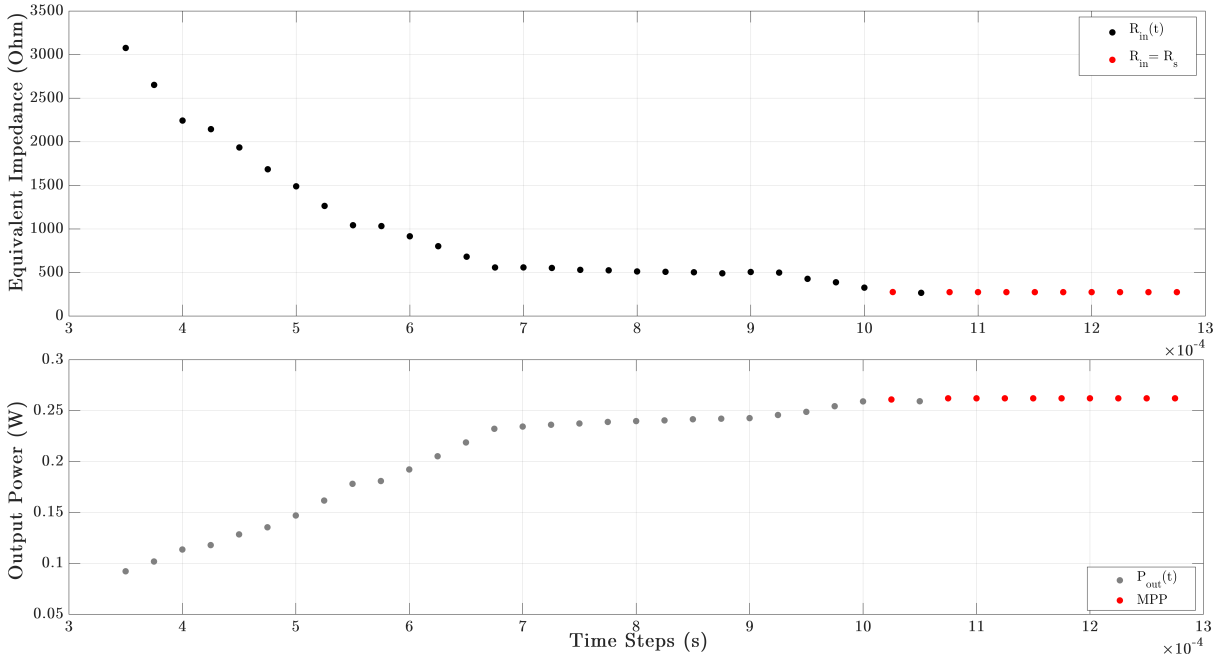

Figure 4.19: The experimental results of transforming the load equivalent impedance and the corresponding output power against time at the minimum flow rate.

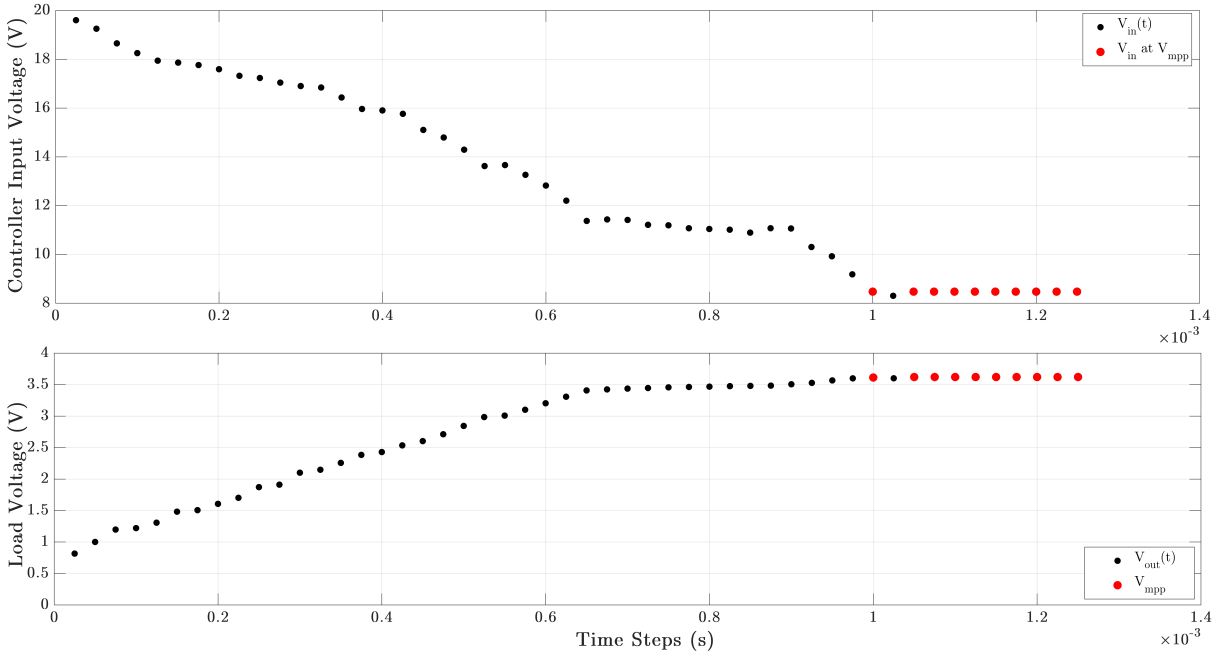

Figure 4.20: The experimental results of the Seesaw MPPT controller input and output voltages against time at the minimum flow rate.

4.3.3.2 Seesaw control operation at different power levels

The previous section reported results of the proposed Seesaw controller in tracking the MPP at various water flow rates individually. This section reports the results on MPPT when the operational point changes with changing power levels (i.e. varying flow rate). It presents the results on tracking the MPP from higher to lower power levels and vice versa.

Figure(4.21) shows the output power of the Seesaw controller when the water flow rate changed from a higher level Q_1 to a lower level Q_2 against the controller's output-to-input voltage ratio. The findings demonstrate the controller tracking of the MPPs under changing operational conditions. Initially, the operational point was controlled towards the MPP available at flow rate of Q_1 (indicated in Figure (4.21) as point **A**). Following a sudden decrease to a flow rate of Q_2, the output power decreased (point **B**). The controller successfully tracked the MPP available at Q_2 (point **C**). Figures (4.22) and (4.23) further show the corresponding controlling process in terms of the load voltage and impedance.

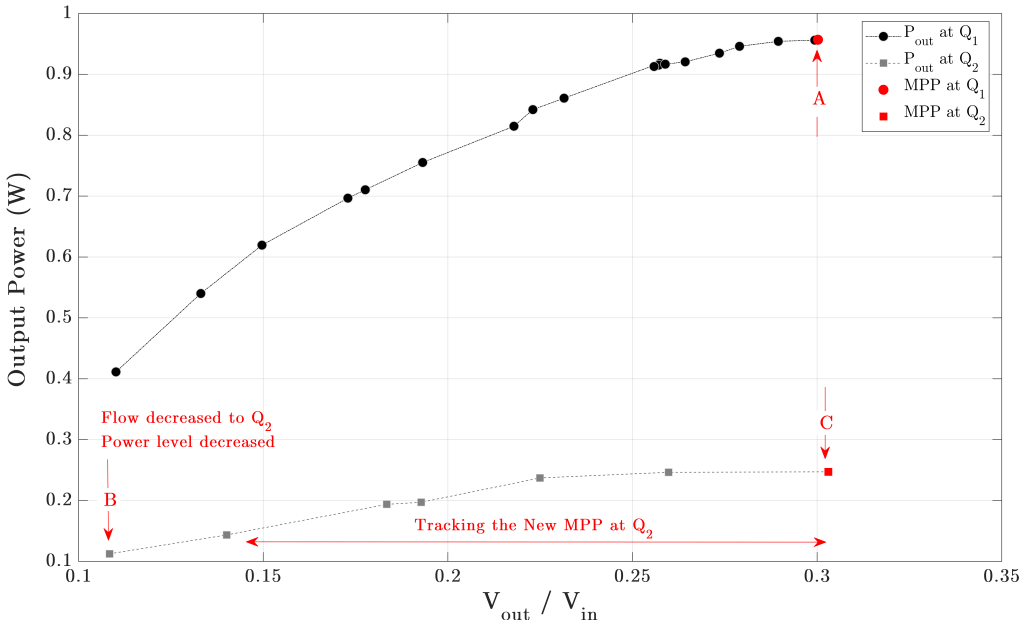

Figure 4.21: The Seesaw MPPT controller output power at a low flow rate of Q_2 from a higher flow rate of Q_1 ($Q_1 > Q_2$) as a function of the controller output-to-input voltage.

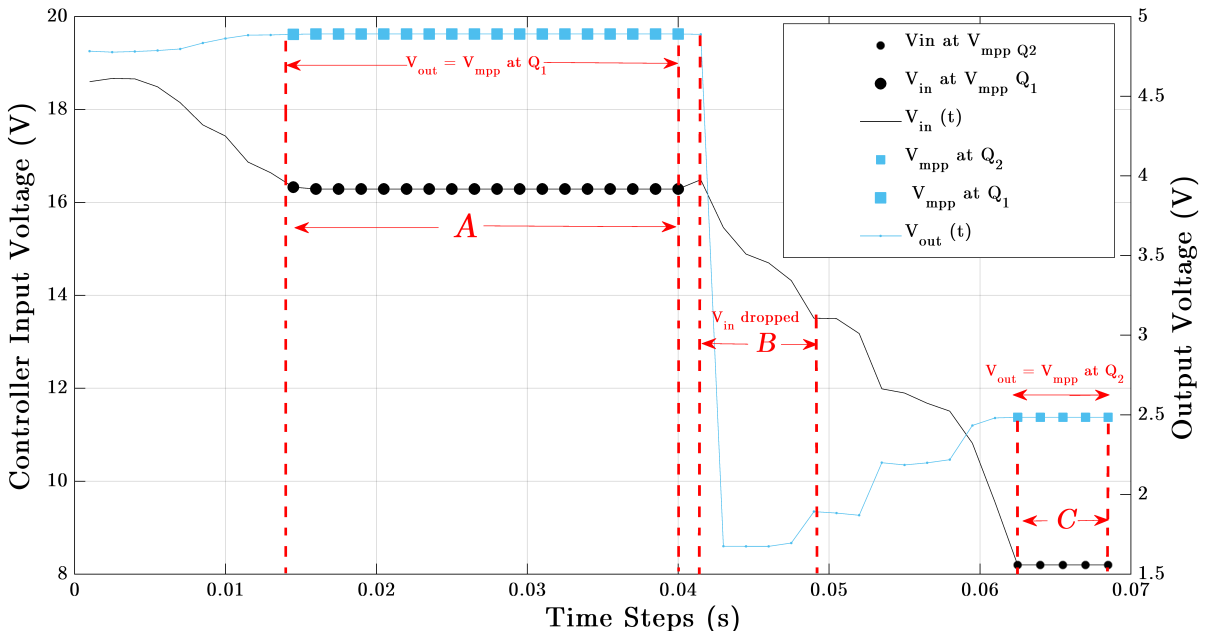

Figure 4.22: The controller input and output voltages in responding to the MPPT control operation at a flow rate of Q_2 from a higher flow of Q_1 ($Q_1 > Q_2$) against time.

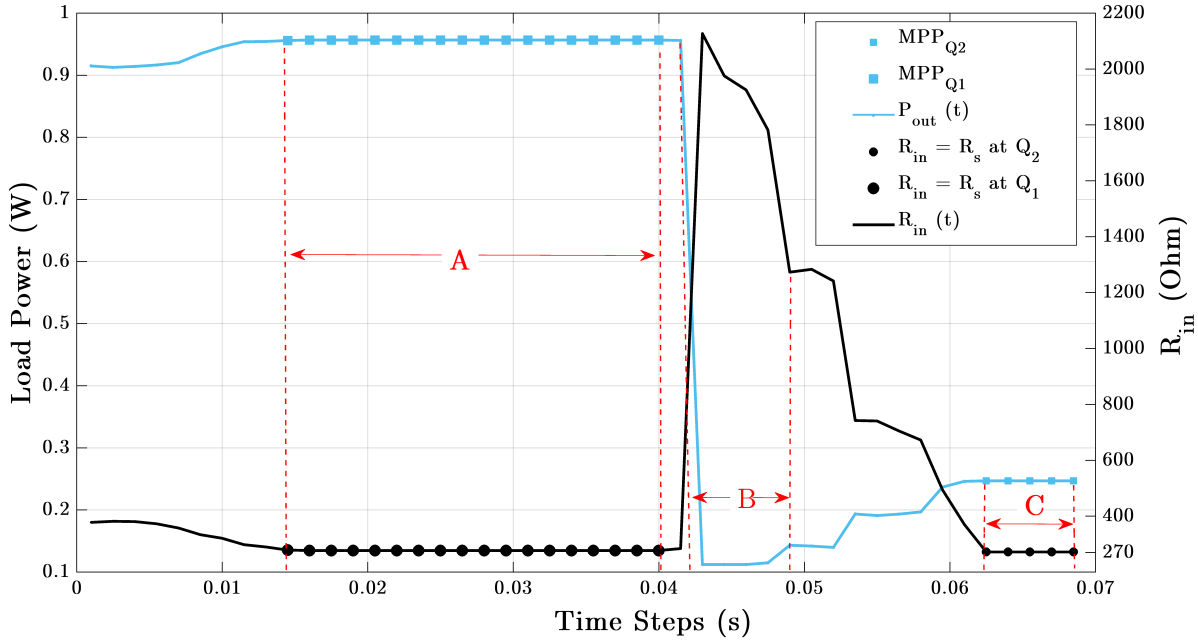

Figure 4.23: The controller output power and input equivalent impedance in responding to the MPPT control operation at a flow rate of Q_2 from a higher flow at Q_1 ($Q_1 > Q_2$) against time.

From Figures (4.22) and (4.23), region **A** indicates when the output voltage was initially controlled at V_{mpp} relative to the MPP_{Q_1}. However, a sudden decrease in the flow rate to Q_2 resulted in a drastic drop in V_{out}, hence P_{out} (region **B** in Figure (4.22)). In response to that, the controller tracked MPP_{Q_2} by increasing V_{out} towards V_{mpp} relative to MPP_{Q_2}. The power delivered to the load raised accordingly (beyond region **B**). The operational point was then matched to the MPP_{Q_2}, when the controller input impedance reduced to R_s (i.e. 270Ω) (region **C**).

As well as, the Seesaw tracking control of the MPP from a low to a higher water flow levels was validated and captured by the findings in Figure (4.24). In this example, the MPP was tracked from a low power level MMP_{Q_2} to a higher power level MMP_{Q_1}. That was achieved by feeding the output voltage forward, which led to increasing the load voltage towards V_{mpp}. Ultimately, the operational point coincided with MMP_{Q_1} when the load impedance was transformed to R_s (region **C** in Figure(4.26)).

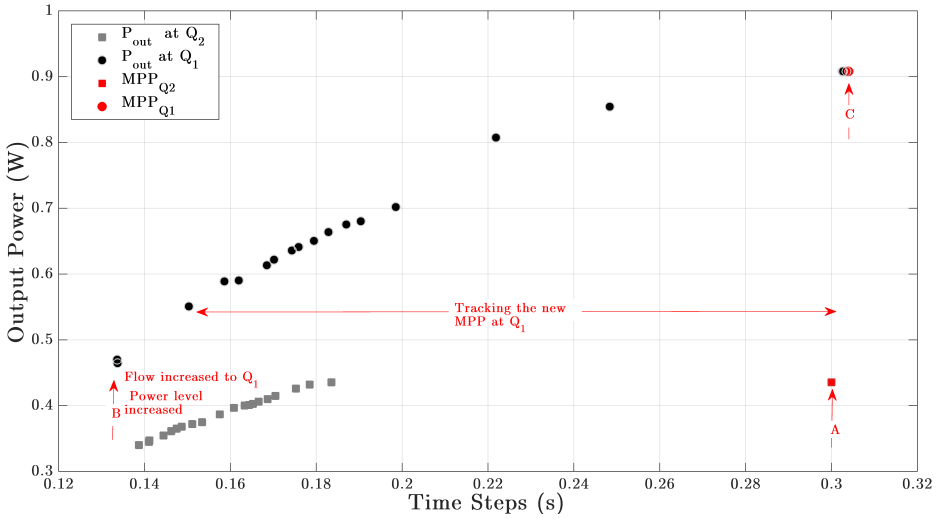

Figure 4.24: The Seesaw MPPT controller output power at a high flow rate Q_1 from a lower flow rate of Q_2 ($Q_1 > Q_2$) as a function of the controller output-to-input voltage.

The Seesaw controller tracking process of the MPP when the power increased from a low level at Q_2 to a higher level at Q_1 is further illustrated by findings captured in Figures (4.25) and (4.26). Whereas Figure (4.25) shows the controller input and output

voltage during the process as a function of time, Figure (4.26) reports the corresponding load power and equivalent impedance.

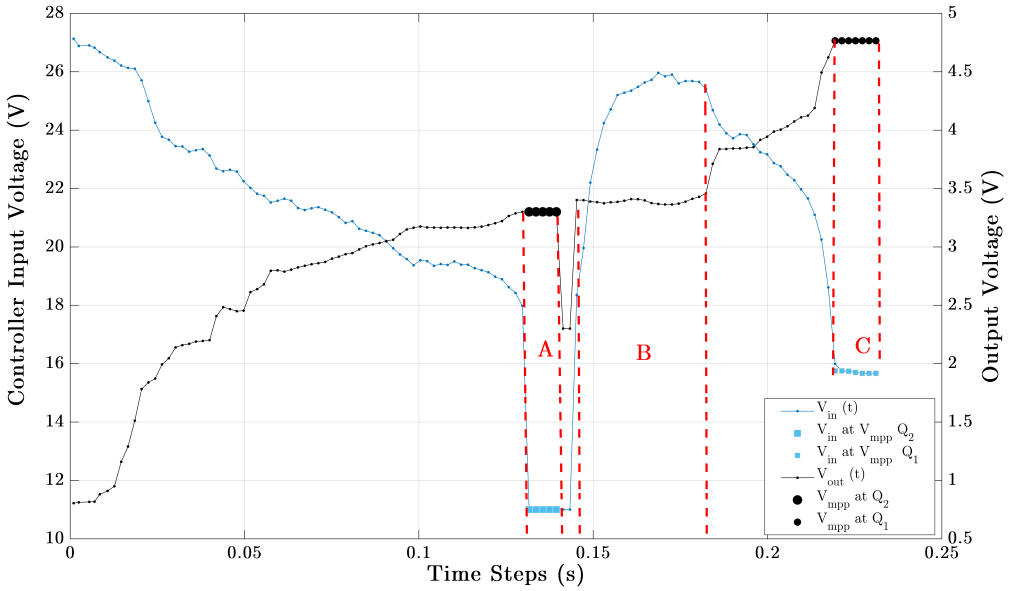

Figure 4.25: The input and output control voltages in corresponding to MPPT control operation at a flow rate of Q_1 from lower flow of Q_2 ($Q_1 > Q_2$) against time.

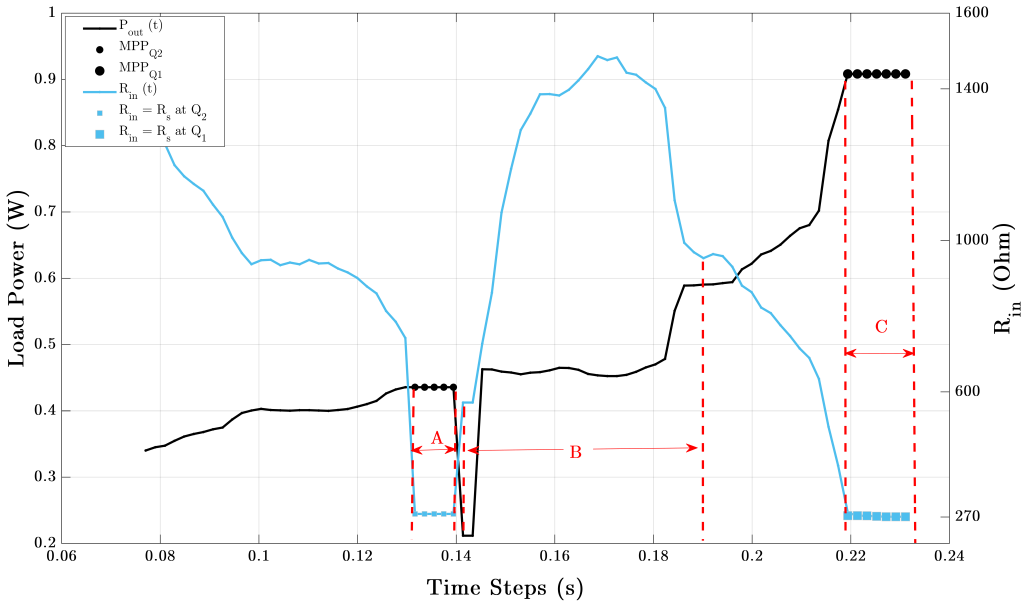

Figure 4.26: The controller output power and input equivalent impedance in corresponding to MPPT control operation at a flow rate of Q_2 from higher flow at Q_1 ($Q_1 > Q_2$) against time.

4.3.3.3 Seesaw for battery charging control

As well as MPPT control, the proposed controller features load power regulation. This is made possible by the load-side, constant-voltage control mechanism here, the controller can set a limit to the voltage, and hence the electrical current, drawn to the load. This can have an effective role in battery charging regulation applications. Thus, the proposed controller can as well match the battery's voltage to that of the generator through the same principles explained earlier in this chapter for the load impedance transformation. That offers a means of overcharging protection achieved by controlling the battery to be charged within its maximum capacity.

Figure (4.27) shows the output current and voltage in relation to the input voltage when the controller was set to regulate the charging voltage to 4 V. Similarly, findings captured in Figure (4.28) resulted from regulating the output voltage at a lower level (2V(0.079A)). It is worth mentioning that for health and safety concerns a resistive load was use to prove the principles.

The results demonstrate the controller regulation of the output parameters (I_{out} and V_{out}) over a wide range of input voltages. Whereas, for a maximum charging voltage of $V_{C_{max}}$ the output voltage V_{out} regulation range with respect to the input voltage V_{in} is given by Equation (4.10), the output current I_{out} control for a maximum charging current of $I_{C_{max}}$ can be written as in Equation (4.11).

$$0 < V_{out}(V_{in}) \leq V_{C_{max}} \tag{4.10}$$

$$0 < I_{out}(V_{in}) \leq I_{C_{max}} \tag{4.11}$$

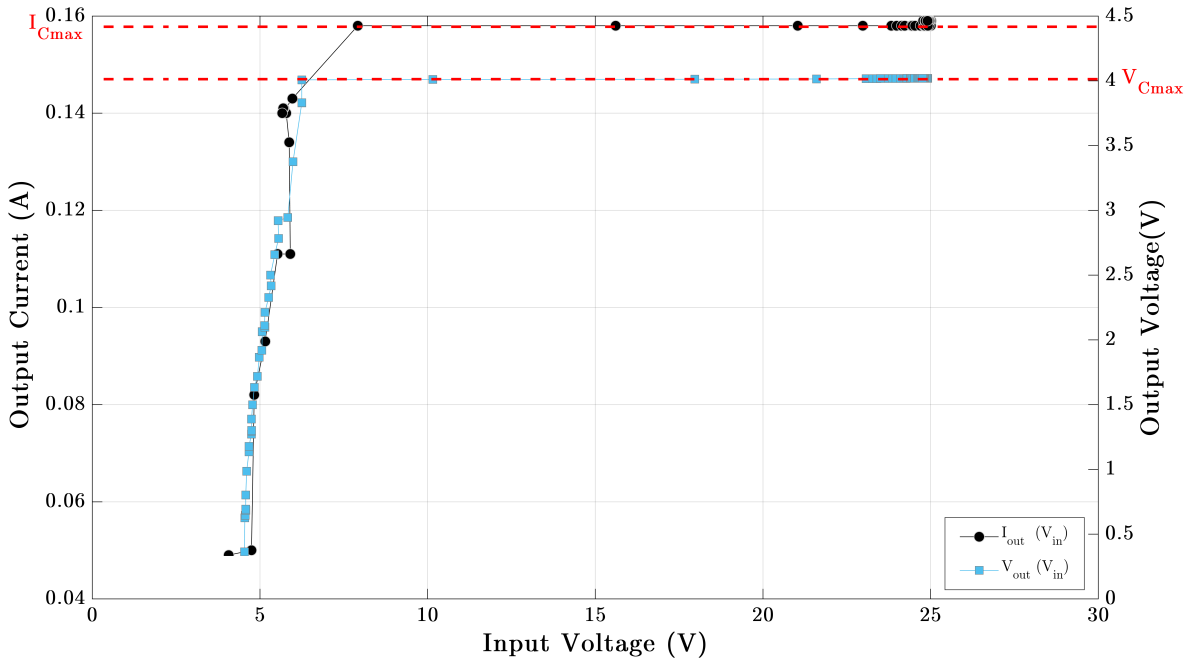

Figure 4.27: The regulator output current and voltage as a function of the input voltage resulting from regulating the load voltage to $4V$.

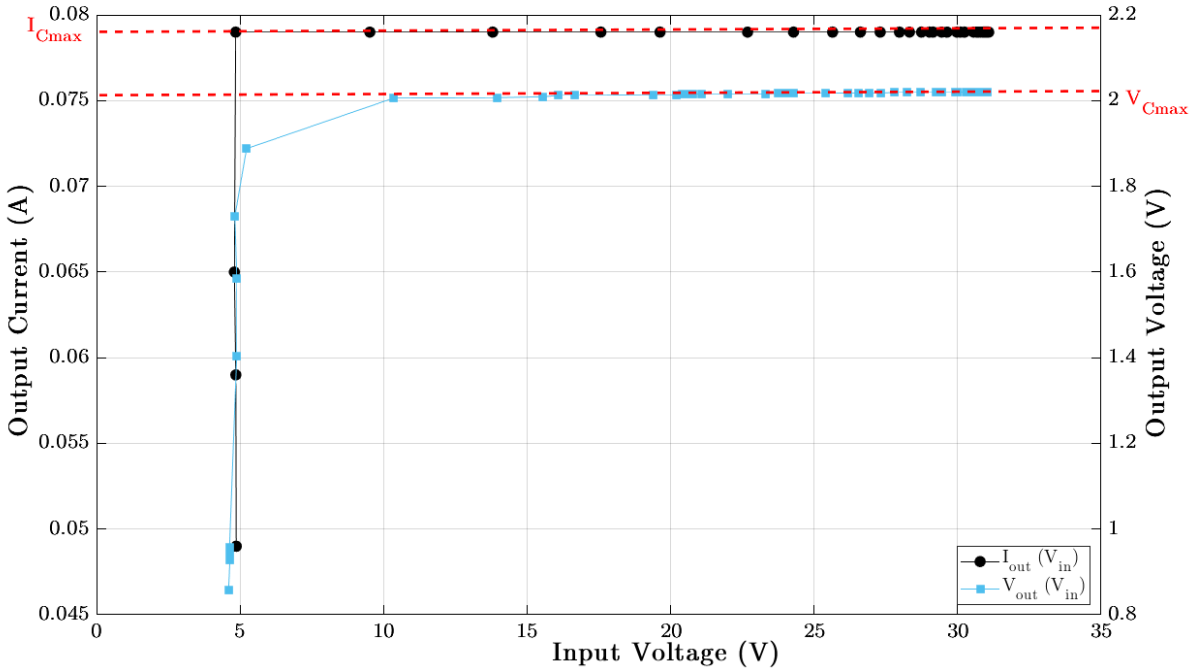

Figure 4.28: The regulator output current and voltage as a function of the input voltage resulted from regulating the load voltage to $2V$.

Having reported on the controlling mechanism for load voltage regulation, a testing trial for a battery charge was conducted. Findings in Figure (4.29) report the input and output voltages when $V_{C_{max}} = 3.073$ against time. The output voltage regulation with respect to $V_{C_{max}}$ is in indicated in the figure. Also, the output current regulation was also investigated in a different charging scenario and shown in Figure (4.30). In both cases the controller demonstrated control of both voltage and current load.

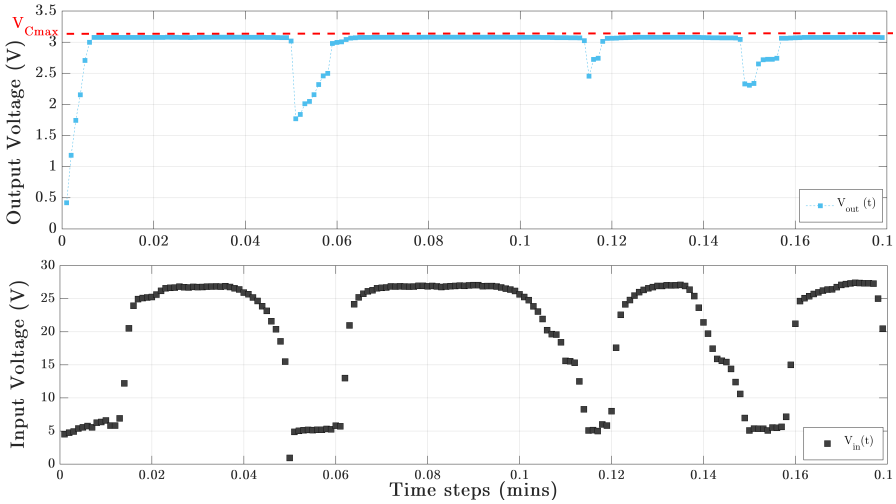

Figure 4.29: The empirical results of the output voltage regulation in relation to $V_{C_{max}}$ and the corresponding input voltage against time.

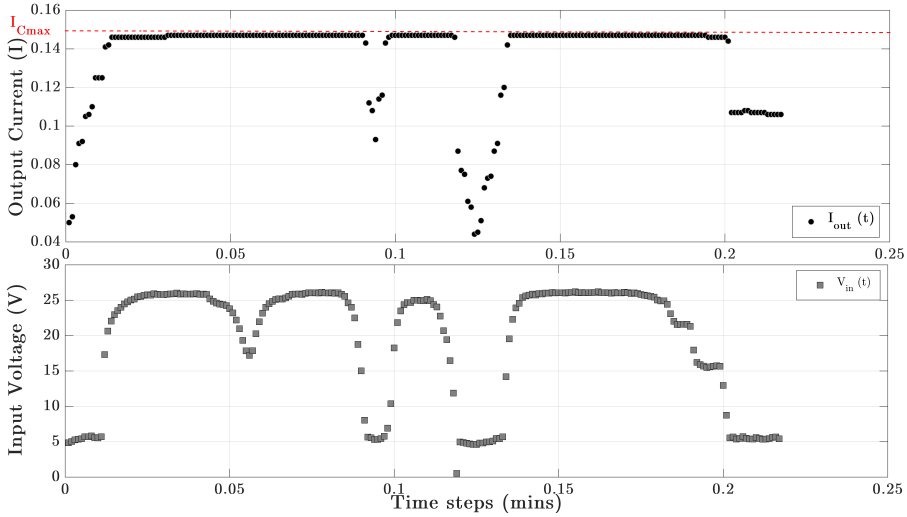

Figure 4.30: The empirical results of the output current regulation in relation to $I_{C_{max}}$ and the corresponding input voltage against time.

4.4 Conclusion

This chapter presented a novel constant-voltage load-side MPPT controller based on I-V characteristics of the source generator. The chapter began by detailing the operational principles of the proposed Seesaw MPPT optimising controller. In particular, the feed-forward mechanism under current-mode control operation for optimal operation was studied.

Also, the control system design was discussed. That included: the utilisation of the I-V characteristic instead of the power-characteristic, traditionally used, which reduced the control complexity; the study of the impedance transformation through a buck-boost converter which maximised the power into any given load; and the use of output parameters that enhanced power conversion efficiency whereby optimum power delivery from the supply to the load was guaranteed. The proposed MPPT presented here tracked the MPP under various weather conditions.

As well as MPPT, the Seesaw controller offers constant output voltage regulation. That is done through matching the load's voltage (i.e. battery) to that of the generator using the same principles as for the load impedance transformation. That offers the means of overcharging protection, achieved by controlling the battery to be charged within its maximum capacity.

Chapter 5

Investigation of Water Micro Leakage Detection

5.1 Introduction

It is evident from reported literature that water losses from residences could account for a significant portion of the water supply. In the UK, between 7.6 m^3 and 76 m^3 of water is lost in each residence annually through leaks [86]. However, studies of water leakage at the domestic level have been limited. Identification of large flow rate leaks (e.g. litres per minute (L/min.) with floods or bursts) through the analysis of the household water consumption is already available. In contrast, micro-leak losses (i.e. milliletres per minute (mL/min.)) might seem insignificant but temporal and geographic aggregation leakage water ultimately leads to major water loss. This, alongside increasing awareness of water quality and resource protection mandates further investigation of micro-leak detection systems.

This chapter reports a novel water micro-leak detection measurement system which features the new technique of shunt measurement using a very sensitive ultrasonic flowmeter to analyse different leak scenarios. The micro-leak detection system is completely

autonomous as it employs a USB-powered voltmeter, flowmeter and switches. The autonomous water flow meter is self-powered through the 2x2 arrangement of MHPGs presented in section (3.4.2). This is remotely controlled which ensures large-scale data collection and system control across the globe. In order to test and investigate the system within a laboratory environment, it was incorporated in an intelligent low-cost hydropower emulator, which is detailed in section (3.3.1). Different household water consumption patterns are emulated. Unlike conventional leak detection systems, the automated system presented here is highly sensitive. Findings from practical experiments detected leaks of just 1 mL/min without impeding main flow. A completely new wavelet analysis for the flowmeter measurements was then derived so as to detect the isolated micro-leak events by removing undesirable background noise. This system detects the water leaks on any scale, anywhere in the world. This feature is beyond the reach of the usual complex conventional detection methods.

5.2 Principles of shunt measurement in the hydraulic analogy

A shunt is an element that is employed in an electrical circuit to redirect the current flow. The diversity of shunt applications in electronics ranges from current measurement, electrical noise bypassing, to over-voltage protection. In electrical current measurement, a shunt resistor is used to create low resistance path, whereby the circuit is interrupted and the interruption is bypassed by the measuring instrument. Analogies between electrical current and water flow imply a potential applicability in fluid dynamics. A shunt water flow measurement method is therefore proposed, whereby a shunt flow meter is placed in parallel with the main water meter creating an alternative fluid pathway. This has a large resistance to flow which enables micro flow rates to be detected. Thus, such a bypass

allows all of the water flow to travel through the main flow meter and dose not disturb the water flow. In other words, when water is been consumed in the house the flow will be measured through the main meter. However, in the event of a water leakage and when no water is been consumed, the leakage flow signals travel through the large resistance path.

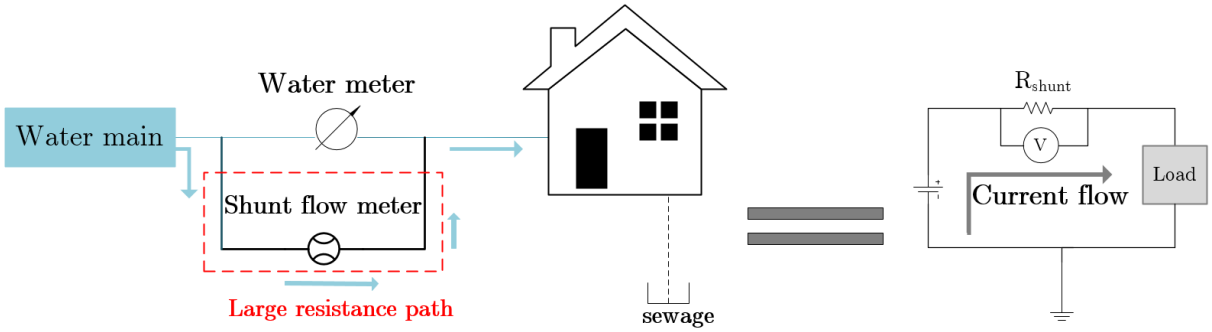

Figure 5.1: Block diagram of the proposed shunt measurement for water flow rate signals.

Figure (5.1) illustrates the electrical analogy of the shunt measurement system. The nature of the analogy developed an understanding of the quantities in an electric circuit, whereby the volume flow rate in litres/min is analogous to the electric current flow in amperes. Similarly, a battery is analogous to a pump in hydraulics; a pump drives the water at low pressure and ejects it at high pressure in the same way the battery takes the charge at low voltages and ejects it at high voltages. The addition of the large resistance path, flow meter in this case, allows small flow rates to go through the shunt device. The fact that the ultrasonic flow meter neither impedes the pressure nor the flow of the water made it a good choice for the proposed leakage measurement system.

A highly ultrasonic flow meter was used in this application, other sensors can serve of course. This feature of the measurement configuration makes it possible to detect any flow, including leakages.

5.3 Principles of wavelet threshold de-noising

Signal noise reduction is an attractive feature of wavelet transform. The key in signal de-noising lies in the suppression of unwanted noise while recovering the original data. A signal contaminated with noise can be expressed as in Equation (5.1), where $x(t)$ represents signal (i.e. low frequency characteristics) and $e(t)$ defines the noise (i.e. high frequency characteristics).

$$S(t) = x(t) + e(t), \qquad t = 0, 1, ..., n-1. \tag{5.1}$$

In its basic form the de-noising process includes thresholding of the high frequency coefficients of the wavelet transform to eliminate the high frequency coefficients and restrain the undesired complements of the original signal [126]. The de-noised signal is then acquired through wavelet reconstruction. Due to the high sensitivity of the flow meter, micro signals are likely to contain noise components. The process proceeds in three stages, namely:

- **Decomposition**

  Firstly, the wavelet and the decomposition level are chosen. The wavelet decomposition at level 'N' is then computed. Generally, decomposition levels between 2-5 are arbitrarily selected [127]. This is determined through visual inspection of the details and approximation components.

- **Thresholding**

  At this stage a threshold for each level is selected to eliminate high frequency coefficients (i.e. de-noise). The universal threshold T_{UV} is given in Equation (5.2) [128].

$$T_{UV} = (\sqrt{2 \log n})\sigma \tag{5.2}$$

where n is the number of data points and σ is an estimate of the noise level. The guaranteed noise-free reconstruction is the main feature of this method.

- **Reconstruction**

  This includes computing the wavelet reconstruction based on the original approximation coefficients of level 'N'.

5.4 Outlines of the water monitoring system

This section reports on the practical implementation of the proposed micro leakage detection method. It presents empirical results obtained from testing the shunt measurement on the laboratory hydraulic emulator detailed previously in section (3.3.1); these findings are published in [24]. The water monitoring system prototype is shown in Figure (5.2). A high-flow rate sensing was established through the optimised set of MHPGs. An off-the-shelf hall-effect water sensor was used to sense the high-flow rate. The flow rate signals were monitored through an Mbed microcontroller. The use of ultrasonic (mL/min) sensor in parallel allowed micro-leaks to be detected.

5.4.1 Implementation and results of the self-powered water flow sensor

This section highlights the implementation of the autonomous water flow meter powered by MHPGs. The specifications of the sensor are listed in Table (5.1). The SeeedStudio water flow sensor was powered by the optimised 2x2 arrangement of MHPGs in the house inlet. The power characteristics of the optimised configuration are previously detailed in section (3.4.2). The flow signals were observed using an Mbed microcontroller allowing remote flow measurement.

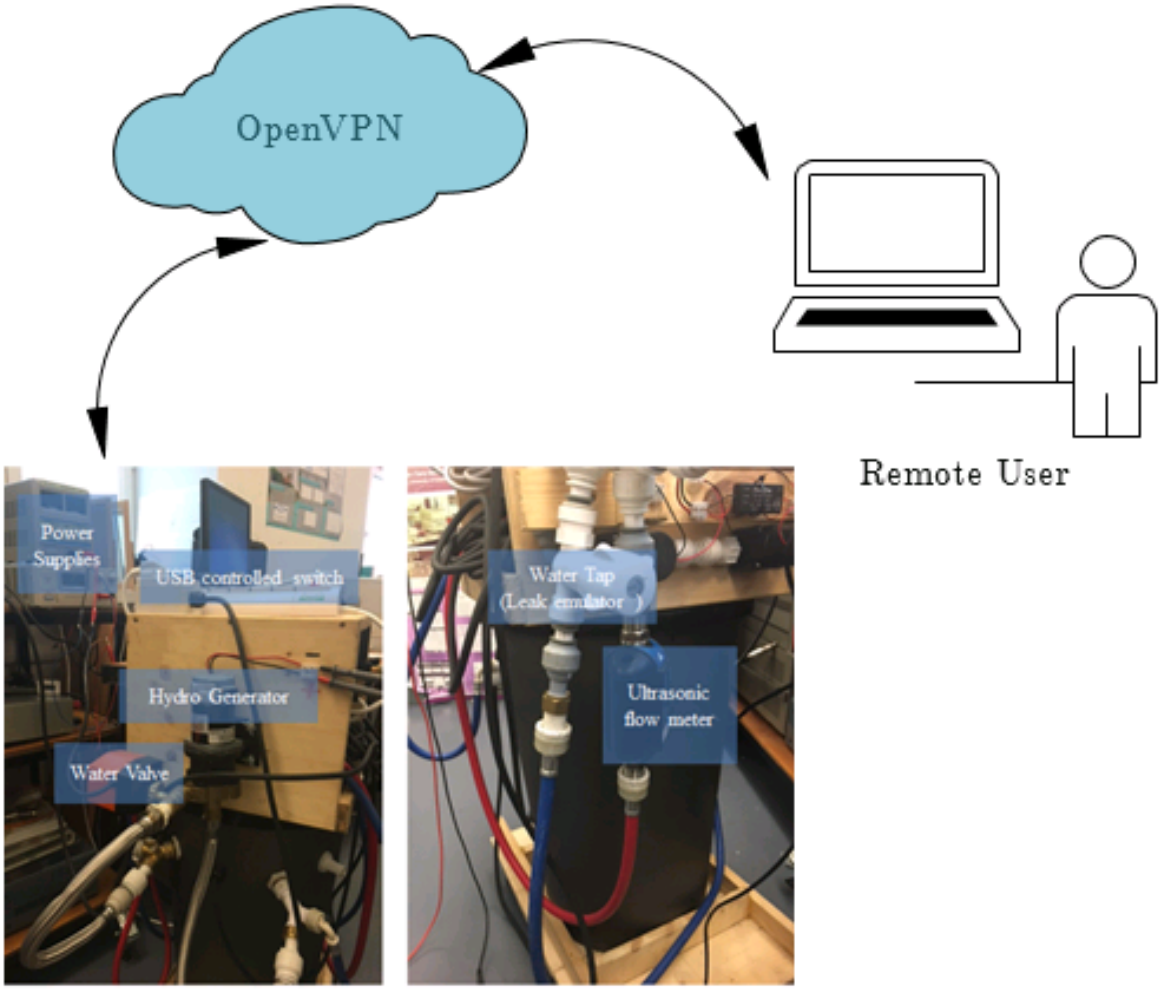

Figure 5.2: Overview of the remotely accessed automated water monitoring system prototype

Table 5.1: Specifications of the SeeedStudio water flow sensor

Parameter	**Value**
Flow rate range	2 to 60 L/min
Operating temperature range	0 to 80 ^0C
Operating voltage	5-24 V
Maximum current	15mA

The relationship between the frequency and the flow rate is given in Equation (5.3). An outline of the autonomous water flow sensing is shown in Figure (5.3).

$$F = 7.5Q_n \tag{5.3}$$

where F is the frequency in Hz and Q_n is the flow rate in L/min.

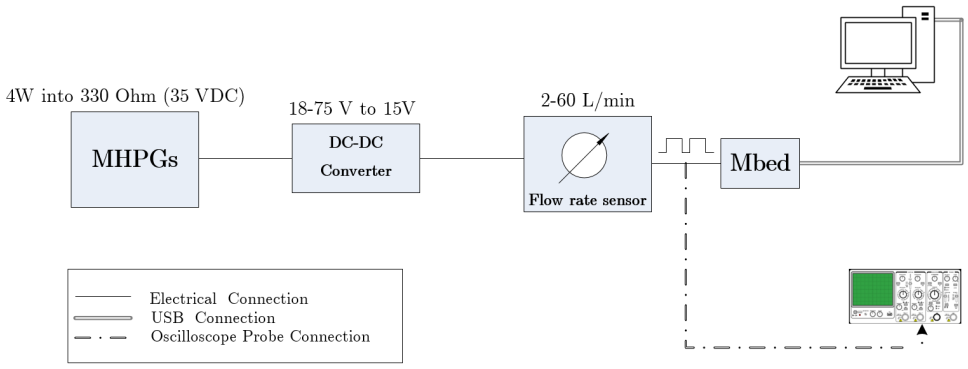

Figure 5.3: Outlines of the water flow measurements through MHPGs.

The flow signals were measured through an Mbed controller and observed on the oscilloscope at various flow rates Q_n, $Q_1 > Q_2 > Q_3$ as shown in Figures (5.4), (5.5) and (5.6), respectively.

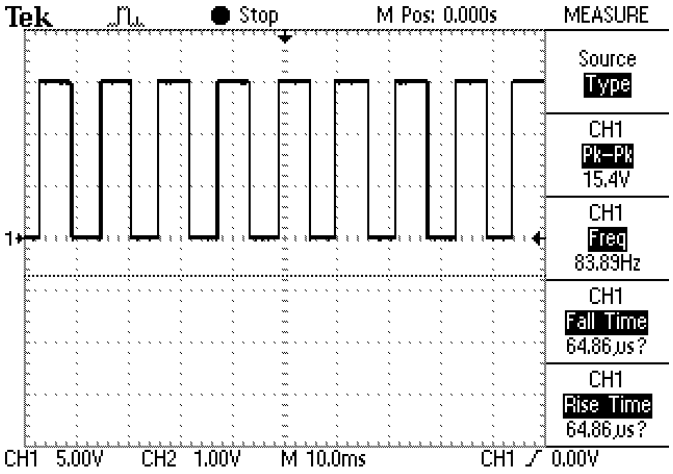

Figure 5.4: Flow rate signals measured through MHPGs at Q_1 of $\approx$ 11 L/min as observed on the oscilloscope.

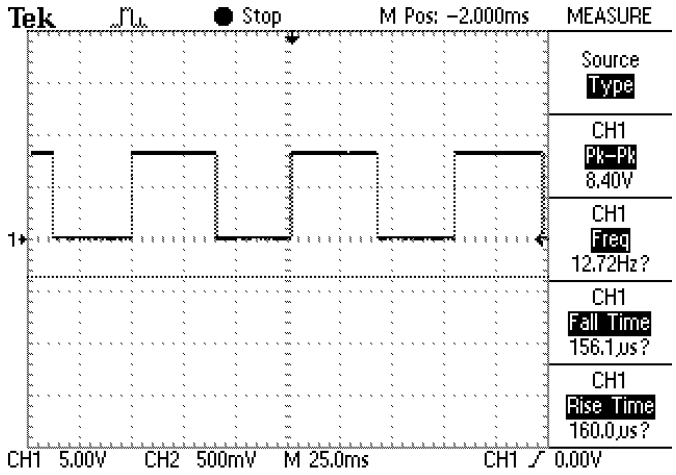

Figure 5.5: Flow rate signals measured through MHPGs at Q_2 of $\approx$ 2 L/min as observed on the oscilloscope.

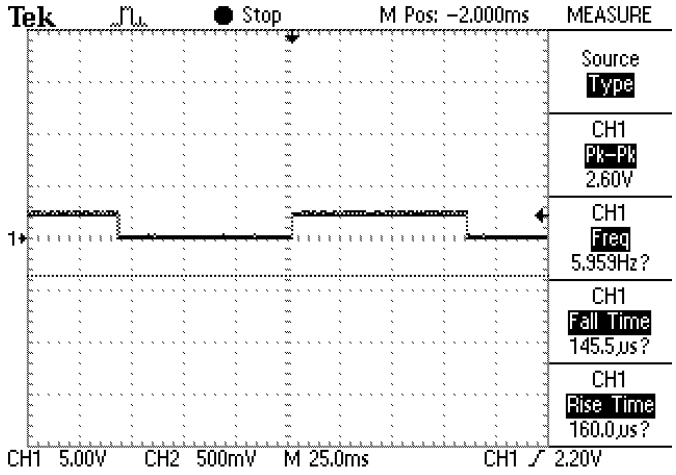

Figure 5.6: Flow rate signals measured through MHPGs at Q_3 of $\approx$ 0.8 L/min as observed on the oscilloscope.

5.4.2 Implementation and results of the shunt measurement for micro-leakage detection

This section reports on the shunt measurement for leakage detection established through the addition of a sensitive flow meter in parallel with an autonomous meter. The state of the art of the proposed leakage detection system lies in the use of shunt measurement

across the mains water supply. At its heart, the detection system features a highly sensitive ultrasonic flow meter (1mL/min). The Atrato low-flow ultrasonic meter can monitor flow over a range of 200 : 1 with accuracy better than ±1.5%. Also, it is USB-powered and features real-time monitoring and data logging of various parameters such as water flow rate and the total measured water. Figure (5.7) outlines the configuration of the measurement system. The specifications of the Atrato ultrasonic flow meter are tabulated in Table (5.2). A water tap was used to emulate the water leakage scenarios.

Table 5.2: Specifications of the Atrato ultrasonic flow meter

Parameter	**Value**
Flow rate range	0.002 to 20 L/min
Fluid temperature range	-10 to 60 ^0C
Accuracy	±1.5%

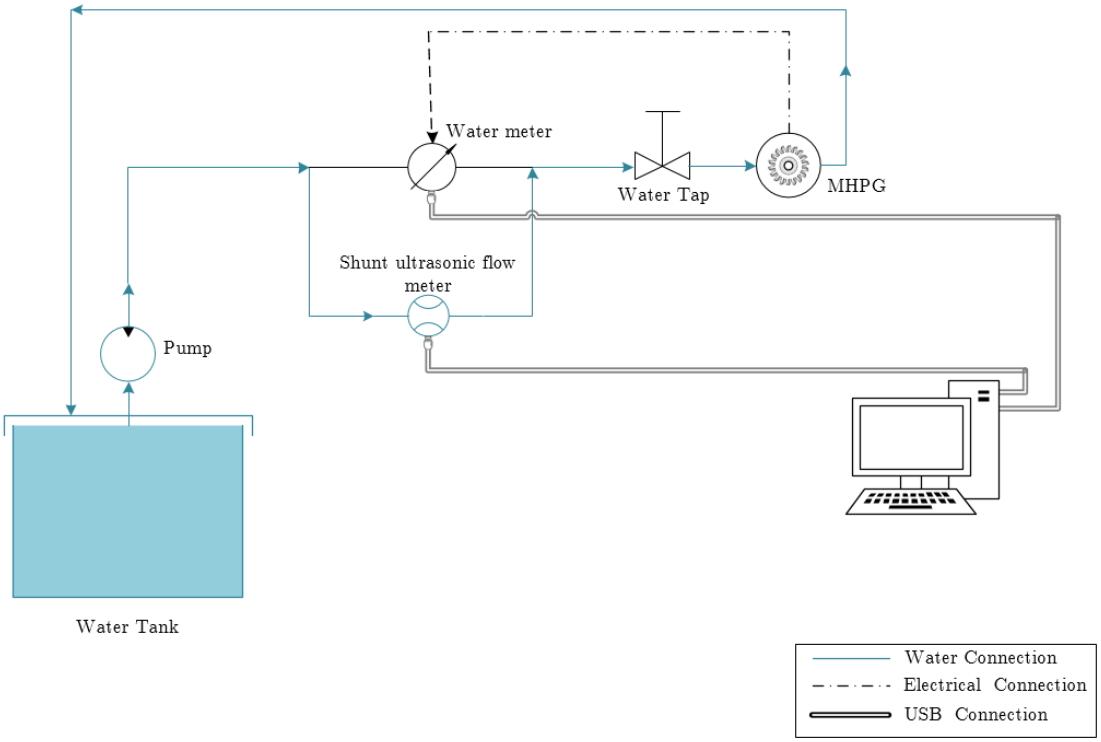

Figure 5.7: An outline of the automated shunt measurement for water leakage detection.

In order to test the performance of the shunt measurement system, water leakage events were emulated using a water tap as shown in Figure (5.7). The flow rate measurement of water leakage events and the corresponding total accumulated water in litres over a period of time are shown in Figures(5.8, 5.9, 5.10). The shunt measurement for the water leakage has proven to be very sensitive. It can be seen that the leaks of 1mL/min were detected. Considering the total accumulated water in Figure(5.10), such leaks tend to be visually and audibly unnoticeable. This indicates a low likelihood of them being detected before they become apparent. Usually a leak is recognised after structural damage has occurred.

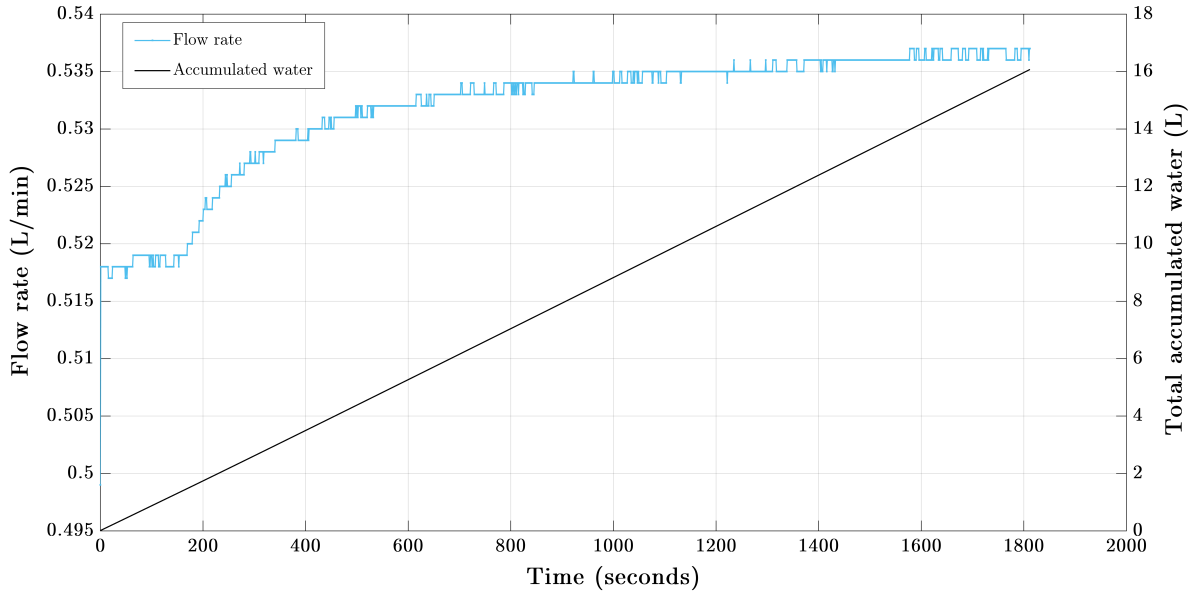

Figure 5.8: Flow rate measured by the shunt flow meter and total accumulated water from such leakage over a period of time ($\approx$ 30 minutes).

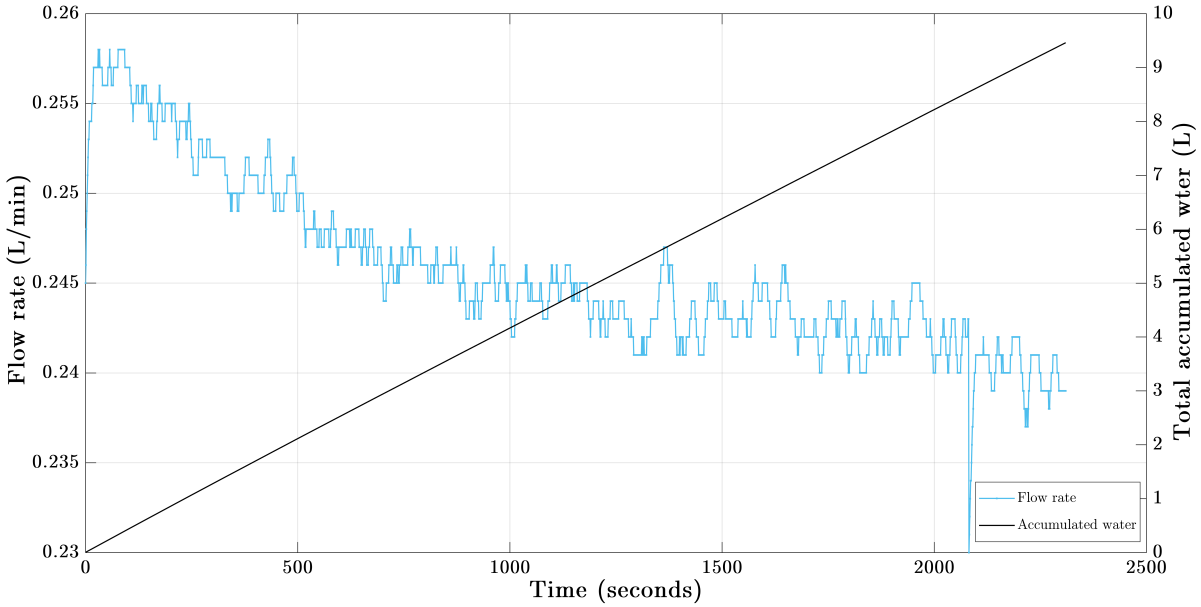

Figure 5.9: Flow rate measured by the shunt flow meter and total accumulated water from such leakage over a period of time (≈ 38.5 minutes).

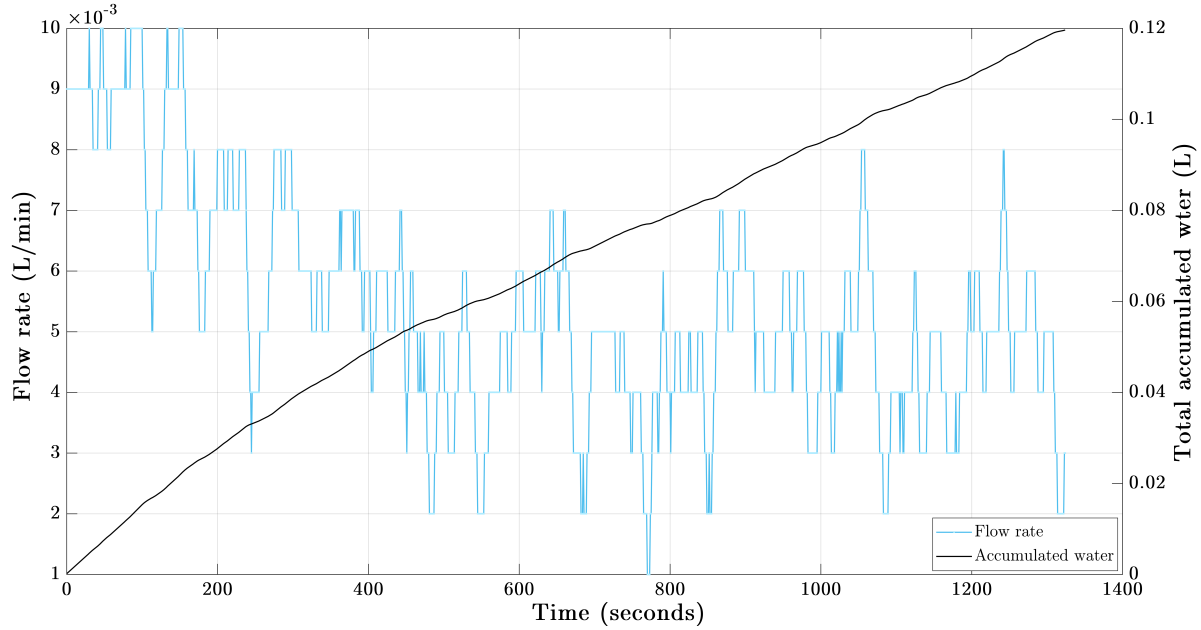

Figure 5.10: Flow rate measured by the shunt flow meter and total accumulated water from such leakage over a period of time (≈ 22 minutes).

5.4.3 De-noising water flow signals of micro flow rates (mL/min)

It is obvious from Figure (5.10) that the signal for the leakage at a micro flow rate is contaminated with noise which could be misleading in the analysis of micro-leakage. Thus, the de-noising property of wavelet transform is carried out on the data to eliminate the noise.

Figure (5.12) shows the approximations and details at 6 levels using the Haar wavelet. The analysis was carried out using the MATLAB Wavelet Analyzer toolbox. The decomposition levels were chosen based on experimental trials. A Haar wavelet transform at level 1 is shown in Figure (5.11). Decomposition at level 6 was observed to be the optimum level for the investigated data as captured in Figure (5.12).

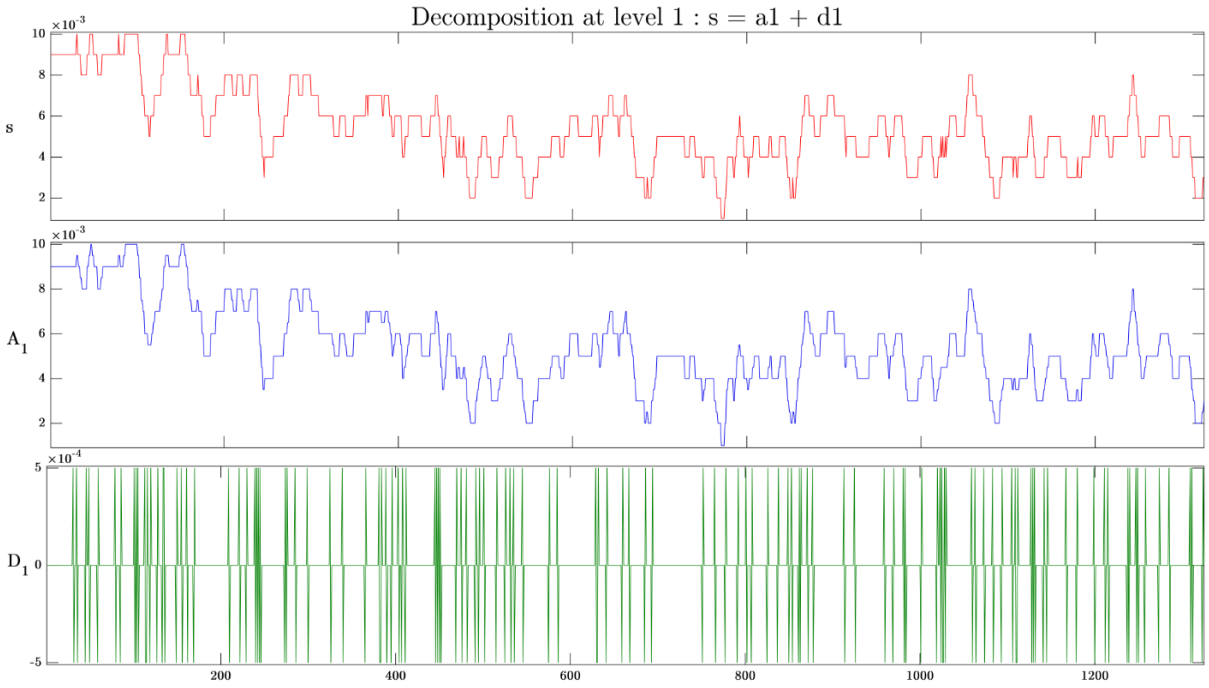

Figure 5.11: The Haar wavelet transform decomposition tree at 1 level. **(s)** The original flow rate signal. (A_1) A 1- level Haar transform decomposition approximation of the signal **s**. (D_1) A 1- level Haar transform decomposition detail of the signal **s**.

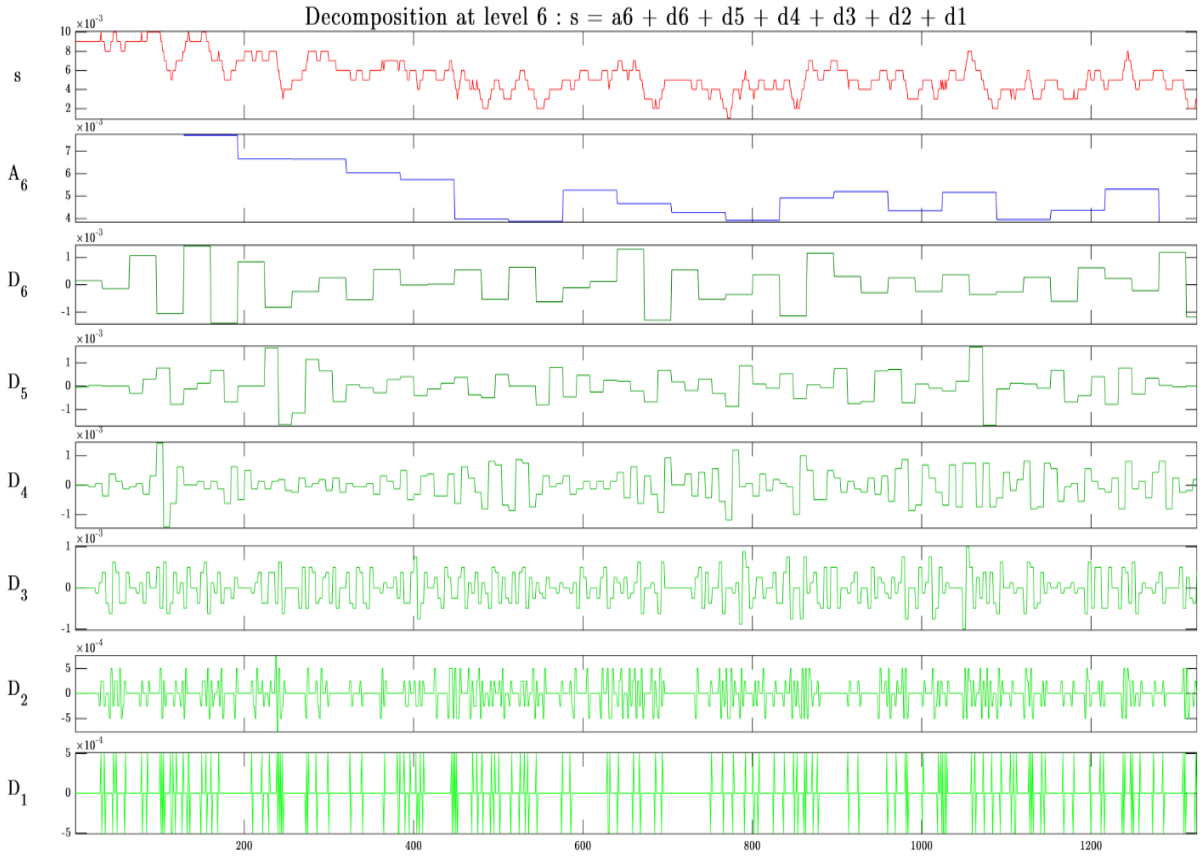

Figure 5.12: The Haar wavelet transform decomposition tree at 6 levels. **(s)** The original flow rate signal. (A_6) The 6^{th}-level Haar transform decomposition approximation of the signal **s**. (D_n) The n^{th}-level Haar transform decomposition detail of the signal **s**.

Comparing the decomposition detail at level 1 to 6 in Figure (5.12) with that of level 1 in Figure (5.11), it can be seen that the noise contributes a large number of small magnitude values to the transform of the signal (i.e. D_2). While the transform captures the original flow signal **s** , to a high percentage (i.e. full decomposition) with magnitudes greater than a threshold $T_s > 0$, the noise signal's transform values are represented by magnitudes below a noise threshold T_n, $T_n < T_s$. Therefore, by thresholding the signal transform the noise can be removed. That was achieved by setting all the signal's transform values with magnitude below the noise threshold T_n to 0. A global threshold was used in this analysis as stated above.

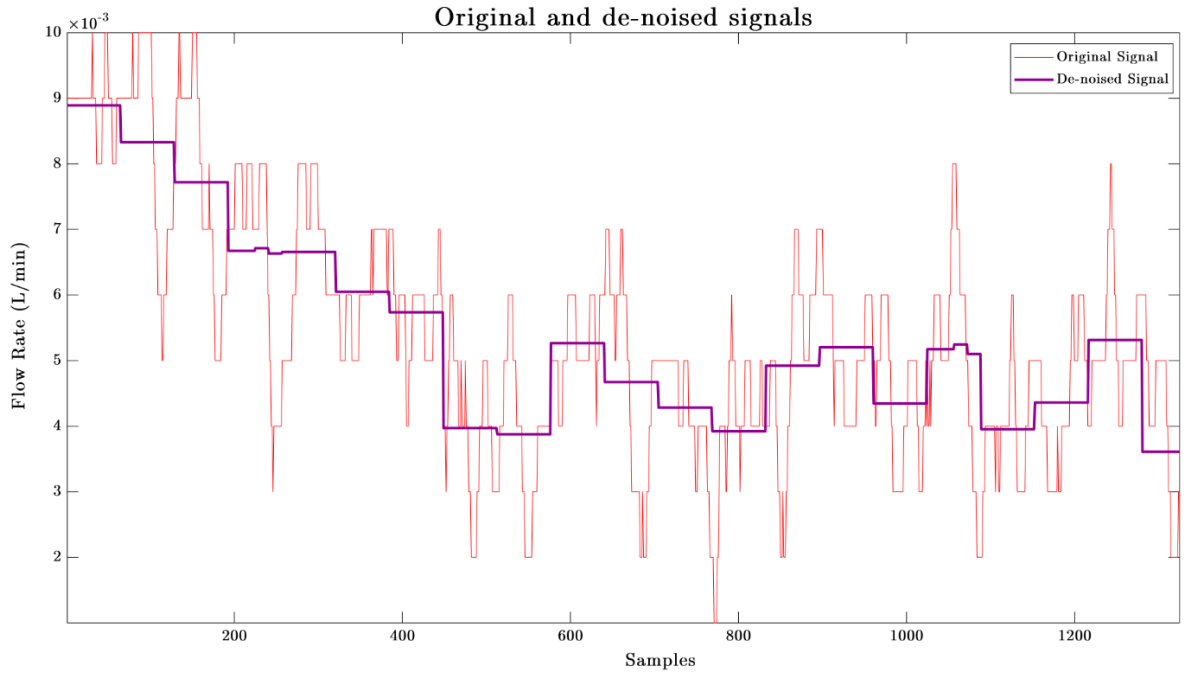

Figure 5.13: The original flow rate signal and the wavelet de-noised signal by a Haar wavelet transform.

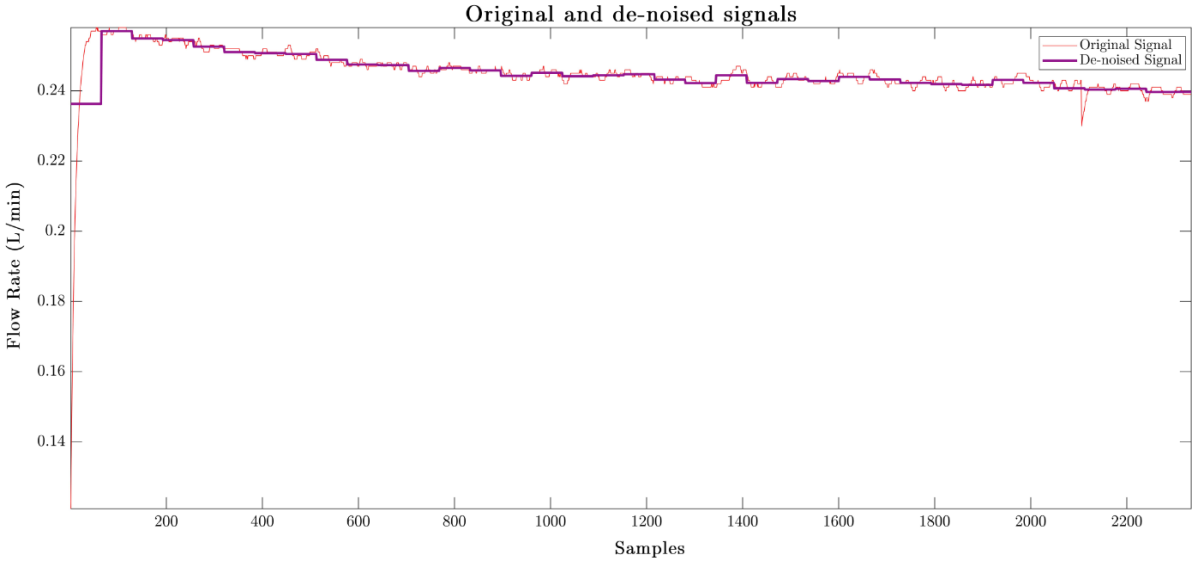

Figure 5.14: The original flow rate signal and the wavelet de-noised signal by a Haar wavelet transform.

Figure (5.13) shows the original signal and de-noised signal with the noise removed using a Haar wavelet transform for a low flow signal (mL/min). The results of the de-

noising effect on a flow signal of a higher flow was studied and shown in Figure (5.14). Overall, the de-noising was effective and the recovered signal had less noisy components. Among other wavelet transforms, the Haar transform guarantees effective reconstruction [129]. The conceptually simple wavelet transform offers robust analysis [130].

These analyses allow leaks of micro flow rates to be recognised and measured. Further pattern recognition analyses can assist in the identification of the leakage origin.

5.5 Conclusion

In this chapter an innovative shunt measurement method for water flow measurement was presented. The principles of the shunt measurements in the hydraulic analogies were discussed. Novelty lies in the introduction of a large resistance path which allows small water flow signals to pass through the shunt device. Highlights of the de-noising property of wavelet transform were included.

Two features of the water management system were detailed. This includes the implementation and results of a water monitoring prototype which features autonomous high-flow sensing through MHPGs. Also, the use of a sensitive flow meter in parallel with the self-powered flow meter (i.e. shunt configuration) which allowed leaks of micro flow rates to be detected. Leaks of just 2 mL/minute were detected and the system did not impede the main flow.

Further, a Haar wavelet analysis was carried out on the flow meter measurements investigated individual micro-leak events by removing undesirable background noise. In that, decomposition at level 6 was observed to be the optimum level for the investigated data.

Chapter 6

Conclusions and Future Work

6.1 Summary and discussion

The performance of power conversion systems under various operational conditions continues to challenge the efficiency of power control systems. An insight into power conversion systems properties is imperative. The work described in this thesis was aimed at this problem while mainly concentrating on microgeneration, MPPT optimisation and the application of MHPGs. This has been achieved by examining three different MHPGs incorporated into a prototype residential hydro power emulator and presenting experimental and simulation results. A challenging task in MPPT control optimisation was to obtain a good trade-off between design cost effectiveness and complexity, and conversion efficiency. In this regard, a simple but robust feed-forward Seesaw MPPT controller was proposed to maximise the power into a given load. Knowledge of the interconnections between MHPG electrical properties and flow dynamics showed a potential application of hydropower for water management systems.

The study of MHPGs characteristic impedance reported in Chapter **3** was drawn from examining three different MHPGs within a controlled environment under different operational conditions. These empirical results introduced a new understanding of MHPG

properties. Arguably, the most useful was the observation of constant ohmic impedance in these generators. Constant source impedance was observed for MHPG combinations as well as for single units. This exhibited a linear system performance regardless of varying environmental conditions (i.e. flow rate), and explained the interconnections between MHPG electrical properties and fluid dynamics, owing to the analogy between power generated from the MHPG and its hydraulic principles. A second major finding concerns the multi-flow correlation between the voltage and current at MPP, which coincided with $50\%V_{oc}$ and $50\%I_{sc}$. A novel heuristic model for a hydroelectric power generator was then described and validated through MATLAB-Simulink simulations. These novel heuristic MHPG models are expected to assist with emerging hydropower generation strategies.

A new simple, low-cost, model independent analogue MPPT controller based on the classical theory of feed-forward was presented in Chapter 4. The Seesaw controller combined a current-mode-controlled buck-boost converter to transform the load impedance to that of the generator through a positive feedback mechanism on the load side for maximum power operation. The impedance transformation through a buck-boost DC-DC converter maximised the power into any given load above or below the MPP. The use of I-V characteristics reduced the control requirements for mathematical operation functions. Optimising the load power by maximising the output voltage is another novelty of the Seesaw controller, in that only one sensor was required. The feed-forward control of the output voltage proved rapid response to varying operational conditions (μ seconds).

The theory and design properties of the Seesaw controller were verified experimentally using an off-the-shelf, DC-DC buck-boost converter and a commercially available 1.8W impulse MHPG incorporated into a controllable hydropower emulator. The theoretical predictions and experimental data were in excellent agreement. The experimental results evaluating the performance of the Seesaw controller under dynamic varying conditions are given in Chapter 4. It is hoped that the proposed MPPT optimisation method described

in this thesis will prove valuable in improving power conversion efficiency for HPCSs as well as other PCSs including PV solar systems.

In addition to the MPPT control, the proposed controller features load power regulation. This was made possible by the load-side, constant-voltage control mechanism, in which the controller set a limit to the voltage, and hence the electrical current drawn to the load. This can have an effective role in battery charging regulation applications by controlling the battery to be charged within its maximum capacity.

An autonomous water flow meter powered through a set of commercially available MHPGs in the house water inlet was described in Chapter **5**. Typically, 4W (into 300 ohm) was produced by an optimised arrangement of 2x2 15V, 1W MHPGs on an intermittent, battery-backup basis. The flow data of the automated flow meter was delivered into an Mbed NXPLPC1768 microcontroller and was remotely controlled enabling large-scale data collection and system control across the globe. The major breakthrough of the water management system development was the shunt combination of high-flow rate sensing (via turbines) and a very sensitive ultrasonic sensor in parallel to detect water leakages. Other types of sensors will serve as well, of course. The remotely controlled, completely automated system (i.e. USB-powered voltmeter, flowmeter and switches) allowed large-scale data collection and system control across the globe. This latter feature is beyond the reach of the complex conventional detection methods. Indeed, the global data collection and control of water flow rates signals is of paramount importance to water resources protection.

Findings from the practical experiments reported in Chapter 5 showed that the detection system was highly sensitive (leaks of just 1 mL/min are detectable) and did not impede the main flow. Wavelet de-noising analysis of flow rate signals using a Haar wavelet at 6 levels removed undesirable background noise and further enhanced the detection sensitivity. The experimental demonstrations and forensic analysis of water flow

signals opens up the prospects for improved leakage detection through machine learning methods.

6.2 Future work

The experimental and theoretical work described in this thesis highlighted both the merits and challenges associated with the analysis of MHPGs power generation and control. This section presents an account of suggested further experimental work.

Optimum arrangement for MHPGs

An optimum arrangement of 2x2 1W MHPGs examined in Chapter **3** produced 4W which is enough power to supply a flow meter as reported in Chapter **5**. However, the output power can be further enhanced through a different type of MHPG (1.8W impulse MHPG presented in section **(3.4.1)** for instance). Furthermore, even utilisation of the generators can be achieved using a combinational optimisation tool similar to that proposed in [131] for PV cells, where, to ensure full energy source utilization, series or parallel combinations of MHPGs are selected. A future direction would thus be to implement a prototype of combinational MHPGs evenly utilised through a cyclic optimisation tool where the maximum power generated would be optimised through the Seesaw MPPT controller.

Seesaw in solar PV applications

The Seesaw MPPT controller tracked the MPP effectively under varying water flow rates. An extension to that work would be to examine the controller for PV solar systems under varying insolation levels. The Seesaw controller fast tracking response under rapid changing operational conditions could have a great role in optimising solar power conversion. The fact that the Seesaw MPPT controller is model independent and maximises the output power as a function of the output voltage makes MPPT highly feasible for PV

systems. Although the controller was developed for a low power application, the principles apply for higher power levels as well. This would be a significant contribution to the Seesaw controller, so an investigation in that direction should be conducted through simulation and experimental studies. Another recommendation would be to investigate the operation of the Seesaw controller for a hybrid system (that incorporates MHPGs and solar PV). The feed-forward operation under current-mode control would ensure that the maximum power available from the sources is extracted regardless of the operational conditions.

Micro-leakage identification through pattern recognition

The micro-leakage identification problem has not been tackled here. However, the ability to measure micro-leaks along with flow rate signals as reported in Chapter **5** opens up the potential for water monitoring analysis through pattern recognition, whereby, using statistical models the nature of the water event can be predicted with the aid of the features selection approach. Given the knowledge of the water consumption pattern, the source of the leak could then be estimated. Given that, research efforts on water consumption pattern recognition has shown great improvement in identifying leakage-free water consumption patterns [93, 98]. Unlike in [132] analysis of leakage-free scenarios would thus not be a precondition. Moreover, a semi-supervised learning approach could then be used to easily classify the water leakage patterns. Such analysis can be carried out on MATLAB. Further, these analyses could pave the way for a highly sensitive leakage forecasting system. The automated remote controlled leakage measurement system could therefore have a significant role in the emulation of different leakage scenarios. The model can be varied using real life household water consumption patterns. Additionally, further research will investigate remote monitoring of water consumption and leakage in agricultural and industrial environments.

Bibliography

[1] P. Lautier, C. O'Neil, C. Deschenes, H. J. N. Ndjana, and R. Eraser, "Variable Speed Operation of a New Very Low Head Hydro Turbine with Low Environmental Impact," in *Electrical Power Conference, Canada*, pp. 85–90, IEEE, 2007.

[2] S. Williamson, B. Stark, and J. Booker, "Experimental Optimisation of A Low-head Pico Hydro Turgo Turbine," in *Third International Conference on Sustainable Energy Technologies (ICSET)*, pp. 322–327, IEEE, 2012.

[3] A. M. Haidar, M. F. Senan, A. Noman, and T. Radman, "Utilization of Pico Hydro Generation in Domestic and Commercial Loads," *Renewable and Sustainable Energy Reviews*, vol. 16, no. 1, pp. 518–524, 2012.

[4] D. Hoffmann, A. Willmann, R. Göpfert, P. Becker, B. Folkmer, and Y. Manoli, "Energy Harvesting from Fluid Flow in Water Pipelines for Smart Metering Applications," in *Journal of Physics: Conference Series*, vol. 476, p. 012104, IOP Publishing, 2013.

[5] B. MMSRS, S. Anbuudayasankar, K. Balaji, *et al.*, "Power Generation by High Head Water in a Building using Micro Hydro Turbine : A Greener Approach," *Environmental Science and Pollution Research*, vol. 23, no. 10, pp. 9381–9390, 2016.

[6] S. Lalitha, "Micro-generation of Electricity from Tap Water," *International Journal of Emerging Technology and Advanced Engineering*, vol. 3, no. 10, 2013.

[7] M. J. A. Khan, *Adaptive Power Tracking Control of Hydrokinetic Energy Conversion Systems*. Phd thesis, Memorial University of Newfoundland, 2010.

[8] L. Belhadji, S. Bacha, I. Munteanu, A. Rumeau, and D. Roye, "Adaptive MPPT Applied to Variable-Speed Microhydropower Plant," *IEEE Transactions on Energy Conversion*, vol. 28, no. 1, pp. 34–43, 2013.

[9] J. Khan, T. Iqbal, and J. Quaicoe, "Evaluation of Maximum Power Point Tracking in Hydrokinetic Energy Conversion Systems," *The Journal of Engineering*, vol. 1, no. 1, 2015.

[10] M. Khan, M. Iqbal, and J. Quaicoe, "Effects of Nonlinear Efficiency Characteristics on the Power-Tracking Control: A Case Study of Hydrokinetic Energy Conversion System," in *Energy Conversion Congress and Exposition, 2009.*, pp. 2657–2666, IEEE, 2009.

[11] H. Zhou, "Maximum Power Point Tracking Control of Hydrokinetic Turbine and Low-Speed High-Thrust Permanent Magnet Generator Design," tech. rep., Missouri University of Science and Technology Rolla, 2012.

[12] Q. Lu, Y. Sun, and S. Mei, *Nonlinear Control Systems and Power System Dynamics*, vol. 10. Springer Science & Business Media, 2013.

[13] E. E. S. Michaelides, *Alternative Energy Sources*. Springer Science & Business Media, 2012.

[14] D. P. Quoc, Q. N. Nhat, N. T. D. Vu, A. N. Bao, H. H. Lee, *et al.*, "The New Combined Maximum Power Point Tracking Algorithm Using Fractional Estimation

in Photovoltaic Systems," in *International Conference on Power Electronics and Drive Systems (PEDS)*, pp. 919–923, IEEE, 2011.

[15] D. Raveendhra, B. Kumar, D. Mishra, and M. Mankotia, "Design of FPGA Based Open Circuit Voltage MPPT Charge Controller for Solar PV System," in *International Conference on Circuits, Power and Computing Technologies (ICCPCT)*, pp. 523–527, IEEE, 2013.

[16] T. Esram and P. L. Chapman, "Comparison of Photovoltaic Array Maximum Power Point Tracking Techniques," *IEEE Transactions on Energy Conversion*, vol. 22, no. 2, pp. 439–449, 2007.

[17] S. Malathy and R. Ramaprabha, "Maximum Power Point Tracking Based on Look Up Table Approach," in *Advanced Materials Research*, vol. 768, pp. 124–130, Trans Tech Publ, 2013.

[18] J. Ghaisari, M. Habibi, and A. Bakhshai, "An MPPT Controller Design for Photovoltaic (PV) Systems Based on the Optimal Voltage Factor Tracking," in *Electrical Power Conference, 2007. EPC 2007. IEEE Canada*, pp. 359–362, IEEE, 2007.

[19] D. Shmilovitz, "On the Control of Photovoltaic Maximum Power Point Tracker via Output Parameters," *IEE Proceedings-Electric Power Applications*, vol. 152, no. 2, pp. 239–248, 2005.

[20] S. Chun and A. Kwasinski, "Analysis of Classical Root-Finding Methods Applied to Digital Maximum Power Point Tracking for Sustainable Photovoltaic Energy Generation," *IEEE Transactions on Power Electronics*, vol. 26, no. 12, pp. 3730–3743, 2011.

[21] M. Veerachary, T. Senjyu, and K. Uezato, "Voltage-based Maximum Power Point Tracking Control of PV System," *IEEE Transactions on Aerospace and Electronic Systems*, vol. 38, no. 1, pp. 262–270, 2002.

[22] M. Veerachary, T. Senjyu, and K. Uezato, "Maximum Power Point Tracking of Coupled Inductor Interleaved Boost Converter Supplied PV System," *IEE Proceedings-Electric Power Applications*, vol. 150, no. 1, pp. 71–80, 2003.

[23] S. A. Alarefi and S. D. Walker, "Intelligent Low-Cost Micro-Hydro Power Emulator for Domestic Applications," in *3rd International Renewable and Sustainable Energy Conference (IRSEC), 2015*, pp. 1–5, IEEE, 2015.

[24] S. A. S. Alarefi and S. Walker, "Innovative Shunt Measurement for Residential Water Micro-Leakage Detection," in *8th International Renewable Energy Congress (IREC)*, pp. 1–6, IEEE, 2017.

[25] I. Staffell, D. J. Brett, N. P. Brandon, and A. D. Hawkes, *Domestic Microgeneration: Renewable and Distributed Energy Technologies, Policies and Economics*. Routledge, 2015.

[26] "Energy Act 2004," July 2004.

[27] "Domestic Energy Fact File and Housing Surveys and Energy and Climate Change: Evidence and Analysis," December 2012. Updated 24 January 2013.

[28] "Climate Change Act 2008: Chapter 27," 2008.

[29] P. Balcombe, D. Rigby, and A. Azapagic, "Investigating the Importance of Motivations and Barriers Related to Microgeneration Uptake in the UK," *Applied Energy*, vol. 130, pp. 403–418, 2014.

[30] "Monthly Central Feed-in Tariff Register Statistics,." Online, July 2017.

[31] E. W. V. Goodright, "Energy Consumption in the UK (2015): Overall Energy Consumption in the UK since 1970," July 2015.

[32] P. Balcombe, D. Rigby, and A. Azapagic, "Motivations and Barriers Associated with Adopting Microgeneration Energy Technologies in the UK," *Renewable and Sustainable Energy Reviews*, vol. 22, pp. 655–666, 2013.

[33] I. D. Jones *et al.*, *Assessment and Design of Small-Scale Hydro-Electric Power Plants*. PhD thesis, University of Salford, 1988.

[34] "World Energy Resources,2016, Excutive Summary." Online, 2016.

[35] P. Pascall, "Hydropower." Online, January 2016. Institution of Civil Engineers,Energy Briefing Sheet.

[36] "World Energy Resources 2013 Survey." Online, 2013.

[37] F. Manzano-Agugliaro, M. Taher, A. Zapata-Sierra, A. Juaidi, and F. G. Montoya, "An overview of Research and Energy Evolution for Small Hydropower in Europe," *Renewable and Sustainable Energy Reviews*, vol. 75, pp. 476–489, 2017.

[38] "Sub-regional Feed-in Tariffs Statistics." Online, July 2013.

[39] E. . I. S. Department for Business and E. Agency, "Harnessing Hydroelectric Power, Part of Low Carbon Energy and Water: How Hydroelectric Power Works, Regional Schemes and Information on Installing your own Micro-Hydro Scheme.." Online, January 2013.

[40] P. Novak, *Developments in Hydraulic Engineering*. CRC Press, 2005.

[41] D. Egré and J. C. Milewski, "The Diversity of Hydropower Projects," *Energy Policy*, vol. 30, no. 14, pp. 1225–1230, 2002.

[42] H. L. Willis, *Distributed Power Generation: Planning and Evaluation*. CRC Press, 2000.

[43] M. Khan, G. Bhuyan, M. Iqbal, and J. Quaicoe, "Hydrokinetic Energy Conversion Systems and Assessment of Horizontal and Vertical Axis Turbines for River and Tidal Applications: A Technology Status Review," *Applied Energy*, vol. 86, no. 10, pp. 1823–1835, 2009.

[44] J. Khan, T. Iqbal, and J. Quaicoe, "Power Tracking Control Challenges in Hydrokinetic Energy Conversion Systems," in *Power and Energy Society General Meeting*, pp. 1–6, IEEE, 2011.

[45] V. J. Ginter and J. K. Pieper, "Robust Gain Scheduled Control of A Hydrokinetic Turbine," *IEEE Transactions on Control Systems Technology*, vol. 19, no. 4, pp. 805–817, 2011.

[46] I. Buehring and L. Freris, "Control Policies for Wind-Energy Conversion Systems," in *IEE Proceedings C (Generation, Transmission and Distribution)*, vol. 128, pp. 253–261, IET, 1981.

[47] M. A. Abdullah, A. Yatim, C. Tan, and R. Saidur, "A Review of Maximum Power Point Tracking Algorithms for Wind Energy Systems," *Renewable and Sustainable Energy Reviews*, vol. 16, no. 5, pp. 3220–3227, 2012.

[48] A. M. Knight and G. E. Peters, "Simple Wind Energy Controller for an Expanded Operating Range," *IEEE Transactions on Energy Conversion*, vol. 20, no. 2, pp. 459–466, 2005.

[49] J. D. De Kooning, L. Gevaert, J. Van de Vyver, T. L. Vandoorn, and L. Vandevelde, "Online Estimation of the Power Coefficient Versus Tip-Speed Ratio Curve of Wind

Turbines," in *39th Annual Conference of the Industrial Electronics Society, IECON* , pp. 1792–1797, IEEE, 2013.

[50] K. Tan and S. Islam, "Optimum Control Strategies in Energy Conversion of PMSG Wind Turbine System Without Mechanical Sensors," *IEEE Transactions on Energy Conversion*, vol. 19, no. 2, pp. 392–399, 2004.

[51] A. Tapia, G. Tapia, J. X. Ostolaza, and J. R. Saenz, "Modeling and Control of A Wind Turbine Driven Doubly Fed Induction Generator," *IEEE Transactions on energy conversion*, vol. 18, no. 2, pp. 194–204, 2003.

[52] S. Ganjefar, A. A. Ghassemi, and M. M. Ahmadi, "Improving Efficiency of Two-Type Maximum Power Point Tracking Methods of Tip-Speed Ratio and Optimum Torque in Wind Turbine System using A Quantum Neural Network," *Energy*, vol. 67, pp. 444–453, 2014.

[53] M. Nasiri, J. Milimonfared, and S. Fathi, "Modeling, Analysis and Comparison of TSR and OTC Methods for MPPT and Power Smoothing in Permanent Magnet Synchronous Generator-Based Wind Turbines," *Energy Conversion and Management*, vol. 86, pp. 892–900, 2014.

[54] A. Aitouche and E. Kamal, "Intelligent Control of Wind Energy Conversion Systems," in *Wind Farm-Impact in Power System and Alternatives to Improve the Integration*, InTech, 2011.

[55] M. Ermiş, H. Ertan, E. Akpinar, and F. Ülgüt, "Autonomous Wind Energy Conversion System with A Simple Controller for Maximum-Power Transfer," in *IEE Proceedings B (Electric Power Applications)*, vol. 139, pp. 421–428, IET, 1992.

[56] K. E. Johnson, L. J. Fingersh, M. J. Balas, and L. Y. Pao, "Methods for Increasing Region 2 Power Capture on a Variable-Speed Wind Turbine," *Journal of Solar Energy Engineering*, vol. 126, no. 4, pp. 1092–1100, 2004.

[57] R. Datta and V. Ranganathan, "A Method of Tracking the Peak Power Points for a Variable Speed Wind Energy Conversion System," *IEEE Transactions on Energy Conversion*, vol. 18, no. 1, pp. 163–168, 2003.

[58] D. Kumar and K. Chatterjee, "A Review of Conventional and Advanced MPPT Algorithms for Wind Energy Systems," *Renewable and Sustainable Energy Reviews*, vol. 55, pp. 957–970, 2016.

[59] K. T. Atta, A. Johansson, M. J. Cervantes, and T. Gustafsson, "Phasor Extremum Seeking and its Application in Kaplan Turbine Control," in *IEEE Conference on Control Applications (CCA)*, pp. 298–303, IEEE, 2014.

[60] S. M. R. Kazmi, H. Goto, H.-J. Guo, and O. Ichinokura, "A Novel Algorithm for Fast and Efficient Speed-Sensorless Maximum Power Point Tracking in Wind Energy Conversion systems," *IEEE Transactions on Industrial Electronics*, vol. 58, no. 1, pp. 29–36, 2011.

[61] L. J. Fingersh and P. W. Carlin, *Results from the NREL Variable-Speed Test Bed*. National Renewable Energy Laboratory, 1997.

[62] L. J. Fingersh and K. E. Johnson, "Baseline Results and Future Plans for the NREL Controls Advanced Research Turbine," in *Proc. 23rd ASME Wind Energy Symposium*, pp. 87–93, Reno, Nevada: CiteSeer, 2004.

[63] K. Yuen, S. Apelfröjd, and M. Leijon, "Implementation of Control System for Hydrokinetic Energy Converter," *Journal of Control Science and Engineering*, vol. 2013, p. 5, 2013.

[64] K. T. Atta, A. Johansson, M. J. Cervantes, and T. Gustafsson, "Maximum Power Point Tracking for Micro Hydro Power Plants Using Extremum Seeking Control," in *IEEE Conference on Control Applications (CCA)*, pp. 1874–1879, IEEE, 2015.

[65] M. R. Halfawy and J. Hengmeechai, "Automated Defect Detection in Sewer Closed Circuit Television Images Using Histograms of Oriented Gradients and Support Vector Machine," *Automation in Construction*, vol. 38, pp. 1–13, 2014.

[66] J. M. Mirats Tur and W. Garthwaite, "Robotic Devices for Water Main In-Pipe Inspection: A Survey," *Journal of Field Robotics*, vol. 27, no. 4, pp. 491–508, 2010.

[67] M. Fahmy and O. Moselhi, "Detecting and Locating Leaks in Underground Water Mains using Thermography," in *Proceedings of the 26th International Symposium on Automation and Robotics in Construction (ISARC 2009), Austin, TX, USA*, vol. 2427, 2009.

[68] B. Shakmak and A. Al-Habaibeh, "Detection of Water Leakage in Buried Pipes using Infrared Technology; A Comparative Study of using High and Low Resolution Infrared Cameras for Evaluating Distant Remote Detection," in *Conference on Applied Electrical Engineering and Computing Technologies (AEECT), Jordan*, pp. 1–7, IEEE, 2015.

[69] T. Inagaki and Y. Okamoto, "Diagnosis of the Leakage Point on a Surface using Infrared Thermography in Near Ambient Conditions," *NDT & E International*, vol. 30, no. 3, pp. 135–142, 1997.

[70] A. M. Obeid, F. Karray, M. W. Jmal, M. Abid, S. M. Qasim, and M. S. BenSaleh, "Towards Realisation of Wireless Sensor Network-Based Water Pipeline Monitoring Systems: A Comprehensive Review of Techniques and Platforms," *IET science, measurement and technology*, vol. 10, no. 5, pp. 420–426, 2016.

[71] S. P. Gupta, A. Mahalwar, and P. Udaykumar, "Analysis of Different Techniques for Locating Leaks in Pipes in Water Distribution System using WSN," in *Innovative Applications of Computational Intelligence on Power, Energy and Controls with their Impact on Humanity (CIPECH)*, pp. 173–177, IEEE, 2014.

[72] R. Pilcher, "Leak Detection Practices and Techniques: A Practical Approach.," *Water 21*, pp. 44–45, 2003.

[73] D. D. Silva, J. Mashford, and S. Burn, "Computer Aided Leak Location and Sizing in Pipe Network," *Urban Water Security Research Alliance Technical Report*, no. 17, 2011.

[74] M. Fantozzi and E. Fontana, "Acoustic Emission Techniques: The Optimum Solution for Leakage Detection and Location in Water Pipelines," *Insight*, vol. 43, no. 2, pp. 105–107, 2001.

[75] S. Rashid, S. Qaisar, H. Saeed, and E. Felemban, "Performance Analysis of Wavelet Transforms for Leakage Detection in Long Range Pipeline Networks," in *Conference on Systems, Process and Control (ICSPC)*, pp. 10–15, IEEE, 2013.

[76] A. F. Colombo, P. Lee, and B. W. Karney, "A selective Literature Review of Transient-Based Leak Detection Methods," *Journal of Hydro-environment Research*, vol. 2, no. 4, pp. 212–227, 2009.

[77] J. P. Vítkovskỳ, J. A. Liggett, A. R. Simpson, and M. F. Lambert, "Optimal Measurement Site Locations for Inverse Transient Analysis in Pipe Networks," *Journal of Water Resources Planning and Management*, vol. 129, no. 6, pp. 480–492, 2003.

[78] J. P. Vítkovskỳ, M. F. Lambert, A. R. Simpson, and J. A. Liggett, "Experimental Observation and Analysis of Inverse Transients for Pipeline Leak Detection," *Jour-*

nal of Water Resources Planning and Management, vol. 133, no. 6, pp. 519–530, 2007.

[79] X. Xu and B. Karney, "An Overview of Transient Fault Detection Techniques," in *Modeling and Monitoring of Pipelines and Networks*, pp. 13–37, Springer, 2017.

[80] B. Brunone, M. Ferrante, D. Covas, H. Ramos, and A. B. De Almeida, "Detecting Leaks in Pressurised Pipes By Means of Transients," 2004.

[81] A. C. Caputo and P. M. Pelagagge, "Using Neural Networks to Monitor Piping Systems," *Process Safety Progress*, vol. 22, no. 2, pp. 119–127, 2003.

[82] W. Moczulski, R. Wyczółkowski, K. Ciupke, P. Przystałka, P. Tomasik, and D. Wachla, "A Methodology of Leakage Detection and Location in Water Distribution Networks The Case Study," in *3rd Conference on Control and Fault-Tolerant Systems (SysTol)*, pp. 331–336, IEEE, 2016.

[83] G. Sanz, R. Pérez, and A. Escobet, "Leakage Localization in Water Networks Using Fuzzy Logic," in *20th Mediterranean Conference on Control & Automation (MED)*, pp. 646–651, IEEE, 2012.

[84] J. M. Alkasseh, M. N. Adlan, I. Abustan, H. A. Aziz, and A. B. M. Hanif, "Applying Minimum Night Flow to Estimate Water Loss Using Statistical Modeling: A Case Study In Kinta Valley, Malaysia," *Water Resources Management*, vol. 27, no. 5, pp. 1439–1455, 2013.

[85] M. M. Gamboa-Medina, L. R. Reis, and R. C. Guido, "Feature Extraction in Pressure Signals for Leak Detection in Water Networks," *Procedia Engineering*, vol. 70, pp. 688–697, 2014.

[86] B. Kingdom, R. Liemberger, and P. Marin, "The Challenge of Reducing Non-revenue Water (NRW) in Developing Countries," 2006.

[87] R. Beuken, C. Lavooij, A. Bosch, and P. Schaap, "Low Leakage in the Netherlands Confirmed," in *Water Distribution Systems Analysis Symposium* , pp. 1–8, 2008.

[88] B. D. Negewo, *Renewable Energy Desalination: An Emerging Solution to Close the Water Gap in the Middle East and North Africa*. World Bank Publications, 2012.

[89] World Health Organization and World Plumbing Council, *Health Aspects of Plumbing*. World Health Organization, 2006.

[90] P. W. Mayer, W. B. DeOreo, E. M. Opitz, J. C. Kiefer, W. Y. Davis, B. Dziegielewski, and J. O. Nelson, "Residential End Uses of Water," 1999.

[91] P. Mayer, W. DeOreo, E. Towler, L. Martien, and D. Lewis, "The Impacts of High Efficiency Plumbing Fixture Retrofits in Single-Family Homes," *Tampa Water Department and the United States Environmental Protection Agency*, 2004.

[92] P. N. Troy, D. Holloway, and W. Randolph, *Water Use and the Built Environment: Patterns of Water Consumption in Sydney*. City Futures Research Centre Sydney, 2005.

[93] K. A. Nguyen, R. A. Stewart, and H. Zhang, "An Intelligent Pattern Recognition Model to Automate the Categorisation of Residential Water End-use Events," *Environmental Modelling and Software*, vol. 47, pp. 108–127, 2013.

[94] S. Anjana, M. Sahana, S. Ankith, K. Natarajan, K. Shobha, and A. Paventhan, "An IoT Based 6LoWPAN Enabled Experiment for Water Management," in *International Conference on Advanced Networks and Telecommuncations Systems (ANTS)*, pp. 1–6, IEEE, 2015.

[95] L. Gama-Moreno, J. Reyes, M. Sanchez, C. Ochoa-Franco, and C. Noguerón, "Instrumentation of a Water-Leaks Detection System Controlled via the Short Message

Service through the GSM Network," in *Electronics, Robotics and Automotive Mechanics Conference (CERMA)*, pp. 654–659, IEEE, 2010.

[96] H. Elkamchouchi and A. ElShafee, "Design and Prototype Implementation of SMS Based Home Automation System," in *International Conference on Electronics Design, Systems and Applications (ICEDSA)* , pp. 162–167, IEEE, 2012.

[97] S.-C. Hsia, S.-W. Hsu, and Y.-J. Chang, "Remote Monitoring and Smart Sensing for Water Meter System and Leakage Detection," *IET Wireless Sensor Systems*, vol. 2, no. 4, pp. 402–408, 2012.

[98] K. A. Nguyen, R. A. Stewart, and H. Zhang, "An Autonomous and Intelligent Expert System for Residential Water End-Use Classification," *Expert Systems with Applications*, vol. 41, no. 2, pp. 342–356, 2014.

[99] G. Oren and N. Y. Stroh, "Mathematical Model for Detection of Leakage in Domestic Water Supply Systems by Reading Consumption from an Analogue Water Meter," *International Journal of Environmental Science and Development (IJESD),*, vol. 4, no. 4, 2017.

[100] G. Boracchi and M. Roveri, "Exploiting Self-Similarity for Change Detection," in *International Joint Conference on Neural Networks (IJCNN)*, pp. 3339–3346, IEEE, 2014.

[101] M. T. Nasir, M. Mysorewala, L. Cheded, B. Siddiqui, and M. Sabih, "Measurement Error Sensitivity Analysis for Detecting and Locating Leak in Pipeline using ANN and SVM," in *11th International Multi-Conference on Systems, Signals AND Devices (SSD)*, pp. 1–4, IEEE, 2014.

[102] G. Jasmin, A. Leroux, and D. Mukhedkar, "Electronic Simulation of A Hydro-Turbine with its Penstock, Speed Regulator and Damping Unit," *IEEE Transactions on Power Apparatus and Systems*, no. 9, pp. 3023–3030, 1983.

[103] M. Steinbring, M. Pacas, and M. Alnajjar, "Emulation of A Micro-Hydro-Turbine for Stand-Alone Power Plants with Z-Source Inverter," in *38th Annual Conference on IEEE Industrial Electronics Society*, pp. 5291–5296, IEEE, 2012.

[104] M. M. Othman, J. A. Razak, M. R. Ayob, M. A. Rosli, S. G. Herawan, and K. Sopian, "Development of Model System for Cost-Effective Pico-Hydro Turbine," in *3rd International Symposium & Exhibition in Sustainable Energy and Environment (ISESEE)*, pp. 17–21, IEEE, 2011.

[105] M. Mauri, F. C. Dezza, and G. Marchegiani, "A Novel Small-Scale Variable Speed Hydropower Emulator Using an Inverter-Controlled Induction Motor," in *European Conference on Power Electronics and Applications*, pp. 1–7, IEEE, 2007.

[106] E. Duran, M. Piliougine, M. Sidrach-de Cardona, J. Galán, and J. Andujar, "Different Methods to Obtain the I–V Curve of PV Modules: A Review," in *33rd Photovoltaic Specialists Conference* , pp. 1–6, IEEE, 2008.

[107] Online, 2018. [Last Accessed 16 August 2018].

[108] Online. [Last Accessed 16 August 2018].

[109] Online. [Last accessed 16 August 2018].

[110] H. U. Fuchs, "Storage and Flow of Fluids and Electricity," *The Dynamics of Heat*, pp. 17–50, 2010.

[111] W. Durfee and Z. Sun, "Fluid Power System Dynamics," *Center for Compact and Efficient Fluid Power*, 2009.

[112] H. A. Sher, A. F. Murtaza, A. Noman, K. E. Addoweesh, K. Al-Haddad, and M. Chiaberge, "A New Sensorless Hybrid MPPT Algorithm Based on Fractional Short-Circuit Current Measurement and P&O MPPT," *IEEE Transactions on Sustainable Energy*, vol. 6, no. 4, pp. 1426–1434, 2015.

[113] D. Baimel, R. Shkoury, L. Elbaz, S. Tapuchi, and N. Baimel, "Novel Optimized Method for Maximum Power Point Tracking in PV Systems Using Fractional Open Circuit Voltage technique," in *International Symposium on Power Electronics, Electrical Drives, Automation and Motion (SPEEDAM)*, pp. 889–894, IEEE, 2016.

[114] W. Xiao, N. Ozog, and W. G. Dunford, "Topology Study of Photovoltaic Interface for Maximum Power Point Tracking," *IEEE Transactions on Industrial Electronics*, vol. 54, no. 3, pp. 1696–1704, 2007.

[115] A. Kislovski and R. Redl, "Maximum-Power-Trackin using Positive Feedback ," in *25th Annual Power Electronics Specialists Conference, PESC'94 Record.*, vol. 2, pp. 1065–1068, IEEE, 1994.

[116] K. A. Aganah and A. W. Leedy, "A Constant Voltage Maximum Power Point Tracking method for Solar Powered Systems," in *43rd Southeastern Symposium on System Theory (SSST)*, pp. 125–130, IEEE, 2011.

[117] A. Tariq and M. J. Asghar, "Development of an Analog Maximum Power Point Tracker for Photovoltaic Panel," in *International Conference on Power Electronics and Drives Systems, PEDS,* , vol. 1, pp. 251–255, IEEE, 2005.

[118] M. Veerachary, T. Senjyu, and K. Uezato, "Feedforward Maximum Power Point Tracking of PV Systems using Fuzzy Controller," *IEEE Transactions on Aerospace and Electronic Systems*, vol. 38, no. 3, pp. 969–981, 2002.

[119] M. A. Masoum, H. Dehbonei, and E. F. Fuchs, "Theoretical and Experimental Analyses of Photovoltaic Systems with Voltage and Current-Based Maximum Power-Point Tracking," *IEEE Transactions on Energy Conversion*, vol. 17, no. 4, pp. 514–522, 2002.

[120] G. Kumar and A. K. Panchal, "An Advance Geometrical Maximum Power Point Targeting Technique for Solar Photovoltaics using Current-Voltage Curve," in *40th Photovoltaic Specialist Conference (PVSC)*, pp. 1944–1947, IEEE, 2014.

[121] J. Zanotti, W. Dos Santos, and D. Martins, "The Maximum Power Point Tracking for PV systems: Introduction to the Input Characteristic Impedance Method," in *5th International Symposium on Power Electronics for Distributed Generation Systems (PEDG)*, pp. 1–7, IEEE, 2014.

[122] C. Deisch, "Simple Switching Control Method Changes Power Converter into a Current Source," in *Power Electronics Specialists Conference*, pp. 300–306, IEEE, 1978.

[123] H. Beukes and J. Enslin, "Analysis of a New Compound Converter as MPPT, Battery Regulator and Bus Regulator for Satellite Power Systems," in *24th Annual Power Electronics Specialists Conference PESC'93 Record.*, pp. 846–852, IEEE, 1993.

[124] R. Redl and N. O. Sokal, "Near-Optimum Dynamic Regulation of DC-DC Converters using Feed-Forward of Output Current and Input Voltage with Current-Mode Control," *IEEE Transactions on Power Electronics*, no. 3, pp. 181–192, 1986.

[125] D. B. Snyman and J. H. Enslin, "Simplified Maximum Power Point Controller for PV Installations," in *Conference Record of the Twenty Third Photovoltaic Specialists Conference,*, pp. 1240–1245, IEEE, 1993.

[126] D. L. Donoho, "De-noising by Soft-thresholding," *IEEE Transactions on Information Theory*, vol. 41, no. 3, pp. 613–627, 1995.

[127] M. Srivastava, C. L. Anderson, and J. H. Freed, "A New Wavelet Denoising Method for Selecting Decomposition Levels and Noise Thresholds," *IEEE Access*, vol. 4, pp. 3862–3877, 2016.

[128] D. L. Donoho and J. M. Johnstone, "Ideal Spatial Adaptation by Wavelet Shrinkage," *biometrika*, vol. 81, no. 3, pp. 425–455, 1994.

[129] S. James and J. Walker, "A Primer on Wavelets and Scientific Applications," 1999.

[130] F. H. Elfouly, M. I. Mahmoud, M. I. Dessouky, and S. Deyab, "Comparison Between Haar and Daubechies Wavelet Transformations on FPGA Technology," *International Journal of Computer, Information, and Systems Science, and Engineering*, vol. 2, no. 1, 2008.

[131] N. M. Ramli, *An Investigation of Photovoltaic Power Optimization.* PhD thesis, University of Essex, 2017.

[132] M. Fagiani, S. Squartini, M. Severini, and F. Piazza, "A Novelty Detection Approach to Identify the Occurrence of Leakage in Smart Gas and Water Grids," in *International Joint Conference on Neural Networks (IJCNN)*, pp. 1–8, IEEE, 2015.

Appendices

Appendix A

The Seesaw Controller Printed Circuit Board PCB

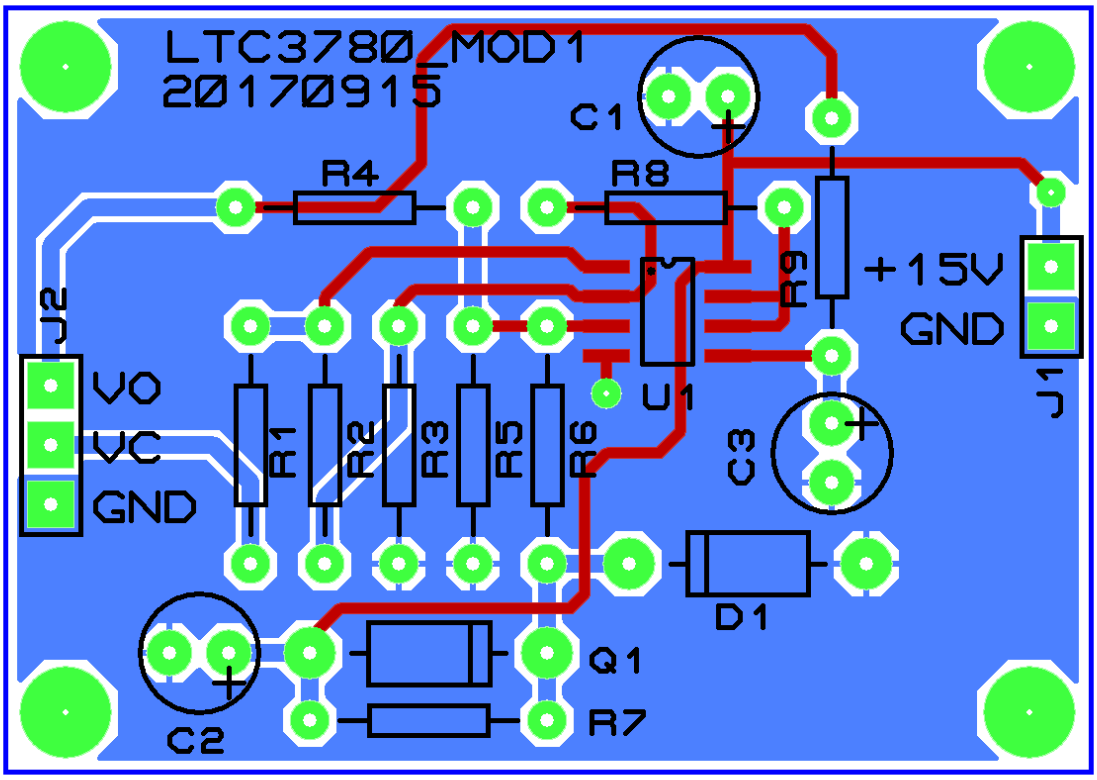

Figure A.1: The Seesaw MPPT printed circuit board.

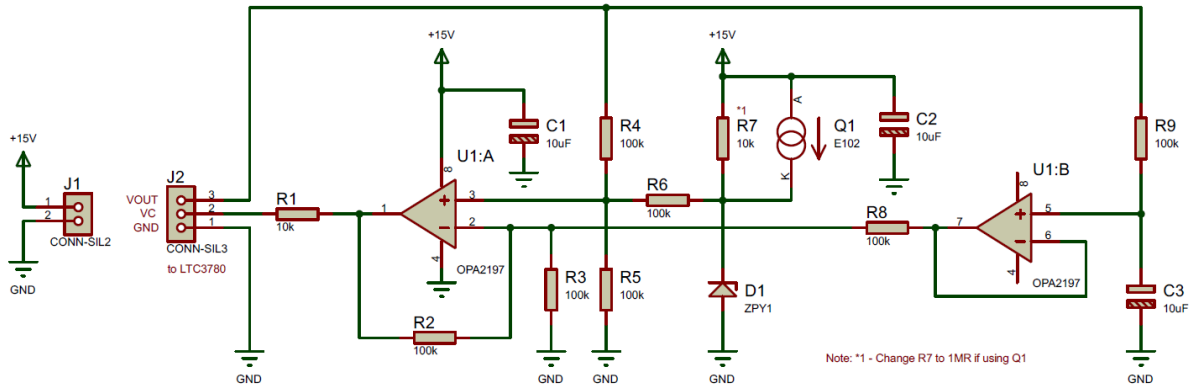

Figure A.2: Circuit diagram for the Seesaw MPPT controller.

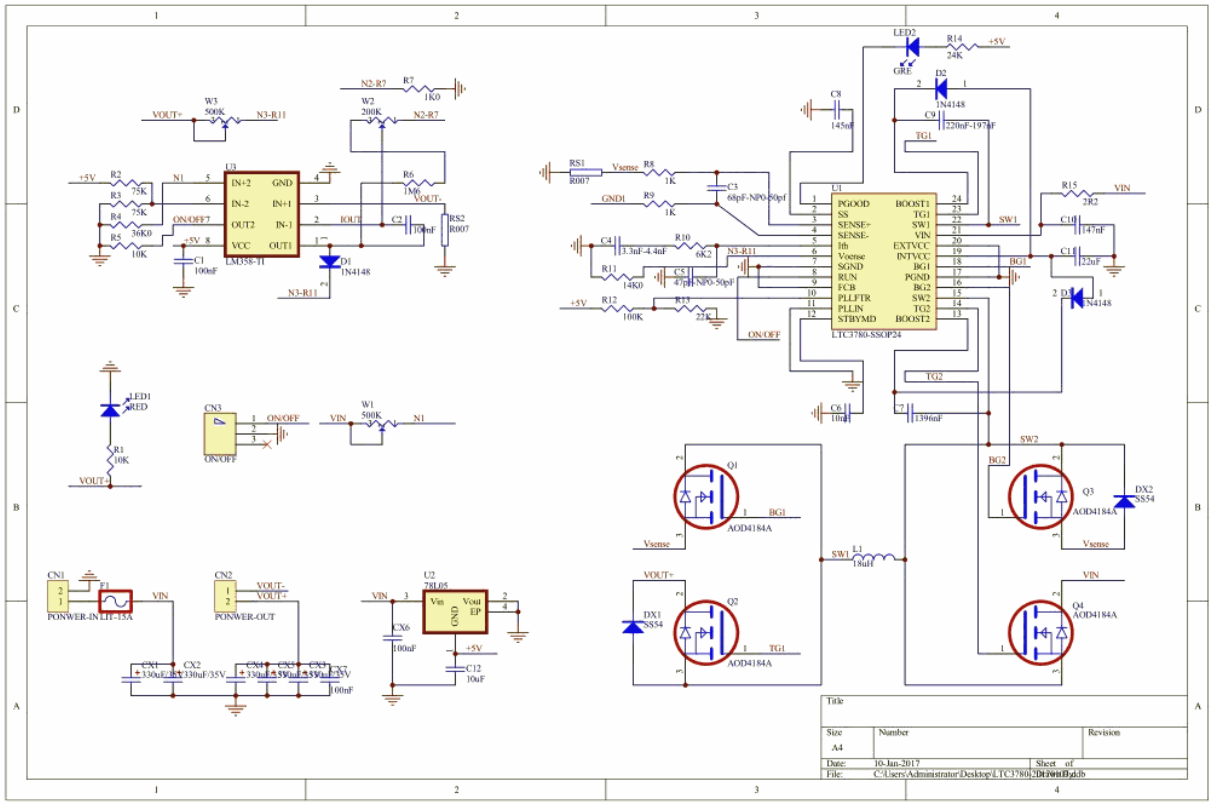

Figure A.3: Circuit connections for the complete maximum power point controller system

Appendix B

Publications and Presentations

N. M. Ramli, **S. A. Alarefi**, and S. D. Walker, "Renewable Power and Microgeneration in Libya: Photovoltaic System Sizing, Wind, Rainfall Potentials and Public Response," *The 6th International Renewable Energy Congress (IREC)*, pp. 1-6, IEEE, 2015.

Renewable Power and Microgeneration in Libya: Photovoltaic System Sizing, Wind, Rainfall Potentials and Public Response

Abstract Renewable generation of electricity within the home has not, thus far, been a notable technology in Libya. To facilitate better take-up, the studies presented here estimate the photovoltaic system sizing; wind and rainfall potentials based on Libyan household energy consumption. Libyan public awareness of such technologies is also investigated. From a Libyan electricity consumers perspective, the vital benefits of deploying microgeneration within a house are to reduce power shortage problems rather than electricity bills. The paper therefore concludes that the public has a positive attitude towards the new technology despite the current lack of provision.

S. A. Alarefi and S. D. Walker, "Intelligent Low-Cost Micro-Hydro Power Emulator for Domestic Applications," *The 3rd International Renewable and Sustainable Energy Conference (IRSEC)*, pp. 1-5, IEEE, 2015.

Intelligent Low-Cost Micro-Hydro Power Emulator for Domestic Applications

Abstract Microgeneration of hydropower for domestic applications is emerging as a promising technology. However, the amount of energy that can be harvested is still modest. The lack of experimental evaluation systems which emulate the power characteristics of such generators for professional development and research has challenged the growth of micro-hydropower generation. This paper describes a laboratory micro-hydropower emulator for research purposes. The core novelty of the system lies in the use of a 2x2 serial/parallel combination of micro-hydro generators. The system features hydro generation with electronically-controllable water flow rates and allows emulation of different household usages.

W. F. Domoney, N. Ramli, **S. Alarefi**, and S. D.Walker, "Smart City Solutions to Water Management Using Self-Powered, Low-Cost, Water Sensors and Apache Spark Data Aggregation," *The 3rd International Renewable and Sustainable Energy Conference(IRSEC)*, pp. 1-4, IEEE, 2015.

Smart City Solutions to Water Management Using Self-Powered, Low-Cost, Water Sensors and Apache Spark Data Aggregation

Abstract We describe a Smart City, self-powered, water monitoring solution that uses low-cost water turbines. These can generate up to 4 W electrical power whilst reporting flow rates at UK domestic water pressure levels. This permits the novel use of stand-alone, remote Apache Spark Streaming as a distributed alternative to the conventional hierarchical Smart Grid. A future Smart City will have innovative features such as high-frequency monitoring of water flows, automated leak detection and shutdown with no requirement for utility electrical power.

S. A. S. Alarefi and S. Walker, "Innovative Shunt Measurement for Residential Water Micro-Leakage Detection," *The* 8^{th} *International Renewable Energy Congress (IREC)*, pp. 1-6, IEEE, 2017.

Innovative Shunt Measurement for Residential Water Micro-Leakage Detection

Abstract In the U.K., between $7.6m^3$ to $76m^3$ of water is lost annually in each residence through leaks. In contrast to the ongoing improvement on water distribution network leakage detection technologies, research on water leakage at the domestic level has been limited. Identification of large flow rate leaks (i.e. L/min. with floods or bursts) through the analysis of the household water consumption is highly feasible. However, micro-flow rate leaks (i.e. mL/min.) tend to be overlooked and can therefore waste hundreds of liters of water before detection. This, alongside increasing awareness of water quality and resource protection, mandates further investigation of micro-leak detection systems. An innovative micro-leak detection system for domestic applications that utilizes an ultrasonic flowmeter in a new shunt configuration is proposed. Unlike conventional water leakage detection systems, the proposed automated system is highly sensitive (detected leaks of 1 mL/min.) and does not impede the main flow. The micro-leak detection system is completely automated as it employs a: USB-powered voltmeter, USB-powered flowmeter and USB-powered switches. An elegant feature is that the system is remotely controlled across the Globe; thus, allowing large-scale data collection and system control. This system circumvents water leaks on any scale, anywhere in the world. This latter feature is beyond the reach of the complex conventional detection methods. The de-noising property of Wavelet transform is carried out on the remotely collected data from the ultrasonic flowmeter to remove unwanted noise.

S. A. S. Alarefi and S. Walker, "Empirical Investigation and Simulink-Simulation Modelling of Hydropower Generator Characteristic Impedance", accepted for publication at *The* 19^{th} *International Conference on Industrial Technology*, IEEE, 2018.

Investigations and Modelling of Hydroelectric Power Generators Characteristics Impedance

Abstract Research on the electrical characteristics of hydroelectric power systems has, to our knowledge not received much attention. However, renewed interest in hydropower microgeneration has created a need to understand the underlying properties. This paper presents a pioneering empirical investigation into the electrical characteristics of micro-hydro power generators (MHPGs). We demonstrate Ohmic characteristic behavior in MHPGs with constant source impedance, even with varying water flow. A novel heuristic model for hydroelectric power generator is then described and validated through Simulink simulations.

S. A. S. Alarefi and S. Walker, "Innovative Shunt Measurement for Residential Water Micro-Leakage Detection" Poster for the *STEM for BRITAIN Competition*, House of Commons, London, 2017.

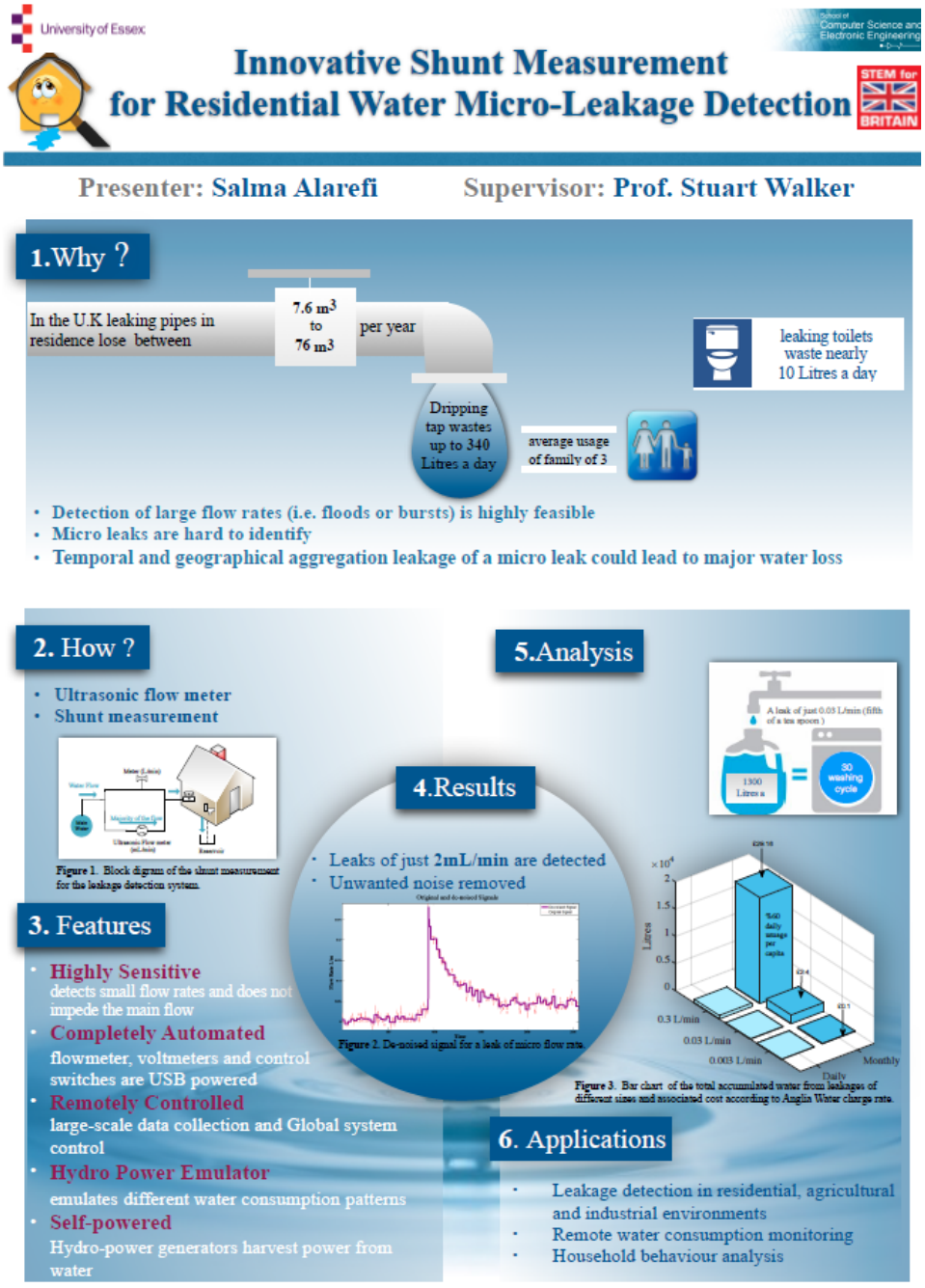

Figure B.1: Poster presented at STEM for BRITAIN Competition 2017.